NASA/TM–20250010561
NESC-RP-25-02088

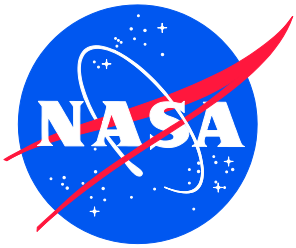

Hubble Space Telescope and Swift Observatory Orbit Decay Study

Heather M. Koehler/NESC, Joseph I. Minow/NESC, William J. Cooke, and Benjamin S. Burger
Marshall Space Flight Center, Huntsville, Alabama

Ashley D. Hill
Amentum Technology, Chantilly, Virginia

Sara R. Wilson/NESC
Langley Research Center, Hampton, Virginia

Abram R. Aguilar
Jacobs Technology, Inc., Dallas, Texas

Max Vovk
University of Western Ontario, Canada

Roger C. Thompson
The Aerospace Corporation, El Segundo, California

November 2025

NASA STI Program Report Series

Since its founding, NASA has been dedicated to the advancement of aeronautics and space science. The NASA scientific and technical information (STI) program plays a key part in helping NASA maintain this important role.

The NASA STI program operates under the auspices of the Agency Chief Information Officer. It collects, organizes, provides for archiving, and disseminates NASA's STI. The NASA STI program provides access to the NTRS Registered and its public interface, the NASA Technical Reports Server, thus providing one of the largest collections of aeronautical and space science STI in the world. Results are published in both non-NASA channels and by NASA in the NASA STI Report Series, which includes the following report types:

- TECHNICAL PUBLICATION. Reports of completed research or a major significant phase of research that present the results of NASA Programs and include extensive data or theoretical analysis. Includes compilations of significant scientific and technical data and information deemed to be of continuing reference value. NASA counterpart of peer-reviewed formal professional papers but has less stringent limitations on manuscript length and extent of graphic presentations.

- TECHNICAL MEMORANDUM. Scientific and technical findings that are preliminary or of specialized interest, e.g., quick release reports, working papers, and bibliographies that contain minimal annotation. Does not contain extensive analysis.

- CONTRACTOR REPORT. Scientific and technical findings by NASA-sponsored contractors and grantees.

- CONFERENCE PUBLICATION. Collected papers from scientific and technical conferences, symposia, seminars, or other meetings sponsored or co-sponsored by NASA.

- SPECIAL PUBLICATION. Scientific, technical, or historical information from NASA programs, projects, and missions, often concerned with subjects having substantial public interest.

- TECHNICAL TRANSLATION. English-language translations of foreign scientific and technical material pertinent to NASA's mission.

Specialized services also include organizing and publishing research results, distributing specialized research announcements and feeds, providing information desk and personal search support, and enabling data exchange services.

For more information about the NASA STI program, see the following:

- Access the NASA STI program home page at http://www.sti.nasa.gov

- Help desk contact information:

https://www.sti.nasa.gov/sti-contact-form/
and select the "General" help request type.

NASA/TM–20250010561
NESC-RP-25-02088

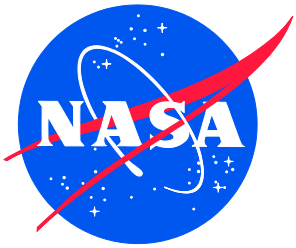

Hubble Space Telescope and Swift Observatory Orbit Decay Study

Heather M. Koehler/NESC, Joseph I. Minow/NESC, William J. Cooke, and Benjamin S. Burger
Marshall Space Flight Center, Huntsville, Alabama

Ashley D. Hill
Amentum Technology, Chantilly, Virginia

Sara R. Wilson/NESC
Langley Research Center, Hampton, Virginia

Abram R. Aguilar
Jacobs Technology, Inc., Dallas, Texas

Max Vovk
University of Western Ontario, Canada

Roger C. Thompson
The Aerospace Corporation, El Segundo, California

National Aeronautics and
Space Administration

Langley Research Center
Hampton, Virginia 23681-2199

November 2025

Acknowledgments

The team is also grateful to the following peer reviewers whose comments and edits improved the quality of this report and clarified the major points of the work: Mr. Joel Sills, Dr. Don Mendoza, Mr. Mike Squire, Mr. Ben Burger, Mr. Chris Broadway, Dr. Sara Wilson, Dr. Jim O'Donnell, Mr. Scott Tashakkor, and Dr. Roger Thompson.

This effort would not have been successful in the shortened period without the help and quick action from MSFC EV40 Management, Mr. Glenn Overbey, Mr. Andy Heaton, Dr. Powtawche Valerino, Mr. Ryan Decker, and Dr. Peter McDonough. Their responsiveness, technical review and most importantly their willingness to make available key experts contributed to the final quality of this assessment.

We acknowledge the valuable peer review and key insights by Dr. Conrad Schiff, Dr. Jer-Chi Liou, Dr. Peter Brown, Dr. Roger Thompson, Mr. Bo Naasz, Ms. Carmel Conaty, and Mr. Jon Holladay. The review inputs provided clarifications and strengthened the findings and recommendations highlighted in this report.

Outstanding team support was provided by Ms. Linda Moore, Ms. Lorrie Hardin, Ms. Linda Burgess, Ms. Melissa Strickland, and Ms. Emily Anthony in managing the financial, team schedule, project coordination, and technical editing respectively. Their efforts went above and beyond to accommodate a compressed timeline and improved the overall product and efficiency of the team.

Available from:

NASA STI Program / Mail Stop 050
NASA Langley Research Center
Hampton, VA 23681-2199

NASA Engineering and Safety Center
Technical Assessment Report

Hubble Space Telescope and Swift Observatory Orbit Decay Study

TI-25-02088

Heather Koehler, NESC Lead

August 28, 2025

Report Approval and Revision History

NOTE: This document was approved at the August 28, 2025, NRB.

Approved: Timmy Wilson Digitally signed by Timmy Wilson Date: 2025.09.29 17:58:19 -04'00'

NESC Director

Version	Description of Revision	Office of Primary Responsibility	Effective Date
1.0	Initial Release	Heather M. Koehler, NASA Technical Fellow, MSFC	8-28-25

Table of Contents

List of Figures

List of Tables

List of Appendices

Technical Assessment Report

1.0 Notification and Authorization

Mr. Todd Ericson, senior advisor to the NASA Administrator, requested the NESC conduct an independent study of the Hubble Space Telescope (HST) orbital decay to inform the timeline to reentry, loss of science and risk to the public for an uncontrolled reentry. The HST reentry and demise have been extensively studied and reported on by numerous groups including the primary organizations such as GSFC Flight Dynamics Facility (FDF) under direction by the Hubble Project Office, and the Orbital Debris Program Office (ODPO) at JSC. As such, the Hubble Space Telescope Project Office and ODPO are considered stakeholders along with head of the office of Chief Engineer (OCE), Joe Pelliciotti.

Request Submitted	April 9, 2025
Out of Board Summary Approved	April 24, 2025
Team Kickoff Meeting	April 11, 2025
Stakeholder Briefing (Draft of Final Results)	May 21, 2025
Final Report Delivery and Stakeholder Update	August 28, 2025

A quick study was requested utilizing different tools and approaches from previous studies. Simplifying assumptions and lower fidelity tools were used to provide reasonable estimates as compared against higher fidelity tools and results in published reports. Additionally, a late request to evaluate the orbital decay of the Neil Gehrels Swift Observatory was included for the NASA Office of Chief Engineer. The NESC lead assigned was Heather Koehler, NASA Technical Fellow for Flight Mechanics.

2.0 Signatures

Submitted by: NESC Lead

Heather Koehler
Digitally signed by Heather Koehler
Date: 2025.09.23 16:15:25 -05'00'

Ms. Heather M. Koehler

Significant Contributors:

Joseph Minow
Digitally signed by Joseph Minow
Date: 2025.09.23 15:41:27 -05'00'

Dr. Joseph I. Minow

WILLIAM COOKE
Digitally signed by WILLIAM COOKE
Date: 2025.09.23 16:05:09 -05'00'

Dr. William J. Cooke

Ashley Hill (affiliate)
Digitally signed by Ashley Hill (affiliate)
Date: 2025.09.23 14:53:46 -05'00'

Mr. Ashley D. Hill

BENJAMIN BURGER
Digitally signed by BENJAMIN BURGER
Date: 2025.09.23 14:21:27 -05'00'

Mr. Benjamin S. Burger

Abram Aguilar (affiliate)
Digitally signed by Abram Aguilar (affiliate)
Date: 2025.09.23 15:56:03 -05'00'

Mr. Abram R. Aguilar

Signatories declare the findings, observations, and NESC recommendations compiled in the report are factually based from data extracted from program/project documents, contractor reports, and open literature, and/or generated from independently conducted tests, analyses, and inspections.

3.0 Team Members

Name	Discipline	Organization/Host Center	* New to NESC Assessments
Core Team			
Heather Koehler	NESC Lead	NESC/MSFC	
Dr. Joseph Minow	Environments Technical Fellow	NESC/MSFC	
Dr. William Cooke	Meteoroid Environments Office (MEO)	MSFC	
Abram Aguilar	Orbital Mechanics Analyst	JSC	*
Ben Burger	Flight Mechanics, 6DOF Simulation	MSFC	
Ashley Hill	6DOF Simulation	ESSCA/MSFC	*
Zach Muscha	6DOF Simulation	ESSCA/MSFC	*
Joshua Stephenson	6DOF Simulation	ESSCA/MSFC	*
Michael Sanders	6DOF Simulation	ESSCA/MSFC	*
Max Vovk	DRAMA Analyst	University of Western Ontario, Canada	*
Dr. Roger Thompson	Orbital Mechanics/Reentry	Aerospace Corp.	
Dr. Sara Wilson	Statistician	NESC/LaRC	
Consultants			
Dr. Peter Brown	ESA Affiliate	University of Western Ontario, Canada	
Dr. David E. Sitton	Simulation	ESSCA/MSFC EV40	
Bo Naasz	ISAM/RPOD SCLT	GSFC	
Nick Jedrich	NASA SMD Chief Engineer	OCE	
Carmel Conaty	NESC Chief Engineer, GSFC	NESC/GSFC	
Dr. Conrad Schiff	Astrodynamics	GSFC 595	
Dr. Peter McDonough	ESSCA Lead, 6DOF Simulation	ESSCA/MSFC EV40	
Dr. Rekesh M. Ali	Multibody Dynamics and Simulation	ESSCA/MSFC EV40	
William J Harlin	Flight Mechanics	ESSCA/MSFC EV40	
Business Management			
Linda Moore (ret.)	Program Analyst	MTSO/LaRC	
Lorrie Hardin	Program Analyst	MTSO/LaRC	
Assessment Support			
Melissa Strickland	Project Coordinator	AMA/LaRC	
Linda Burgess	Planning and Control Analyst	AMA/LaRC	
Emily Anthony	Technical Editor	AS&M/LaRC	

3.1 Acknowledgements

The team is also grateful to the following peer reviewers whose comments and edits improved the quality of this report and clarified the major points of the work: Mr. Joel Sills, Dr. Don Mendoza, Mr. Mike Squire, Mr. Ben Burger, Mr. Chris Broadway, Dr. Sara Wilson, Dr. Jim O'Donnell, Mr. Scott Tashakkor, and Dr. Roger Thompson.

This effort would not have been successful in the shortened period without the help and quick action from MSFC EV40 Management, Mr. Glenn Overbey, Mr. Andy Heaton, Dr. Powtawche Valerino, Mr. Ryan Decker, and Dr. Peter McDonough. Their responsiveness, technical review and most importantly their willingness to make available key experts contributed to the final quality of this assessment.

We acknowledge the valuable peer review and key insights by Dr. Conrad Schiff, Dr. Jer-Chi Liou, Dr. Peter Brown, Dr. Roger Thompson, Mr. Bo Naasz, Ms. Carmel Conaty, and Mr. Jon Holladay. The review inputs provided clarifications and strengthened the findings and recommendations highlighted in this report.

Outstanding team support was provided by Ms. Linda Moore, Ms. Lorrie Hardin, Ms. Linda Burgess, Ms. Melissa Strickland, and Ms. Emily Anthony in managing the financial, team schedule, project coordination, and technical editing respectively. Their efforts went above and beyond to accommodate a compressed timeline and improved the overall product and efficiency of the team.

4.0 Executive Summary

The NASA Engineering and Safety Center (NESC) conducted a comprehensive study on the Hubble Space Telescope (HST) orbital decay to predict its reentry timeline and assess public safety risks. This assessment was initiated to improve understanding of HST's orbital lifespan and develop strategies for managing its eventual uncontrolled Earth reentry. An additional request included a quick evaluation of the orbital decay predictions for the Swift Observatory given its potential near-term reentry, analyses are presented in Appendix C.

The HST demise has been studied extensively (refs. 1, 2, 3, 4) and was found to be highly sensitive to variations in space weather activity and the breakup modelling for estimating casualty risks for populations living under the ground track. The orbiting platform has been serviced 5 times since its launch in 1990 to maintain the observatory, replace critical instruments, and extend the lifetime. Recent studies (ref. 1) estimate the observatory to decay in the mid 2030's with approximately 20% of the mass (ref. 3) of the spacecraft surviving reentry, increasing the probability of casualties on the ground given an uncontrolled reentry. The current NASA requirement for human casualty is 1/10,000 (ref. 5).

This study employed multiple orbital simulation tools and methodologies to analyze various factors affecting HST's decay rate, including historical solar activity and predictions, atmospheric density models, HST attitude orientations, and drag characteristics. The assessment team identified critical factors influencing decay predictions, such as solar activity forecasts, atmospheric density model variations, and spacecraft attitude profiles. To evaluate the resulting footprint and casualty probabilities, two simulations were used to assess multiple reentry conditions and debris-ejection models. A thorough statistical analysis of the decay or reentry time was out of scope for this assessment; however, some Monte Carlo analyses were conducted with simplified assumptions in a 6 degree of freedom (6DOF) simulation.

Key findings revealed significant sensitivity of decay predictions to solar activity forecasts, with variations in F10.7 solar flux values leading to substantial differences in predicted reentry dates. The NESC team also identified inconsistencies in atmospheric density models and the importance of accurately representing HST's attitude profile when calculating effective drag area.

Results of this study conclude that for the nominal predicted solar activity, and average projected surface area, HST is predicted to reenter Earth's sensible atmosphere in 2033, with a debris footprint that ranges approximately 350 kilometers (km) to 800 km along the ground track. While the exact location of reentry and footprint were not estimated, the probability of casualty ranges from and average overall risk of 1:330 over the entire inclination region HST crosses to 1:31,000 over the most remotely inhabited region of the South Pacific Ocean from the two simulations conducted.

The results of the Swift Observatory decay conclude that for the nominal predicted solar activity, and average projected surface area, Swift Observatory is predicted to reenter Earth's sensible atmosphere in 2026. The debris footprint and casualty risk were not computed for this part of the analyses due to time constraints.

The assessment produced several findings, observations, and NESC recommendations for improving decay predictions, including using attitude profiles from observation schedules to estimate drag area variations, conducting updated reentry survivability analyses, and

implementing model improvements for solar activity forecasting. Additionally, the NESC team recommended updating NASA standards for orbital debris risk assessment to incorporate new debris casualty area equations.

In summary, this assessment provides stakeholders with improved methodologies for predicting HST and Swift Observatory orbital decay and evaluating public safety risks, while highlighting the importance of continued refinement of prediction tools and the need for updated survivability analyses using the latest population data and modeling techniques.

5.0 Assessment Plan

This effort aimed to provide an independent check using different tools, environments and assumptions compared against recent results and to address open questions regarding the anticipated decay time and casualty impacts to the population under the HST ground track. This effort was not meant to be an all-encompassing deep dive into the complexities of aerothermal demise fragmentation, nor does it attempt to untangle the complicated relationship between the solar cycle uncertainties and relationships to ballistic and drag coefficients and the thermosphere. Parameter sweeps over various conditions and simplifying assumptions allowed for a rapid assessment of the accuracy of recent reports and offered some interesting findings and observations about the performance of these simulation tools and actionable recommendations for further areas of study.

This effort used an independent simulation to assess the decay rate against predictive solar cycles and historical solar cycle data to evaluate the sensitivity to decay time given HST's current altitude. Two reentry/footprint analysis tools assumed variations in breakup conditions, altitude, orientations and debris fragment characteristics to produce expected debris footprint sizes and casualty risks. With unknown reentry interface locations, HST's 28.5-degree inclination constrains the potential dispersal for debris between +/-28.5 degree latitude. Casualty risks were computed using global population data, scaled for growth, from public websites.

Brief surveys of historical reports characterizing previous Hubble decay results are included in an appendix and findings, observations, and recommendations conclude the technical report.

Response to a late request to independently assess the decay predictions for the Swift telescope against current predictions were included and are in Appendix C. Analyses for reentry, footprint or casualty risk predictions were not conducted. That is considered forward work for the responsible organizations.

6.0 Problem Description and Background

The HST, launched in 1990, will eventually undergo uncontrolled reentry as its orbit naturally decays. Accurately predicting when this reentry will occur and assessing potential risks to the public are critical concerns for NASA. This assessment evaluated and independently checked HST decay prediction methodologies, analyzed potential hazards upon reentry, and provided recommendations for managing associated risks.

HST orbits at an altitude where atmospheric drag gradually reduces its orbital energy. The rate of decay is influenced by numerous factors, including varying solar activity (which affects atmospheric density), the spacecraft's attitude, and its physical characteristics. Current prediction methodologies show significant variations in estimated reentry dates, necessitating a more comprehensive approach to improve accuracy.

Additionally, as HST was not designed for controlled reentry, there are concerns regarding surviving debris reaching Earth's surface and the associated casualty risks. Previous survivability assessments need updating to reflect the current HST configuration after the final servicing mission (SM-4) and to incorporate the latest population density data and risk assessment methodologies.

The orbiting platform has been serviced 5 times since its launch in 1990 to maintain the observatory, replace critical instruments, and extend the lifetime. Recent studies estimate the

observatory to decay in the mid 2030's with approximately 20% of the mass of the spacecraft surviving reentry, increasing the probability of casualties on the ground with an uncontrolled reentry.

HST was located 489 km above Earth's surface as of April 2025 with a 28.46-degree inclination and near circular orbit. Flight Dynamics Facility (FDF) orbital altitude as of March 2025, Figure 6-2, shows the recent trend, losing approximately 45 km since January 2022 and 5-6 km since January 2025. The last servicing mission added ~400 kilograms (kg), resulting in a 12,246 kg telescope.

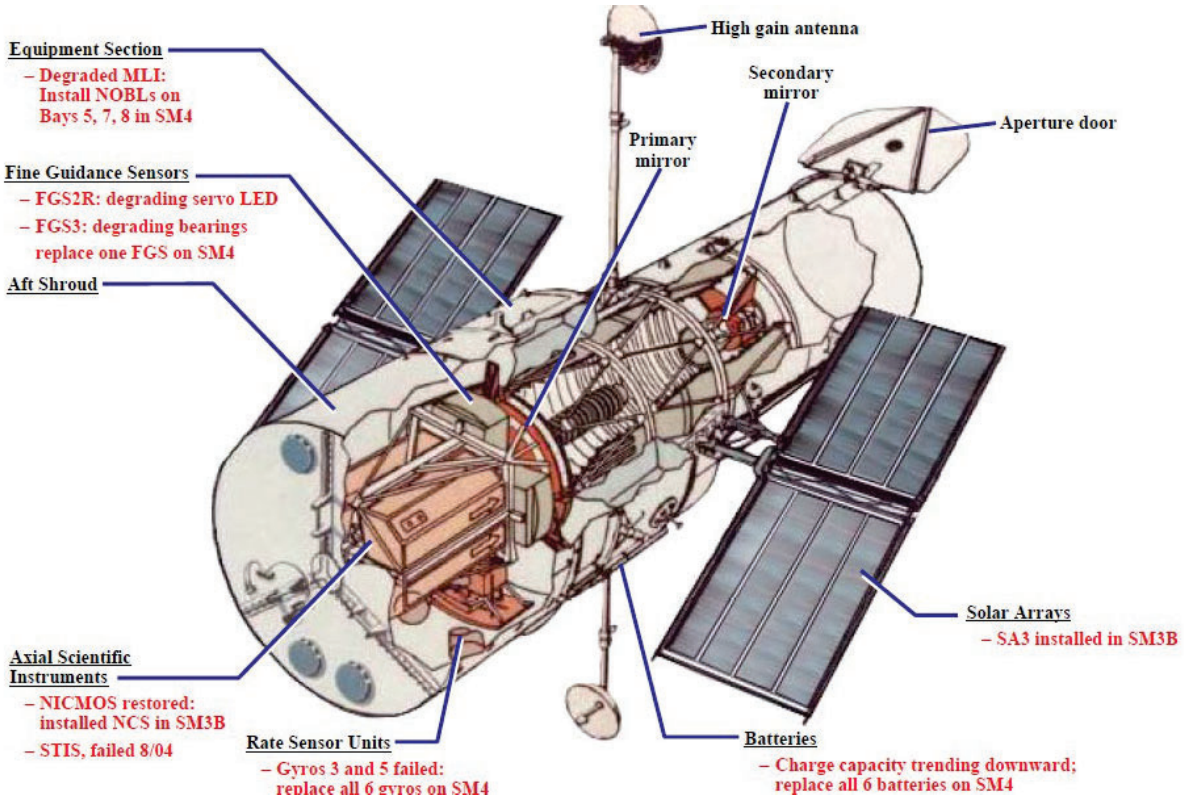

Figure 6-1. HST Current Configuration[1]

[1] https://science.nasa.gov/mission/hubble/observatory/

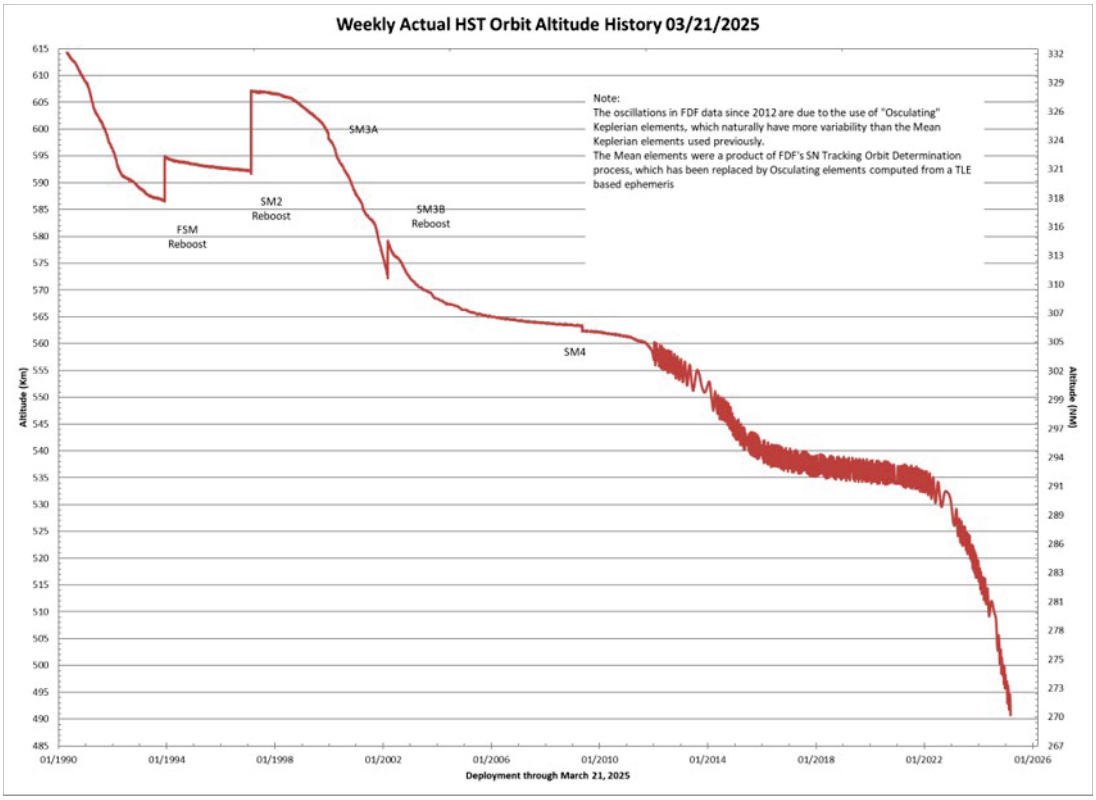

Figure 6-2. FDF Tracked HST Orbit Altitude

Hubble's orbital altitude has been as high as 620 km over the years, but due to atmospheric drag, it has slowly descended over time.

The telescope was boosted into higher orbits multiple times over the years by the space shuttle following servicing. The last servicing mission to boost Hubble was conducted in 2009 and now is under the influences of natural drag driven by the thermosphere and solar activity.

Given the current trend in decay, our analysis attempts to address the question if HST will follow the current trend for an earlier reentry.

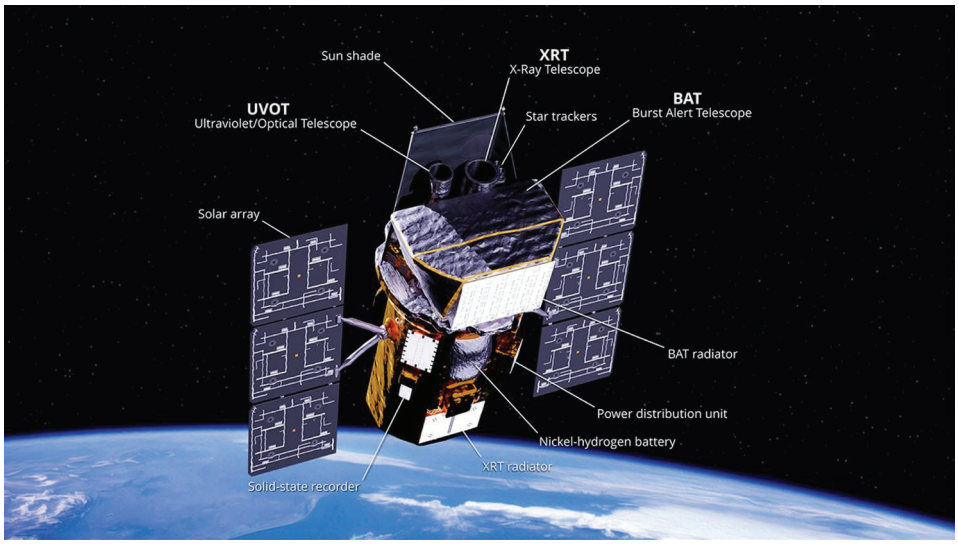

Figure 6-3. Swift Observatory Configuration[2]

7.0 Analysis

"The computation of orbit lifetime is extremely challenging. The abundance of uncertainty makes the results of any one prediction suspect." (ref. 6)

This analysis includes a brief discussion of the driving factors for orbital decay, predictions and modeling of the solar environment, and calculations of HST and the Swift Observatory (found in Appendix C) drag coefficients. Simulation setup and results are presented for the orbital decay analyses followed by reentry modeling setup, results and casualty risk analyses for HST only, Swift analyses is described in Appendix C.

7.1 Solar Environment Discussion

"Virtually every term in the atmospheric drag force equation has a significant uncertainty" (ref. 7)

$$a_{drag} = \frac{1}{2} C_d \rho \frac{A}{m} v^2$$

Equation 1.

The atmospheric drag acceleration equation is a function of a satellite's area-to-mass ratio (A/m), drag coefficient (C_d), speed (v) at which the satellite is traveling relative to the motion of the local atmosphere, and the atmospheric density (ρ). The importance of the atmospheric density term to the drag acceleration varies both in time and space. Atmospheric density increases with decreasing altitude, so atmospheric density contributions to drag acceleration dominate at low altitude. Atmospheric density also exhibits variations over a range of spatial and temporal scales from changes in density between the day and night segments of a single satellite orbit, local time variations over a day due to atmospheric tidal structures, short term variations in density as the atmosphere expands over a period of many hours to days from atmospheric heating by solar photons at ultraviolet (UV) and extreme ultraviolet (EUV) wavelengths during periods of increased solar activity, and energy deposition at high latitudes by charged particles and joule

[2] https://science.nasa.gov/mission/swift/spacecraft/

heating during geomagnetic storms. Finally, there are long period variations in solar activity and corresponding increases and decreases in atmospheric density over a period of 9 to 14 years due to solar UV/EUV activity variations over a solar cycle, as seen in Figure 7.1-1. The physics that drives spatial and temporal changes in atmospheric density are incorporated into standard models of the Earth's neutral atmosphere that have been developed over the years including the Naval Research Laboratory's Mass Spectrometer Incoherent Scatter (NRLMSIS) model, Drag Temperature Model (DTM), Jacchia-Roberts (JR), and Jacchia-Bowman (JB) series of codes (refs. 8, 9, 10, 11, 12, 13, 14, 15, 16). Solar and geomagnetic parameters are used as inputs to these codes to constrain the atmospheric density variations due to heating by solar activity and geomagnetic storms. The JR and MSIS codes are used in this work because they are standard models widely used for studies of orbital decay of satellites and are included in the FreeFlyer software distribution[3].

Energy deposition in the Earth's lower thermosphere by solar UV/EUV photons is the physical process responsible for heating of Earth's upper atmosphere during periods of enhanced solar activity. Direct measurements of solar UV/EUV photons require satellite-borne instruments above the atmosphere and are plagued by issues of variation in instrument sensitivity over time and drift in sensor calibration. More frequently, atmospheric models use the F10.7 index as a proxy for the solar UV/EUV flux because F10.7 correlates well with UV/EUV emissions which are responsible for heating Earth's upper atmosphere but are measured from the surface of the Earth (ref. 17).

F10.7 values are a measurement of the strength of all solar radio emissions over the Earth-facing disk of the Sun in a 100 MHz-wide band centered on a frequency of 2800 MHz (wavelength of 10.7 centimeters (cm)) in a 1-hour period centered on the time reported for the measurement. The 10.7 cm solar flux measurements are reported in solar flux units where 1 solar flux unit (sfu) = 10^{-22} W/m^2-Hz. F10.7 measurements are currently obtained in western Canada at the Dominion Radio Astrophysical Observatory (DRAO), near Penticton, British Columbia. Measurements are made three times a day at 17:00 Universal Time (UT), 20:00 UT, and 23:00 UT from March through October and 18:00 UT, 20:00 UT, and 22:00 UT from November through February. The F10.7 index is obtained from the 20:00 UT measurement, which is local solar noon at DRAO.

In the early years of the 10.7 cm measurement, if the 20:00 UT measurement were contaminated by a large solar radio burst then, efforts were made to remove these values and substitute a quiet value from either the morning or afternoon measurement for the F10.7 index. Some implementations of the F10.7 index today still do this filtering process while others simply accept the 20:00 UT value as measured depending on the intended application (ref. 17).

In summary, geomagnetic indices, Ap and Kp, are measures of magnetic field disturbances and are proxies for magnetospheric energy input to Earth's upper atmosphere. Models of Earth's upper atmosphere use F10.7 solar activity index and the Ap or Kp geomagnetic index to produce neutral density values for computing spacecraft drag force.

Prediction of future solar activity is a difficult problem, some techniques are better than others but, accurate predictions are still a challenge.

[3] https://ai-solutions.com/

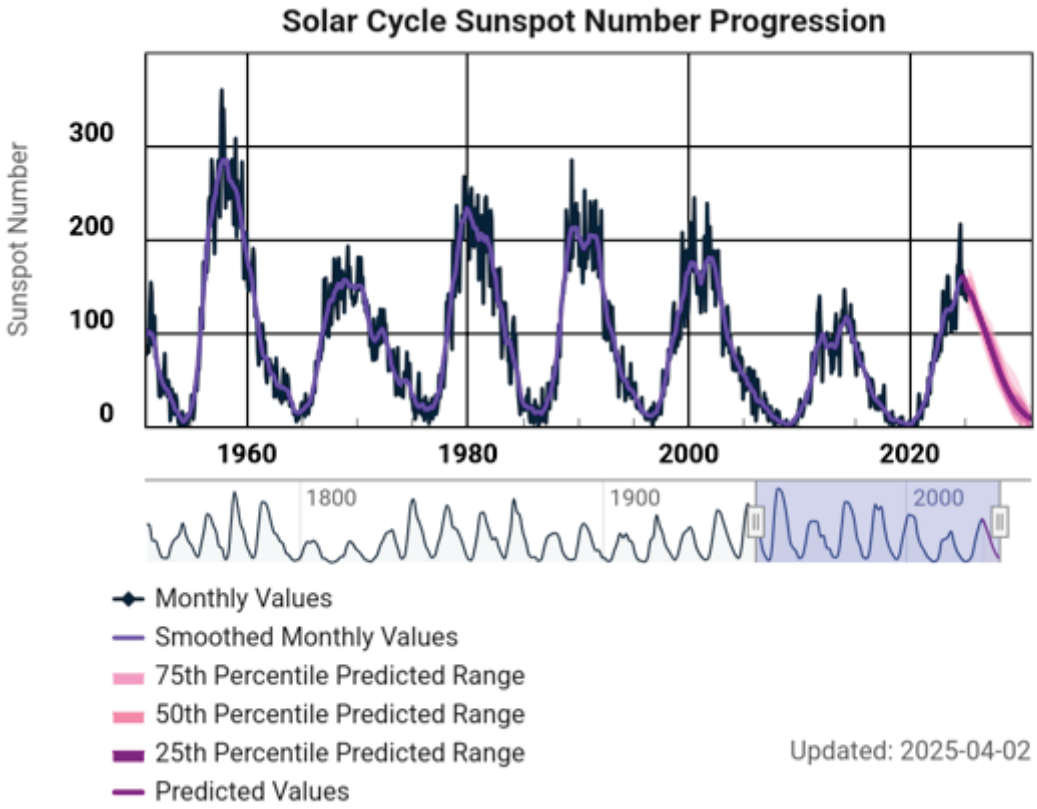

Figure 7.1-1. Solar Cycle Sunspot Number Progression[4]

One such model of Earth's upper atmosphere, NASA Marshall Solar Activity Future Estimation (MSAFE) uses a McNish-Lincoln linear regression method used for predicting the remainder of the current solar cycle. Analysis of the past 24 complete solar cycles is used to generate statistical estimates of the F10.7 index for the next complete solar cycle. The solar forecast is updated monthly using the latest month's observed solar indices to provide estimates for the balance of the current solar cycle. The forecasted solar indices represent the 13-month smoothed values with a best estimate value stated as a 50th percentile value along with approximate +/- 2 sigma values stated as 95 and 5th percentile statistical values, as seen in Figures 7.1-2 and 7.1-3. Most solar activity prediction models generate a "smoothed" profile, removing the natural daily variations, which can be dramatic ranging over hundreds of points day to day.

[4] https://www.swpc.noaa.gov/products/solar-cycle-progression

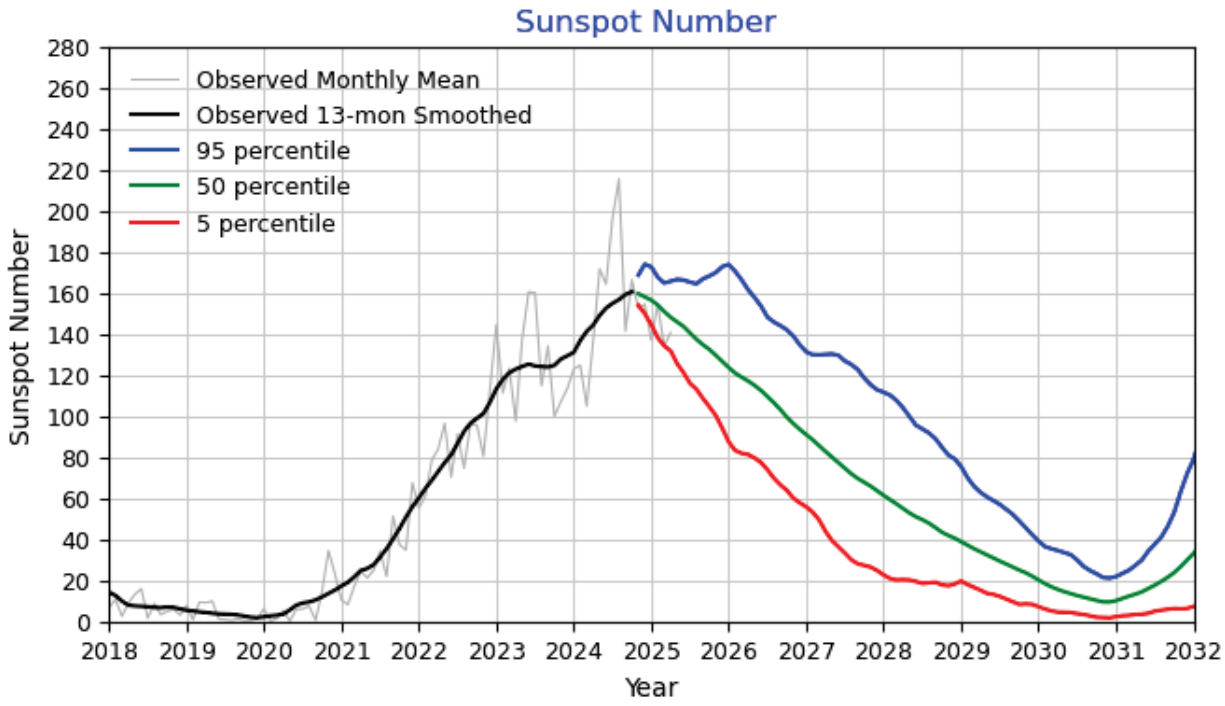

Figure 7.1-2. MSAFE Solar Cycle Sunspot Number Progression[5]

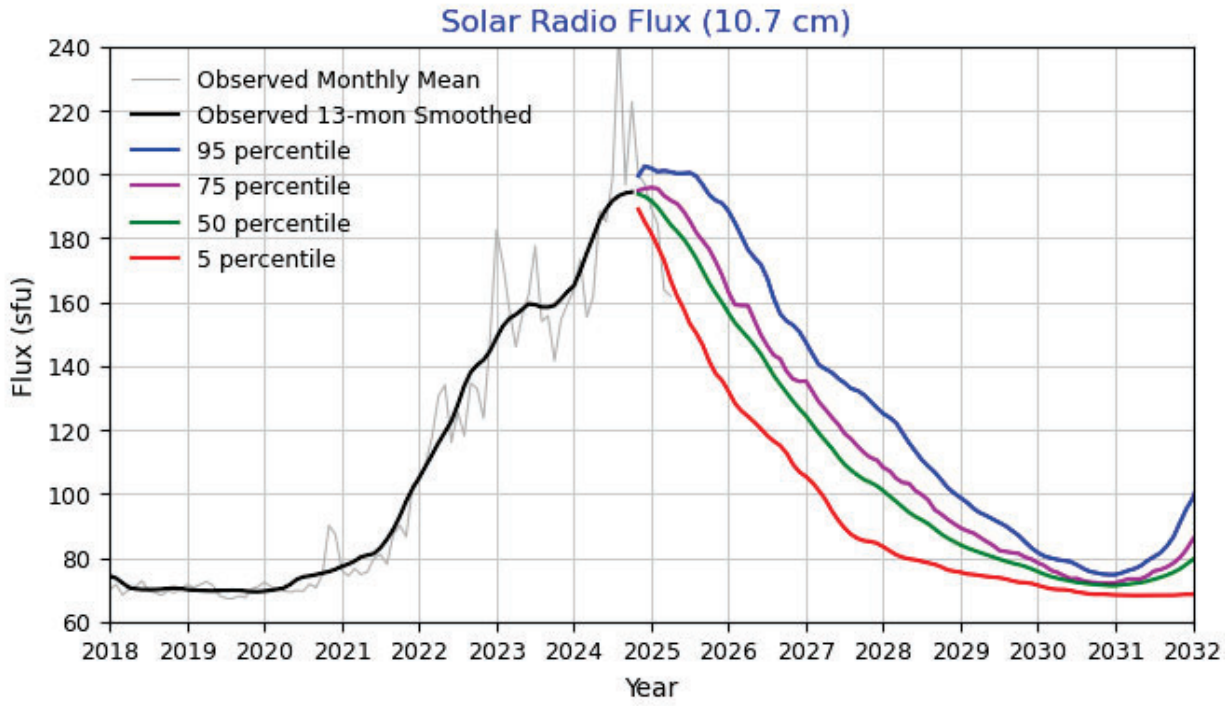

Figure 7.1-3. MSAFE Solar Radio Flux (10.7cm)[6]

[5] https://www.nasa.gov/solar-cycle-progression-and-forecast/

[6] https://www.nasa.gov/solar-cycle-progression-and-forecast/

For these analyses, the NESC team selected FreeFlyer (FF), a commercial off-the-shelf astrodynamics software package, and the MSAFE solar activity model. GSFC FDF used System Tool Kit (STK) and the Schatten solar environment prediction model (ref. 18). Specifically, FF uses a space weather data file from the public website CelesTrak[7] by default. CelesTrak provides free orbital data, satellite catalog element sets, and space weather data, typically direct from the data providers. The website has been published since 1998 and is widely used in astronomy and astrodynamics communities. The space weather file from CelesTrak contains data for F10.7 flux, Kp, Ap and other related values. These data are used for Jacchia Roberts and MSIS atmospheric density modeling. The data file contains both observed values and predicted data; the predictions come from the National Oceanic and Atmospheric Administration (NOAA) and the NASA MSAFE model. (**O-1**)

Because the use of FF and MSAFE provide an alternate method to the GSFC FDF approach for conducting orbital decay analysis, they provide a good independent check. CelesTrak publishes an updated space weather file, frequently updating the daily measured F10.7, Ap, and Kp values. For dates in the future, CelesTrak reports to use the MSAFE 50th percentile F10.7 values. During our analysis, it was discovered that our initial decay predictions from FF were based on an older default space weather file from CelesTrak that contained observed F10.7 values through April of 2024 followed by MSAFE predictive values from April 2024 to the present. That older MSAFE 50th percentile model underpredicted an actual observed 'second peak' of solar activity. Figure 7.1-4 shows the missed second peak (circled in yellow) where the predicted model (in blue) had a smaller average amplitude than the daily measured values (red) for the spring 2024 timeframe. This means that our initial FF simulation was using an under-predictive solar environment than what was actually measured during that period. The underprediction meant the modeling of a weaker solar activity level into the atmosphere influenced the resulting decay predictions for a later date. The figure below also displays a more recent space weather file in green, which had daily F10.7 measured values through April 2025 followed by MSAFE predicted values. Using the up-to-date space weather file (in green) included this observed second high peak of solar activity. This inclusion of additional high peak solar activity impacted the decay predictions of HST and Swift to earlier reentry dates (recomputed to reenter earlier than the first analyses with 'stale data').

[7] https://celestrak.org/

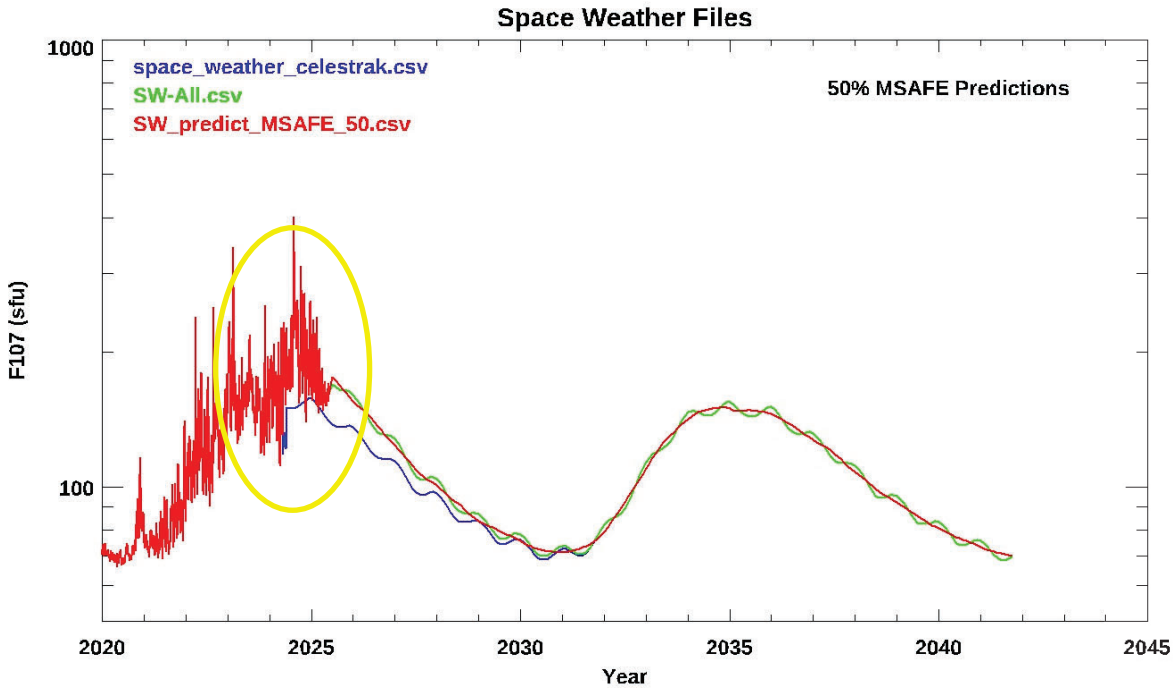

Figure 7.1-4. Comparison Plot of CelesTrak Space Weather Files, Daily Observed F10.7 and MSAFE model predicted values for F10.7

Additionally, the older and newer space weather files showed an oscillation in the predicted MSAFE F10.7 values (blue and green lines). Upon investigation, it was discovered the original NASA MSAFE predictions for F10.7 had been altered to incorrectly account for Earth's variation from the Sun, *an inclusion of a (1/Earth Radius^2) factor.* The Earth's orbit is not perfectly circular, and it was justified to include this small variation in eccentricity when reporting the F10.7 values. In discussion with the original MSAFE model developers, this Earth variation manipulation should not be included, and this information was relayed to the CelesTrak website developer. (F-3) The red line displays the actual daily variations of measured F10.7 up to May 2025, and the unaltered MSAFE predictions of the 50th percentile for the next cycle. This red line data file was included in the FF simulation to correct for both HST and Swift decay predictions.

7.2 Quick Determination of HST and Swift Drag Coefficient

"Virtually every term in the atmospheric drag force equation has a significant uncertainty." (ref. 7)

The previous section described solar activity influence on atmosphere and density modeling as a source of uncertainty, this section will focus on another source of uncertainty in this process.

Recall that the atmospheric drag force equation is a function of the drag coefficient, C_d. Drag force has considerable sources of error and most decay predictions do not provide accurate models of ballistic coefficient (which itself is a kind of fudge factor commonly used to account for a large variety of effects) and is dependent on spacecraft geometry and attitude. Varying spacecraft area and drag coefficient independently (while common) is not desired. The NESC

team first attempted to compute C_d derived from B* in a two-line element (TLE) given its relation to drag force.

TLE's provide the minimum orbital element data necessary to propagate the orbit of a satellite or space object. A single TLE provides a 'snapshot' of an orbiting object's state in time and the orbital elements can be converted into a position and velocity. NORth American Aerospace Defense command (NORAD) tracks thousands of satellites and space debris and makes the TLE data publicly available. TLEs are updated daily sometimes more or less frequently. A single TLE may look like the text below (Figure 7.2-1), with the B* (BSTAR) drag term defined as:

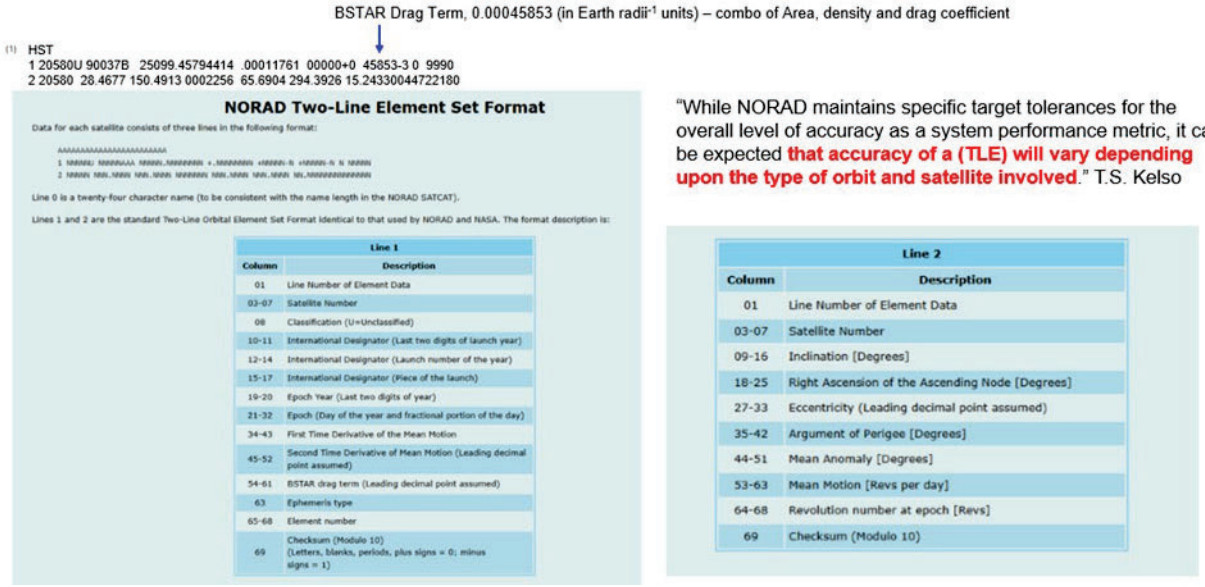

Figure 7.2-1. NORAD TLE Set Descriptions

B* is computed relative to constant atmospheric density ($\rho_0 = 0.15696615$ kg m^2 Re $^{-1}$). Use of B* values from TLEs require care as they are fits to data and only work with a Special General Perturbations 4 (SGP4) propagator used by NORAD. To derive C_d from a TLE is a complex process and may lose accuracy due to the instantaneous measurement from a single TLE. This process requires both the computation of the atmospheric density (ρ) at the TLE epoch (which implies altitude) and use of a scaling factor to reasonably bound density ratio, (ρ/ρ_0). Resulting C_d by this method were 0.3-0.7, which is reasonable for a bullet or rocket, but not HST due to its more complex shape with multiple surfaces. The adopted approach was developed from simple equations for the loss in orbital energy. The deceleration caused by drag on an orbital body is given by:

$$a_{drag} = \frac{1}{2} C_d \rho \frac{A}{m} v^2$$

Equation 2.

where a_{drag} is the deceleration, C_d the drag coefficient, A the spacecraft effective cross-sectional area, m the spacecraft mass and v the vehicle velocity. The total energy of a spacecraft in a circular orbit about Earth is:

$$U = -\frac{GM_e m}{2R}$$

Equation 3.

where GM_e is the geocentric gravitational constant (GM_e = 398600.4 km^3s^{-2}) and R is the radius of the circular orbit. The derivative of the energy with respect to time gives the energy loss due to drag, which can be set equal to the work done by the drag force:

$$\frac{dU}{dt} = \frac{GM_e m}{2R^2} = ma_{drag}\frac{ds}{dt}$$

Equation 4.

where *ds* is the arc length traversed by the satellite in time *dt*. For a circular orbit, this may be replaced by the mean motion, *n*, multiplied by the orbital radius:

$$\frac{ds}{dt} = Rn = \frac{2\pi R}{P} = \sqrt{\frac{GM_e}{R}}$$

Equation 5.

where *P* is the period of the orbit. And so:

$$\frac{dU}{dt} = ma_{drag}\sqrt{\frac{GM_e}{R}}$$

Equation 6.

The above may be used to find the decrease in the orbital radius with time by invoking:

$$\frac{dR}{dt} = \left(\frac{dU}{dR}\right)^{-1}\frac{dU}{dt}$$

Equation 7.

$$\frac{dR}{dt} = 2a_{drag}\sqrt{\frac{R^3}{GM_e}} = \frac{a_{drag}P}{\pi}$$

Equation 8.

Expanding a_{drag} and solving for the drag coefficient yields

$$C_d = -\frac{2\pi m}{A\rho v^2 P}\frac{dR}{dt}$$

Equation 9.

This (*dR*/*dt*) can be obtained from the TLE sets spanning years 2022-2025 (for this case dt is one day as to allow for a reasonable change in the radius of the orbit). The area A was set to be 72.6 m^2 (approximate average area for cylindrical sizes of this proportion) and the mass of HST to 12,246 kg. Density values were obtained from the MSIS atmospheric model used in the FF simulations. Essentially all the uncertainty in the other parameters (Area to Mass, Density, spacecraft velocity) are grouped to get an average C_d in this approach Figure 7.2-2 shows the variation in C_d due to the uncertainties in density and area-to-mass over the various TLE epochs at different altitudes. If the derived C_d value is good, one would not expect to see a variation in the scatter with altitude. Figure 7.2-3 shows the spread in atmospheric density at various altitudes

emphasizing that density is the predominant error source in the drag calculation, affirmed previously in (ref. 19) and recognizing that there have been no significant atmospheric density modeling updates in two decades, and no real improvements in atmosphere models like MSIS and Jacchia Roberts that were useful for reentry predictions (ref. 7). (**O-4**)

Figure 7.2-4 shows the decay of HST's orbital altitude of the computation time span with multiple values for C_d, including the final derived mean value of 1.74. In Figure 7.2-4, FF simulations with higher or lower values for C_d do not completely bound the actual HST decay profile, but a FF simulation with the newly derived C_d completely bounds the actual decay providing confidence of the correct derived value. (**F-1**)

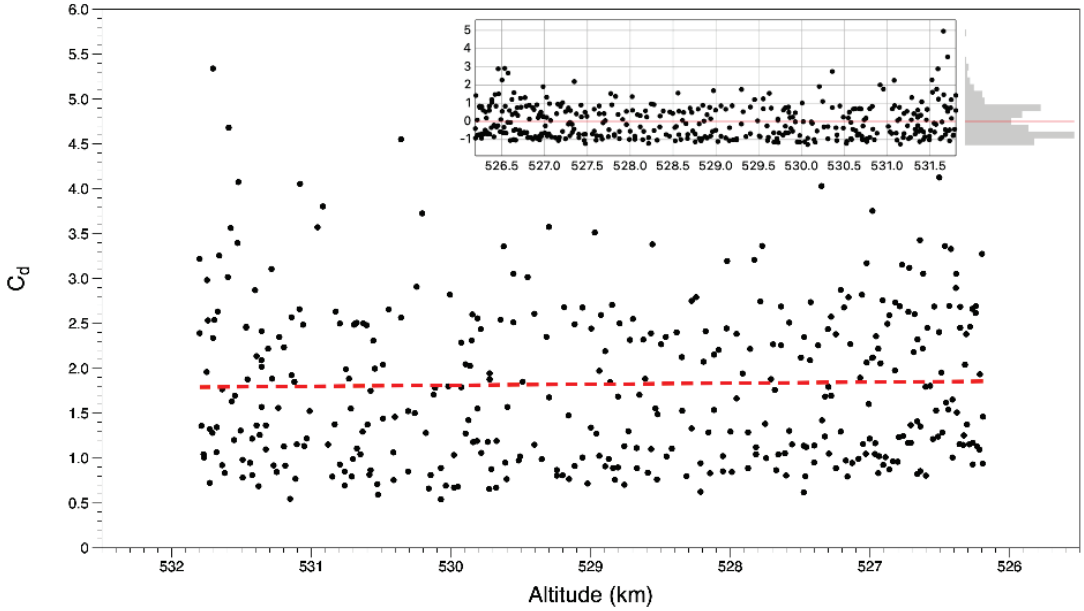

Figure 7.2-2 Scatter Plot of HST TLE Epochs, Varying C_d values Due to Uncertainties

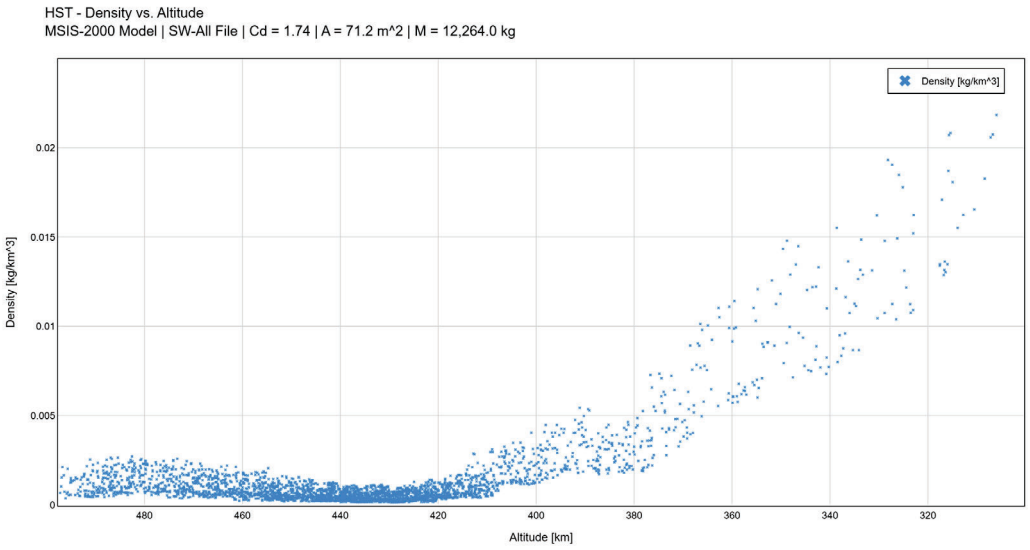

Figure 7.2-3 Scatter of Total Atmospheric Density over Altitude Range

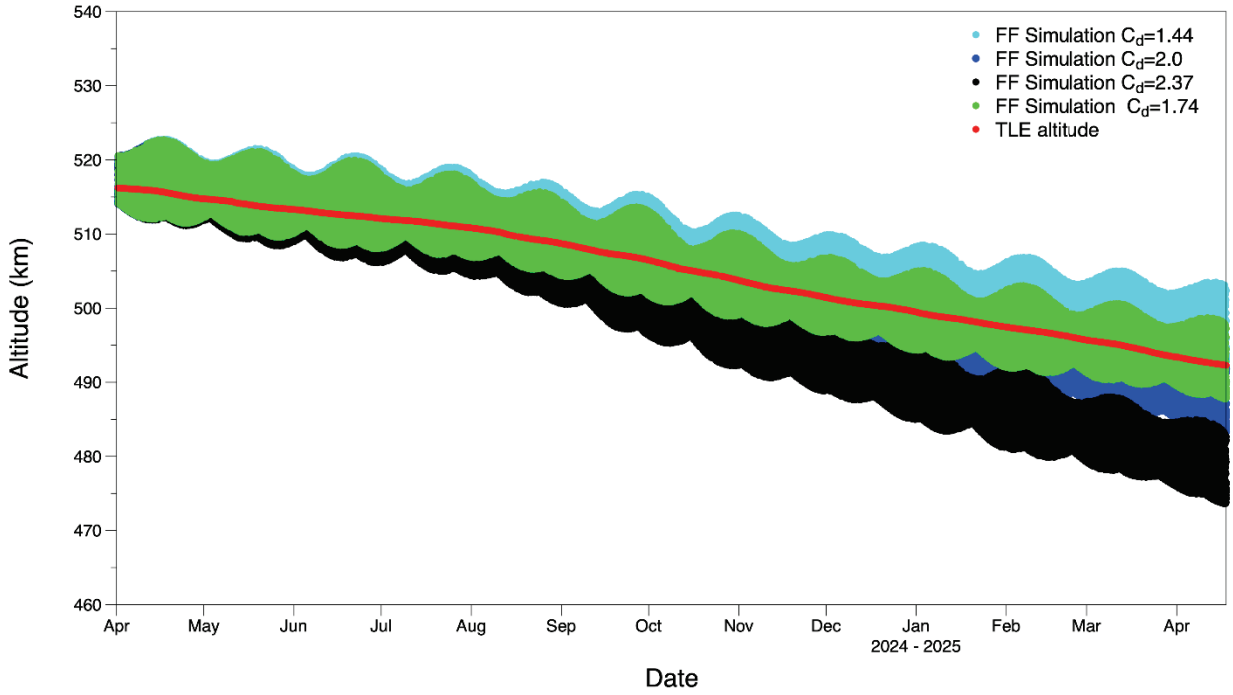

Figure 7.2-4 FF Simulation with Different C_d Values
(green run with derived C_d matches actual decay profile)

7.3 Orbital Decay Simulation

Multiple simulation tools were employed to analyze HST's orbital decay, including propagation methods based on TLE sets and higher-fidelity models. These tools incorporated various atmospheric density models and solar activity forecasts to predict reentry dates.

The NESC team used the FF simulation software produced by AI Solutions. FF is a commercial astrodynamics software package that simulates the flight dynamics for satellite mission design, analysis and operations. It is widely used at NASA in programs such as International Space Station (ISS), James Webb Telescope (JWST), and Lunar Gateway.

Simulation setup included the following assumptions, models, environments and settings:

Force Model Bodies – Sun, Earth, Moon

Solar Radiation Pressure Model (SRP) – spherical

Earth Gravitational Model 96 – 8x8 zonal and tesseral with solid tides

Initializing TLE – Space-Track source, April 09, 2025 10:59:26

Propagator – Bulirsch-Stoer Variation of Parameters (VOP) Integrator with Variable Step Size

HST Dimensions – 13.2 m length, 4.2 m width at base

(2) Solar Panel Dimensions - 7.6 m length, 2.4 m width

HST Mass – 12,246 kg

Decay Altitude cutoff – 100 km (not all runs complete exactly at this altitude due to variable step size). (**O-5**)

Updated space weather file – CelesTrak source, current as of 04/29/2025 with unaltered MSAFE 50th percentile loaded for F10.7 predictions after 04/09/2025

Recent TLEs from Space-Track (NORAD) were used to initialize the state for simulation runs. Typically, the SGP4 propagator is used with a TLE, but the SGP4 propagator does not allow for variations in the drag coefficient or selection of F10.7 values. A numerical propagator suitable for orbital decay studies like Bulirsch-Stoer VOP, was selected. With the adoption of a numerical propagator, FF uses a physics-based model for atmospheric density. In this case, C_d is used to calculate drag force explicitly, and F10.7 is used by atmospheric density models such as MSIS or Jacchia-Roberts to compute density. Together, these allow the simulation to evaluate drag acceleration as part of the numerical integration process. This approach provides higher fidelity and better long-term accuracy. Evaluating the HST trajectory under the influence of a varying physical environment that includes realistic drag forces and solar activity and using a numerical propagator with C_d and F10.7 provides for a better choice over other methods involving SGP4 alone.

To validate the FF simulation and environment settings, the NESC team compared the actual HST decay over the past year for a short-term comparison. The plot below, Figure 7.3-1 (and above, Figure 7.2-4), shows the FF simulation with assumptions bound the actual HST altitude decay as measured by a year of TLE's. Recall, a single TLE is a 'snapshot' of an orbiting object's state in time; any single TLE can have 'noise', so it is best to evaluate multiple TLEs over a time series and is recommended as an exercise for future work. (**O-3**)

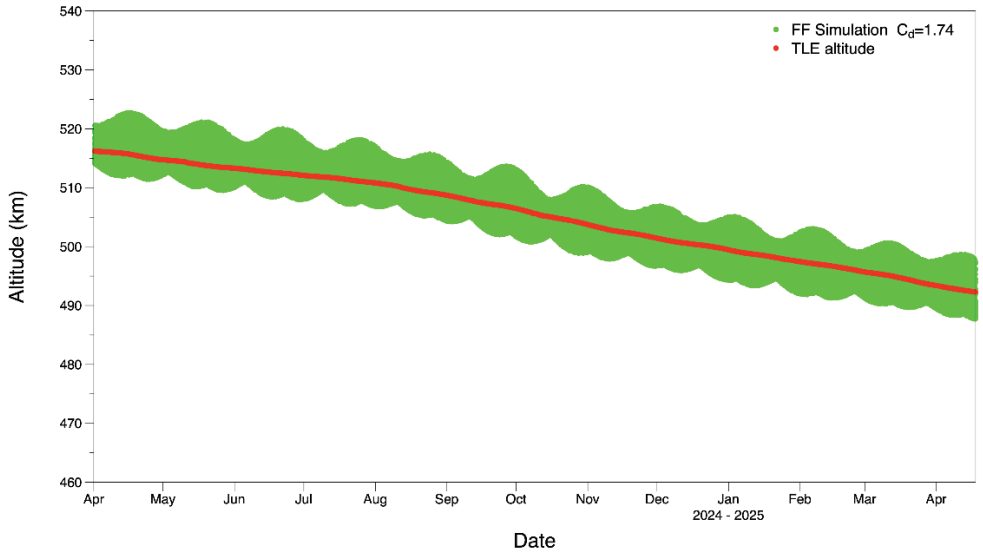

Figure 7.3-1 Simulation is Validated, Bounds the Actual HST Decay

Note the oscillating behavior in the decay plots, which is due to the use of osculating elements in the simulation propagation, and influence of perturbing forces on the HST trajectory. A detailed description of this behavior can be found in General Perturbation theory in most orbital dynamics textbooks. The use of osculating elements captures the true time-varying orbital elements inclusive of all periodic (long and short) and secular effects and represent the high precision trajectory. In contrast, the use of mean elements, which are averaged over some time period, do not account for any short period variations. The red line for TLE altitude drop of HST over time is just altitudes as measured from the TLEs without any propagation.

7.3.1 HST Projected Surface Area

HST is pointing in different directions throughout the year; Reference 19 states HST changed directions 36 times in 1 week, therefore using a time-averaged cross-sectional area as the expected orientation is a good assumption and cited in the Projects Orbital Debris Assessment Report (ODAR). Values for the time-averaged area are approximately 71-74m^2 based on different papers cited above.

To bound the effects of area on the reentry window, cases with a maximum and minimum cross-sectional area, Figure 7.3-2, into the velocity direction were run, along with one other intermediate value.

Worst Case Projected Area – 92.6m^2

Minimum Projected Area - 13.8m^2

Intermediate Projected Area – 55m^2

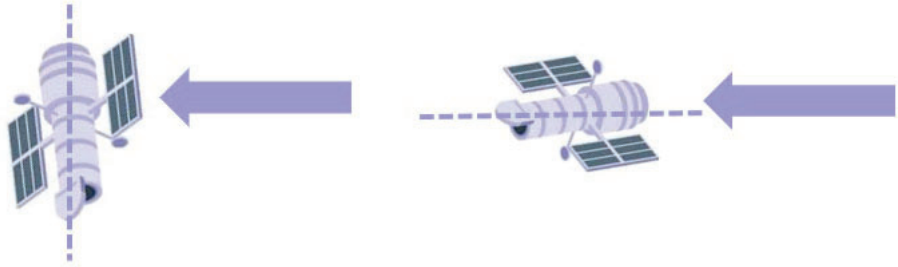

Figure 7.3-2. Hubble Attitude Orientations, Max and Min into Velocity Vector

7.4 HST Decay Prediction Results

"The computation of orbit lifetime is extremely challenging. The abundance of uncertainty makes the results of any one prediction suspect." (ref. 6)

Recall, the difficulty in isolating any one of these variables in the decay equation to apply uncertainties is complex, therefore a run matrix was generated varying areas, drag coefficient values, atmosphere models, TLEs and various interpretations of the solar activity model to produce a range of possible reentry dates. Given the shortened time to produce results, a complete statistical analysis was not possible. Using extreme and average values provides insight into the possible reentry timeframes acknowledging uncertainty exists in every part of this process.

Results for an average cross-sectional area of 71m^2, derived C_d of 1.74, MSIS atmosphere model, and 50th percentile solar activity prediction MSAFE file produces a possible HST reentry in October 2033. (**F-8**)

Assuming a higher projected area which increases drag, shows earlier reentry times as early as Fall of 2030. Using the minimum projected area pushes out that reentry well into the 2050s. Varying drag coefficient to higher values, +1 sigma (derived from the data in Figure 7.2-2), has a stronger effect on drag and reentry leading to a 2026 possibility, while a –1-sigma drag coefficient pushes out the reentry to 2043. Likewise, an extreme solar prediction environment of the 95th percentile produces a 2027 reentry, and a 5th percentile environment produces a 2034 date.

Correcting the MSAFE file in the CelesTrak version, removing the incorrect variation factor due to Earth's eccentricity did not have a big difference in results with variations of only days over this long propagation time. Using a different TLE to initialize the HST also showed little difference in predicted reentry dates. The selection of atmosphere models between Jacchia-Roberts and MSIS did show more significance, but for our analysis the MSIS atmosphere model is believed to be more accurate based on a previous study comparing atmosphere models from the Aerospace Corp.

It is worth noting not all runs terminated exactly at the 100 km altitude. Due to the variable time step associated with the Bulirsch-Stoer propagator, once HST reaches about 200 km, it drops very quickly. The team could have implemented an altitude-based step size change, but a quick comparison showed an impact of just a couple of hours difference in decay. Results are shown in Table 7.4-1 for the parameter combinations evaluated. The (*) for MSAFE files indicate the oscillation of F10.7 due to variations in Earth's eccentricity were removed, and the original MSAFE files were used instead.

Table 7.4-1. HST Run Matrix Results for Various Parameters

Run No.	Solar Weather Pred	Atmosphere	Area (m^2)	Cd	Reentry Date	
1a	Celestrak MSAFE 50%	MSIS	71	2.5	July 07, 2029	
2a	Celestrak MSAFE 50%	MSIS	92	2.5	October 08, 2027	
2ab	Celestrak MSAFE 50%	MSIS	92	1.74	November 08, 2030	
3a	Celestrak MSAFE 50%	MSIS	55	2.5	December 26, 2032	
3ab	Celestrak MSAFE 50%	MSIS	55	1.74	April 14, 2035	
4a	Celestrak MSAFE 50%	MSIS	13.8	2.5	>2050's	
4ab	Celestrak MSAFE 50%	MSIS	13.8	1.74	>2050's	
5a	Celestrak MSAFE 50%	MSIS	74	2.5	February 29, 2029	
6a	Celestrak MSAFE 50%	MSIS	71	1.31	June 15, 2035	25% lwr bd
7a	Celestrak MSAFE 50%	MSIS	71	3.26	September 28, 2027	75% upr bd
8a	Celestrak MSAFE 50%	JR	71	2.5	October 16, 2028	
9a	Celestrak MSAFE 50%	JR	92	2.5	June 11, 2027	
10a	Celestrak MSAFE 50%	JR	55	2.5	August 11, 2031	
11a	Celestrak MSAFE 50%	JR	13.8	2.5	>2050's	
12a	MSAFE 50th (*)	MSIS	71	2.5	July 09, 2029	
13a	MSAFE 50th (*)	MSIS	71	4.19	November 27, 2026	+1 sigma
14a	MSAFE 50th (*)	MSIS	71	0.79	May 01, 2043	-1 sigma
15a	MSAFE 5th (*)	MSIS	71	2.5	January 31, 2034	
16a	MSAFE 95th (*)	MSIS	71	2.5	June 13, 2027	
17a	Celestrak MSAFE 50%	MSIS	71	2.0	April 09, 2031	April 1,2024 TLE
18a	MSAFE 50th (*)	MSIS	71	2.0	May 26, 2030	April 1,2024 TLE
19a	Celestrak MSAFE 50%	MSIS	71	1.74	November 02, 2033	April 9,2025 TLE
19a2	MSAFE 50th (*)	MSIS	71	1.74	October 29, 2033	
20a	Celestrak MSAFE 50%	MSIS	71	1.74	October 02, 2033	April 1,2024 TLE

The major takeaways from this run matrix confirm that extreme area presentations, extreme drag coefficients or extreme environments can dramatically alter the predicted reentry times. (**O-2**)

The NESC simulation results above for the nominal expected environment, area and drag, are within family of the GSFC FDF prediction results. See Figure 7.4-1 below.

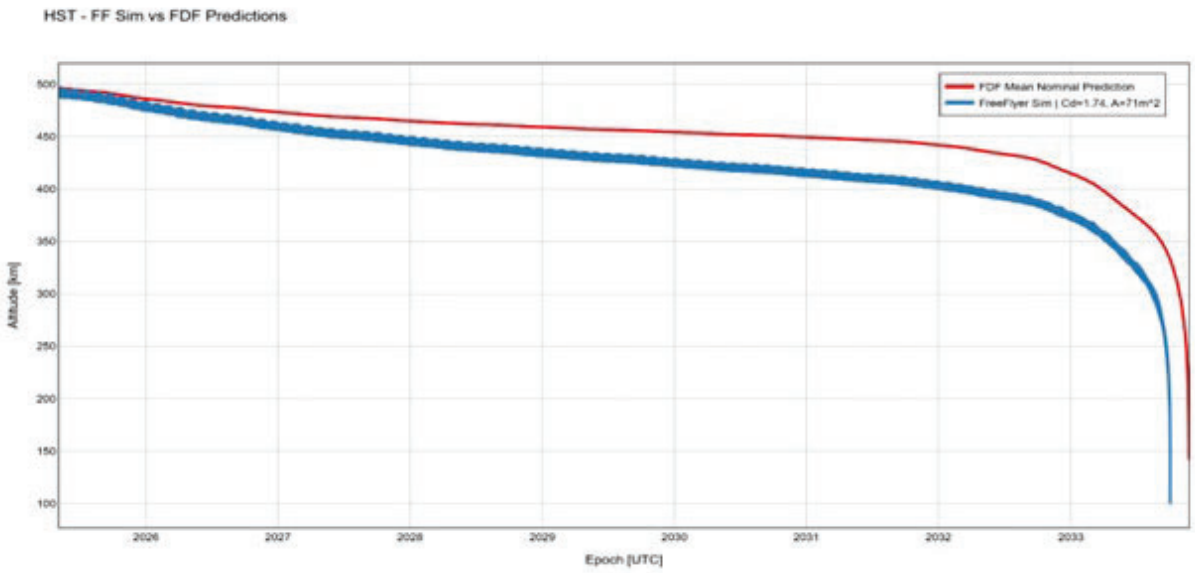

Figure 7.4-1. NESC Prediction Compared to GSFC FDF Prediction

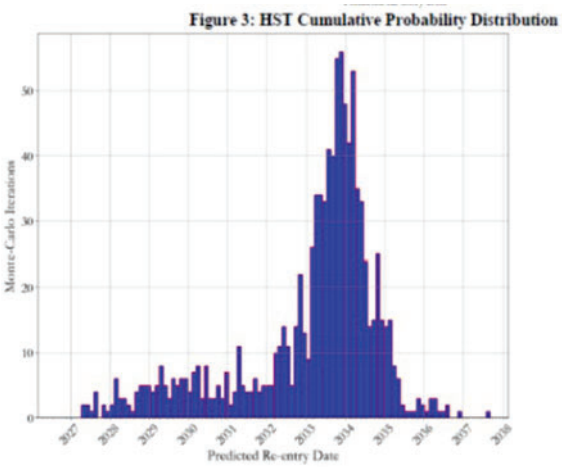

Figure 7.4-2. GSFC FDF Histogram of HST Predictions

The range of NESC results for various parameters are within family of the cumulative probability distribution of possibilities as predicted by GSFC FDF, Figure 7.4-2.

Aerospace Corporation Simulation Results

Additionally, several Aerospace Corporation tools (external and internally developed) were used to do quick assessments with various environment and ballistic coefficient settings. A summary of results is presented below. The average area cases used a cross-sectional area of 72.96 m^2 and the maximum area cases us 92 m^2.

Orbital Element Sets Propagation Methods:

- General Perturbations (TLE) and Improved version called XP
  - Reentry Predictions

        - TLE: 7 April 2032 (does not include varying F10.7, only relies on a fixed value, linear density variation with altitude)
        - XP: 8 September 2033 (includes more perturbations, slightly higher fidelity density model, same fixed F10.7)
- Special Perturbations method (more perturbations, better drag modeling)
    - Reentry Predictions
        - Average Area: September 27, 2031
        - Maximum Area: May 22, 2030

Satellite Orbital Analysis Program (SOAP)

- Numerical integration of equations of motion, (EGM 8x8, SRP, C_d=2.0)
    - Reentry Predictions
        - 03/06/2031 (Average Area, Constant F10.7 = 100, MSIS-2000)
        - 01/15/2027 (Average Area, Constant F10.7=200, MSIS-2000)
        - 11/27/2026 (Maximum Area, Constant F10.7 = 180, MSIS-2000)

AllProp Predictions

- Precision integration tool, (Earth Gravity Model (EGM) 12x12, MSIS-2000, SRP, Sun & Moon gravity, Solid Tides, MSAFE, Average Area)
    - Reentry Predictions
        - 05/19/2030 MSAFE 50th
        - 06/11/27 MSAFE 95th
        - 03/07/2036 MSAFE 5th

Lifetime Predictions (mean element propagation tool developed by Aerospace)

- Used specifically for reentry predictions, similar to STK Lifetime module, (can read internal solar cycle data or MSAFE, EGM 8x8, SRP, C_d=2.0)
    - Reentry Predictions
        - 05/23/2035 (Internal Solar Table 50th, Average Area)
        - 03/04/2037 (MSAFE 50th, Average Area)
        - 10/26/2031 (Internal Solar Table 95th, Average Area)
        - 11/01/2033 (MSAFE 95th, Average Area)
        - 06/29/2034 (Internal Solar Table 50th, Maximum Area)
        - 06/19/2035 (MSAFE 50th, Maximum Area)
        - 04/13/2029 (Internal Solar Table 5th, Maximum Area)
        - 09/08/2032 (MSAFE 50th, Maximum Area)

TRACE (precision integration tool developed by Aerospace)

- Corporate standard for precision orbit propagation (EGM 70x70, MSIS-2000, C_d=2.2, MSAFE, Average Area)
    - Reentry Predictions
        - 11/04/2034 (MSAFE 5th)
        - 03/01/2029 (MSAFE 50th)
        - 03/04/2027 (MSAFE 95th)

The Aerospace analyses assuming variations in ballistic coefficient, constant and extreme environments, with reentry predictions ranging from 2026 to 2037. Ballistic coefficient variations have the greatest effect on reentry predictions. Exceptions include an attitude maintained at a constant orientation relative to the velocity vector, maximum or minimum cross-sectional areas will provide the extremes of the reentry window. Using 5th and 95th solar cycle predictions have the same effect but both extremes with ballistic coefficient (BC) and environments are probably not a reasonable estimate. Early reentry predictions 2029 and earlier were only found for cases where the 95th percentile solar environment or maximum cross-sectional area were used. The overall range of values are also within family of the GSFC FDF results and NESC analysis and show similar trends with extreme environments driving the largest swings.

7.4.1 Historical Scan of Solar Activity and Impacts Against HST Decay

A comprehensive analysis of the HST's orbital decay trends leveraging historical solar cycle data spanning nearly seven decades was conducted. This part of the analysis aimed to understand HST's deorbit behavior against future unknown solar cycle variability, including potential solar activity spikes that could significantly impact the telescope's operational lifetime.

Predicting solar activity and its resulting influence on the Earth's thermosphere presents significant challenges due to the complex nature of solar phenomena and limited measured data available for analysis. To address this challenge, the NESC team developed a historical sweep methodology that evaluated solar cycle activity dating back to October 1, 1957, using monthly TLE epochs propagated forward until orbital decay.

The analysis employed a FF setup with HST's orbital parameters initialized from Space-Track TLE data as of April 24, 2025. The orbit epoch was systematically reset in one-month increments from October 1, 1957 through April 1, 2025 creating a comprehensive dataset spanning multiple complete solar cycles.

7.4.2 Simulation Parameters and Force Modeling

The orbital propagation simulations incorporated detailed spacecraft characteristics derived from HST's End of Mission Plan, SMR-6090 HST End of Mission Plan Rev B. The telescope's drag and solar radiation pressure area was set at 71.2 m², with a drag coefficient of 1.74 and a reflectivity coefficient of 1.5. The spacecraft mass was modeled at 12,264 kg.

The force model employed sophisticated gravitational and environmental factors, including the GGM03C Earth gravity model truncated to 8x8 with 3x3 solid tides, the MSIS-2000 atmospheric density model for drag calculations underpinned by MSAFE 50th percentile predictions, spherical solar radiation pressure modeling, and point mass representations for both the Sun and Moon. The Bulirsch-Stoer integration method was utilized for numerical precision.

During the analysis, a significant technical issue was encountered with the MSIS-2000 atmospheric model. The model, which originates from the Naval Research Laboratory (NRL) and requires the previous day's F10.7 solar flux value to calculate current atmospheric density, experienced computational errors when processing certain out-of-family F10.7 'spikes' that occurred between 2000 and 2011.

These spikes, measured in solar flux units (sfu), reached extreme values including 563.5 sfu on April 6, 2001, 655.6 sfu on December 28, 2001, and 938.6 sfu on March 7, 2011. The MSIS-2000 model's inability to process these anomalous values caused simulation failures for orbits initialized prior to these events and is not an issue with FF itself. (**O-6**) Table 7.4-1 reports all the extreme values that caused errors.

The MSIS model in FF is directly converted from the Fortran code of the original MSIS-2000 model by the NRL. The MSIS model has an issue with computing atmospheric density after those spikes. (**F-2**) AI solutions is aware of the issues and is working toward a patch to handle extreme values. The NRL MSIS-2000 website also produces the same errors if provided the same extreme F10.7 values from the space weather file and produces a "NaN," Figure 7.4-3.

Figure 7.4-3. Screenshot of Website NRL-MSIS Error[8]

To mitigate this limitation, the team implemented a data filtering approach, replacing problematic F10.7 spikes with 3-day average values centered at each peak. This solution allowed the simulations to proceed while maintaining the overall solar activity trends necessary for accurate orbital decay predictions. Table 7.4-1 shows the modified values used in the scan.

[8] NRLMSIS | Instant Run | CCMC

Table 7.4-1. Modified F10.7 Values Replacing Extreme Values

Epoch [UTC]	F10.7 Observed [sfu]	F10.7 Observed 81-Day Avg. [sfu]	F10.7 Observed 3-Day Avg. [sfu]
Apr 06, 2001	563.5	177.2	380.5
Dec 28, 2001	655.6	230.9	398.2
Nov 04, 2003	560.9	144.4	280.6
Sep 09, 2005	707.6	99.2	305.9
Dec 06, 2006	573.4	91.4	266.8
Mar 07, 2011	938.6	115.0	415.9

The comprehensive historical sweep revealed compelling patterns in HST's orbital behavior relative to solar cycle activity. Approximately 97% of all simulation runs resulted in orbital decay within the 25-year analysis window, with propagation halting either when HST's epoch exceeded the last available observed solar cycle data (April 24, 2025) or when elapsed time exceeded 25 years.

The deorbit time analysis showed a clear inverse relationship between solar activity and orbital lifetime. Troughs in deorbit time corresponded directly to peaks in solar activity, demonstrating the significant impact of enhanced solar flux on atmospheric density and subsequent drag forces acting on the spacecraft.

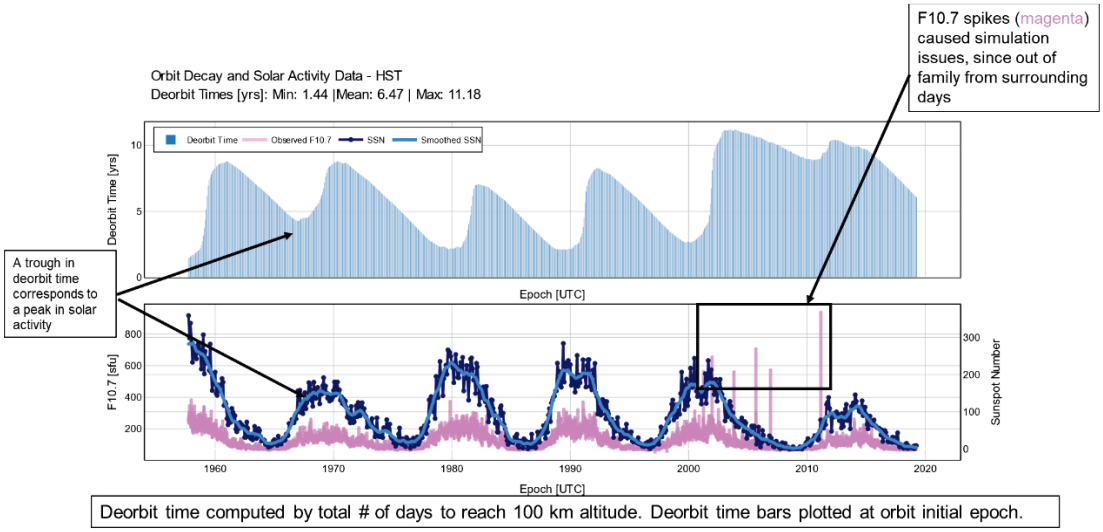

Figure 7.4-4 HST Deorbit Times Using Historical Solar Cycle Scans

Of the runs that met deorbit conditions, approximately 16% resulted in decay within 1-2 years, while 100% of successful runs showed decay within approximately 9.5 years. This distribution provides valuable insight into the range of possible scenarios HST might encounter based on historical solar activity patterns.

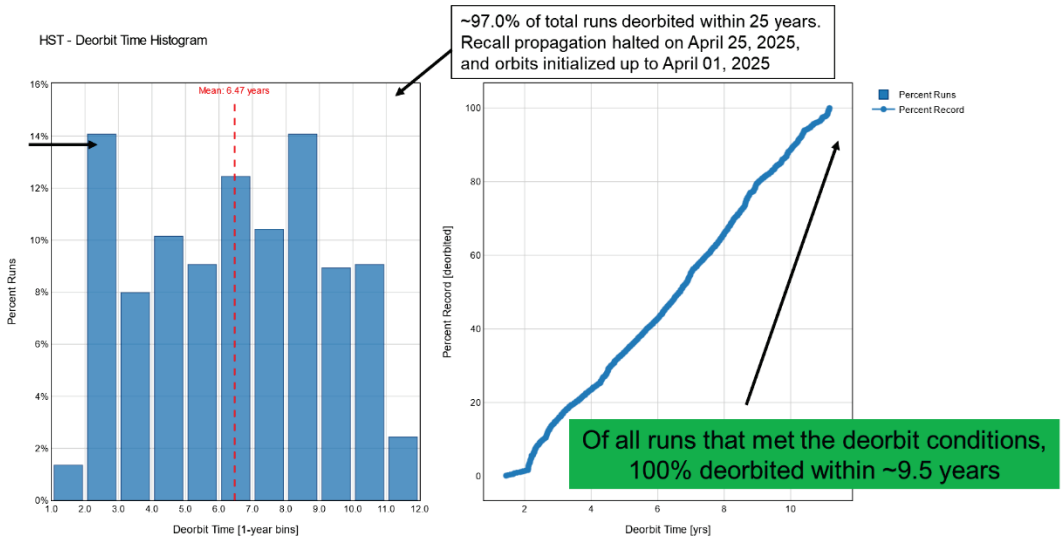

Figure 7.4-5. Histogram of Deorbit Times Against Historical Solar Activity

The team analyzed deorbit times across different solar cycles and activity phases, categorizing results by solar maxima and minima periods. Historical solar cycles from 19 through 25 were examined, with average deorbit times ranging from 4.329 years (Solar Cycle 21) to 8.936 years (Solar Cycle 24), Table 7.4-2.

Notably, orbits initialized during solar maxima showed an average deorbit time of 6.059 years, while those during solar minima averaged 6.815 years. This difference highlights the extended operational lifetime possible during periods of reduced solar activity.

Table 7.4-2. Deorbit Times by Solar Maxima/Minima and Cycle

Solar Cycle	Start	End	Maxima Start	Maxima End	Avg. Deorbit Time [years]
19	2/1/1954	10/31/1964	1/1/1957	12/31/1960	6.496
20	11/1/1964	6/30/1976	1/1/1967	12/31/1971	6.302
21	7/1/1976	9/30/1986	1/1/1978	12/31/1982	4.329
22	10/1/1986	5/31/1996	1/1/1988	12/31/1992	5.031
23	6/1/1996	12/31/2008	1/1/1999	12/31/2003	7.428
24	1/1/2009	12/31/2019	1/1/2012	12/31/2016	8.936
25	1/1/2020	---	1/1/2023	---	---

*Current cycle 25, is more like cycle 23, than 24 with regard to magnitude of the peak.

Solar Maxima/Minima	Avg. Deorbit Time [years]
Maxima	6.059
Minima	6.815

The analysis revealed that the current Solar Cycle 25 exhibits characteristics more similar to Cycle 23 than Cycle 24 in terms of peak magnitude, Figure 7.4-5. **As HST currently transitions from solar maxima toward minima, historical data suggests the deorbit timeline could extend as the solar minimum phase is entered. Recall the initial question as motive for conducting the study, would HST's decay trend continue on its current path or extend out?**

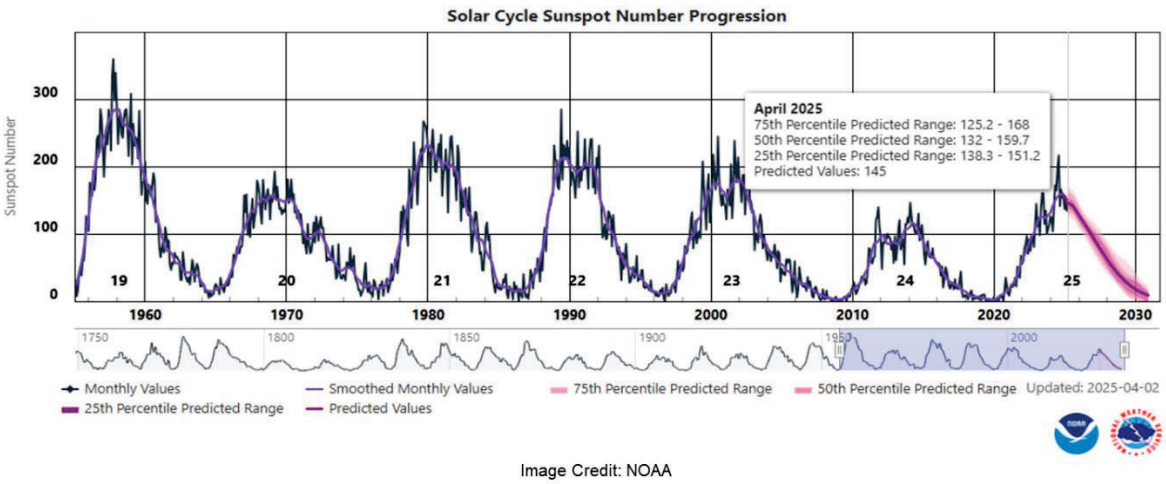

Figure 7.4-5. Historical Solar Activity with Future Predicted Behavior (in pink)

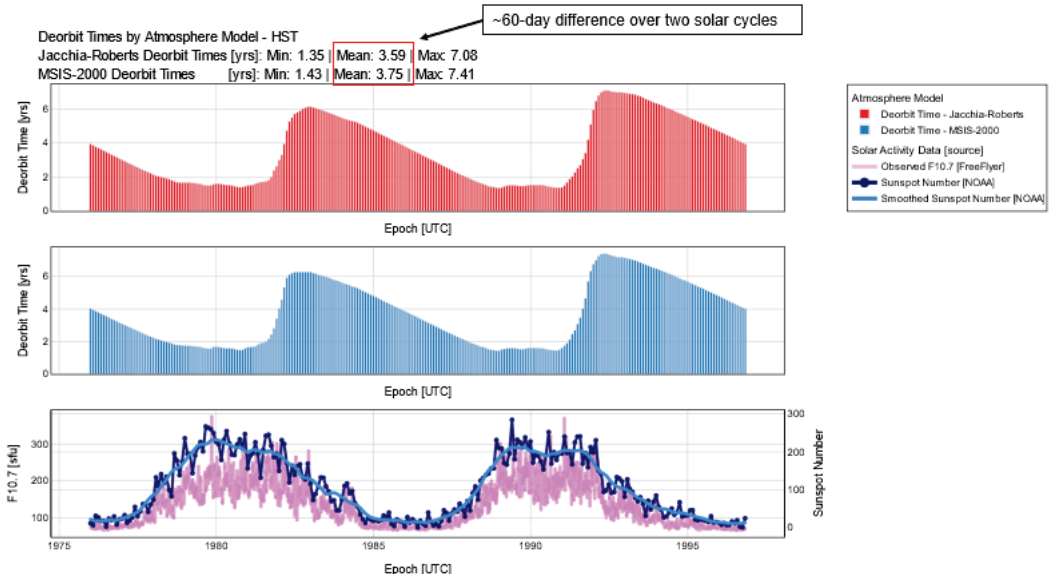

Figure 7.4-6. HST Decay - JR vs MSIS Over Two Solar Cycles

A comparative analysis between the JR and MSIS atmospheric models over two solar cycles showed approximately a 60-day difference in predicted orbital decay times, Figure 7.4-6. This comparison validates the robustness of the MSIS-2000 approach while acknowledging inherent uncertainties in atmospheric modeling.

The historical solar cycle sweep provides insights into HST's potential orbital behavior under various solar activity scenarios. The clear correlation between solar cycle phases and orbital decay times demonstrates that if HST experiences solar activity patterns similar to historical cycles, deorbit times will vary significantly based on the specific solar conditions encountered.

The study confirms that solar cycle variability has a profound effect on spacecraft orbital lifetime, with implications extending beyond HST to other low Earth orbit missions. The methodology developed through this analysis provides a framework for assessing orbital decay risks for current assets operating in similar orbital regimes.

7.5 Reentry Footprint Predictions and Debris Risk

The NASA-STD-8719.14C Process for Limiting Orbital Debris specifies how to show compliance to the requirement that the risk of human casualty from surviving debris shall be less than 0.0001 (1:10,000) for uncontrolled reentry:

- Use DAS (Debris Assessment Software) or ORSAT (Object Reentry Survival Analysis Tool)
- Calculate total debris casualty area (DCA represented by D_A) using Eq. 10 or Eq. 11 (Opiela-Matney)
  - where N is the number of objects that survive reentry at > 15 Joules, and A_i is the average cross-sectional area of each individual surviving piece.
- Calculate human casualty expectation using Eq. 12.
  - where D_A is equal to the total debris casualty area and P_D is equal to the total average population density for the particular orbit.
- E < 0.0001 (1:10,000) for compliance

$$D_A = \sum_{i=1}^{N} \left(0.6\ m + \sqrt{A_i}\right)^2$$

Equation 10.

$$\begin{aligned} &Casualty\ Area\ = \\ &\quad Area\ of\ "Person\ Circle"\ [0.28\ \mathrm{m}^2] \\ &\quad + Area\ of\ Debris \\ &\quad + Perimeter\ of\ Debris\ \times \\ &\quad\ Radius\ of\ "Person\ Circle"\ [0.3\ \mathrm{m}] \end{aligned}$$

Equation 11.

$$E = D_A * P_D$$

Equation 12.

The HST orbital decay and subsequent debris footprint and reentry risk can be studied separately. Two independent methods for modeling the breakup during reentry and associated debris footprint are presented below.

7.5.1 Debris Risk Assessment and Mitigation Analysis (DRAMA)

The European Space Agency (ESA) maintains the Debris Risk Assessment and Mitigation Analysis (DRAMA) software suite, which is a comprehensive set of tools used for compliance analysis of space missions mitigating space debris standards. The tool suite uses a module called Spacecraft Entry Survival Analysis Module (SESAM) to determine the fragments of a satellite that would survive atmospheric reentry, and another module called Spacecraft Entry Risk Analysis Module (SERAM) to compute the on-ground risk of human casualty. DRAMA is a lower fidelity set of tools as compared to the higher fidelity tool suite managed by ESA such as SCARAB or NASA's Orbital Degree Engineering Model (ORDEM). (**O-8**) The advantage of

DRAMA is it is often used as a first quick assessment. For calculation of the HST reentry, a simple geometric model of a cylinder and flat plate solar panels were developed, where the cylinder is a compartment containing geometric objects like spheres, cylinders, boxes and plates characterized by their measure, mass and material properties. The models used for this analysis were found on NASA's public website for the Hubble Project[9]. Typically, it is assumed for object-oriented tools like SESAM that simple objects are released from the compartment (cylindrical body) at certain altitudes. SESAM uses an approach described by the figure in Figure 7.5-1.

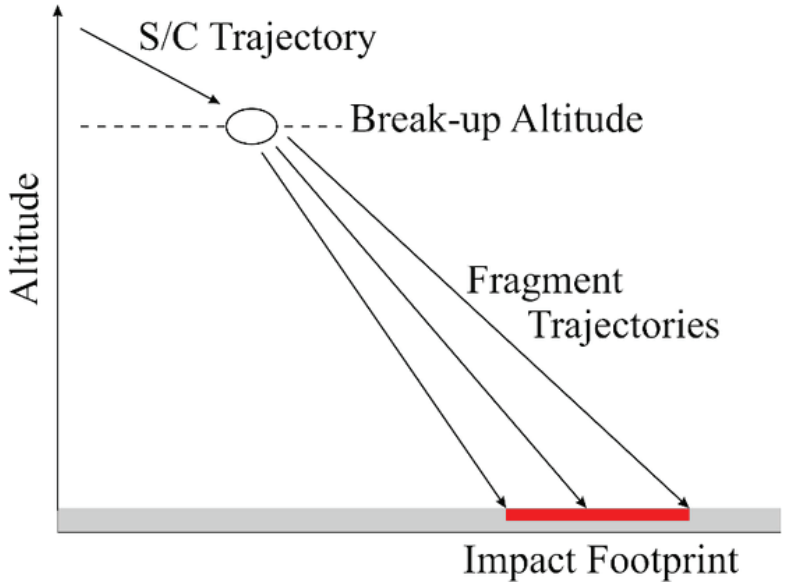

Figure 7.5-1. DRAMA/SESAM Simplified Modeling Approach[10]

7.5.1.1 ESA DRAMA Tool for HST Reentry/Footprint Analysis

An early study used NASA's ORSAT to evaluate the HST demise and resulting impacts to human casualty risks. Here, ESA's open-sourced DRAMA suite was used to compute the reentry trajectory and survivability of spacecraft components. Appendix A and B have the details of the modeling, analysis and results of this independent assessment and are summarized here.

HST's TLE-derived state was initialized well above the atmospheric interface and the reentry trajectory is propagated down to the reentry boundary accounting for long-term orbital decay under atmospheric drag, solar activity and geomagnetic conditions using space weather forecasts and empirical density models provided by ESA. Once HST descends below 150 km, the simulation transitions to the beginning of the aerothermal reentry phase, during which detailed modeling of fragmentation, thermal loads and ground impact risk is performed.

HST is modeled as a composite structure comprising a cylindrical main body with attached solar panels, four magnetic torquers; the main body houses both the payload and the satellite bus subsystems (see Figure 7.5-2).

[9] About Hubble - NASA Science

[10] https://www.htg-gmbh.com/en/htg-gmbh/software/dramasesam/

Sources for the main body geometry and dimensions are publicly available from the NASA HST website, About Hubble - NASA Science.

The analysis assumes the main body demises at approximately 78 km altitude, triggering release of all internal subcomponents (referred to as children).

The breakup altitude reflects dynamic pressure and thermal stress thresholds typically observed in reentry events, consistent with empirical studies from the Aerospace Corporation and modeling assumptions in Reference 3.

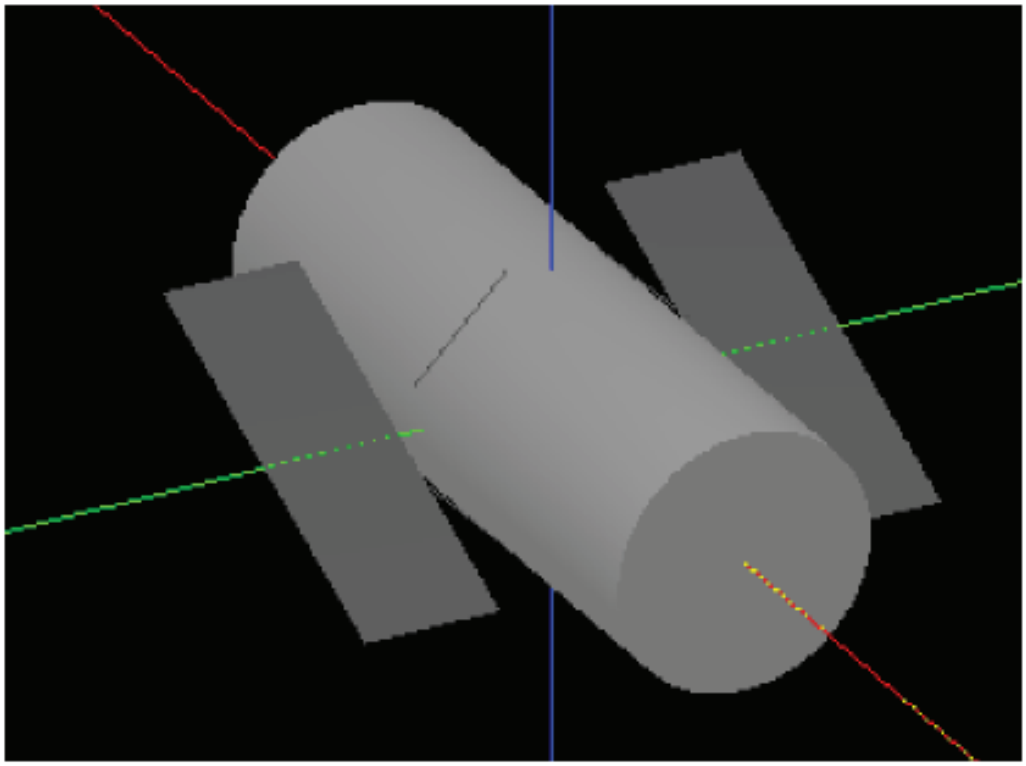

Figure 7.5-2. DRAMA Assembly View of the Hubble Space Telescope

Each geometry will start to lose mass when the average temperature of the body reaches melting temperature (derivations included in the Appendix A).

The main body shields the internal components until it demises or reaches the predefined breakup altitude of 78 km, at which point all children are released at a nominal temperature of 300 Kelvin.

The children at the release are:

- two battery casings (which house 3 battery cells each),
- the two Low Gain Antennas (LGAs), and
- the four Reaction Wheels.

The internal power subsystem is modeled via the battery casing and battery cells. The Attitude and Orbit Control Subsystem (AOCS) is represented by the four magnetorquers and reaction wheels and the communication subsystem is represented by the two LGAs mounted on the bus.

Table 7.5-1 Each Object Mass, Geometry and Material
Children of the Main Body are grouped below it (excluding Magnetic Torquers and Solar Panels)

Name	Quantity	Geometry	Dimensions	Mass [kg]	Material
– Magnetic Torquers –					
TLx MagneticTroquer	1	Cylinder	Radius: 0.066 m, Height: 2.489 m	43.00	drama-Iron
TRx MagneticTroquer	1	Cylinder	Radius: 0.066 m, Height: 2.489 m	43.00	drama-Iron
BLx MagneticTroquer	1	Cylinder	Radius: 0.066 m, Height: 2.489 m	43.00	drama-Iron
BRx MagneticTroquer	1	Cylinder	Radius: 0.066 m, Height: 2.489 m	43.00	drama-Iron
– Solar Panels –					
Rx Solar Panels	1	Box	Width: 2.44 m, Height: 0.01 m, Length: 7.54 m	27.60	drama-SolarPanel-Mat
Lx Solar Panels	1	Box	Width: 2.44 m, Height: 0.01 m, Length: 7.54 m	27.60	drama-SolarPanel-Mat
Aperture Door	1	Box	Width: 3.099 m, Height: 0.038 m, Length: 3.099 m	41.78	drama-AA7075
Main Body	1	Cylinder	Radius: 2.3 m, Height: 13.0 m	1243.15	drama-AA7075
Battery Enclosure	2	Box	Width: 0.914 m, Height: 0.808 m, Length: 0.363 m	49.24	drama-AA7075
Battery-Cells	69	Cylinder	Radius: 0.09 m, Height: 0.236 m	2.34	drama-Inconel718
Primary Mirror	1	Box	Width: 2.195 m, Height: 2.195 m, Length: 0.33 m	1005.16	drama-FusedSilicaProxy
Secondary Mirror	1	Cylinder	Radius: 0.322 m, Height: 0.058 m	12.80	drama-ZerodurProxy
RWA Housing	2	Cylinder	Radius: 0.301 m, Height: 0.527 m	46.72	drama-AA7075
ReactionWheels	2	Cylinder	Radius: 0.24 m, Height: 0.254 m	20.05	drama-A316
Low Gain Antenna Fwd	1	Box	Width: 0.113 m, Height: 0.059 m, Length: 5.224 m	9.89	drama-AA7075
Low Gain Antenna Shield	1	Box	Width: 0.113 m, Height: 0.059 m, Length: 7.812 m	14.79	drama-AA7075
Main Ring	1	Cylinder	Radius: 1.5 m, Height: 0.381 m	449.06	drama-TiAl6v4
Antenna Ballast Block	4	Box	Width: 0.203 m, Height: 0.027 m, Length: 0.041 m	3.68	drama-Tungsten
Axial Fittings	1	Box	Width: 0.146 m, Height: 0.228 m, Length: 0.715 m	23.10	drama-A316
Base Disk	1	Box	Width: 0.07 m, Height: 0.04 m, Length: 0.07 m	1.92	drama-Molybdenum
Bracket Assy	1	Box	Width: 0.357 m, Height: 0.036 m, Length: 0.5 m	6.80	drama-TiAl6v4
Mast Base	1	Cylinder	Radius: 0.089 m, Height: 0.276 m	5.90	drama-TiAl6v4
Opt. Bench Struct.	1	Box	Width: 0.305 m, Height: 0.016 m, Length: 0.381 m	6.10	drama-Invar

Assuming an uncontrolled, circular orbital decay trajectory, the demise altitude triggers the release of child objects. Fragments are classified as uncritical once their impact kinetic energy falls below the 15J casualty threshold. The NESC team used three different population growth scenarios: Low-Variant, Medium-Variant, and High-Variant, and additional fidelity runs were made with the Medium-Variant option for random tumbling (Appendix B).

To compute casualty risk, a one-dimensional (1D) latitude-based population model was used. By assuming a uniform distribution of population along latitude bands, the model captures the dominant effect of the satellite's orbital inclination on the potential impact zones. This approach is useful for general risk estimates when detailed targeting information is not available.

Due to uncertainties in the reentry orientation, three configurations of HST were analyzed:

- Maximum drag orientation – HST aligned to widest cross-section in direction of motion
- Minimal drag orientation – HST aligned with smallest cross-section (tube aligned with direction of motion)
- Random tumbling state

Released subcomponents (children) were assumed to enter a random tumbling state upon separation.

Maximum Drag Results:

Total Number of Fragments = 11

Total Impact Mass = 1068.1 kg

Total Casualty Area = 17.22 m^2

Total Casualty Probability (1D) for different population variant:

Low Variant = 3.82e-4

Medium Variant = 3.80e-4

High Variant = 3.84e-4

Select Surviving Fragments and Associated Risk:

Primary Mirror = 828 kg, average casualty area = 4.69 m^2, casualty probability = 1.04e-4, max downrange = 13,480 km

Reaction Wheels (4 units) = 45 kg total, average casualty area = 1.8 m^2, casualty probability = 3.97e-5, max downrange = 13,122 km

Battery Cells (6 units) = 10.02 kg total, average casualty area = 0.89 m^2, casualty probability = 1.96e-5, max downrange = 13,297 km

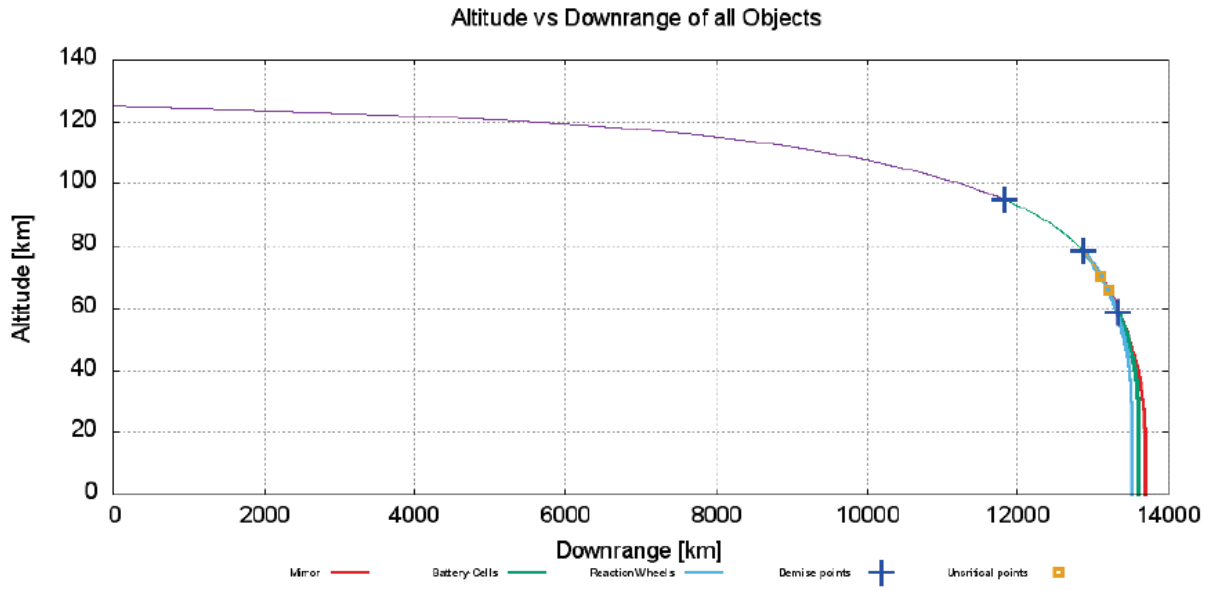

Figure 7.5-3. Altitude vs Downrange Distance for Main Body During Reentry The steep descent profile reflects the high drag configuration of the satellite.

Minimum Drag Results:

Total Number of Fragments = 11

Total Impact Mass = 1052.4 kg

Total Casualty Area = 17.22 m^2

Total Casualty Probability (1D) for different population variant:

Low Variant = 3.98e-4

Medium Variant = 3.94e-4

High Variant = 4.02e-4

Surviving Fragments and Associated Risk:

Primary Mirror = 828kg, average casualty area = 4.69 m^2, casualty probability = 1.07e-4, max downrange = 22188 km

Reaction Wheels (4 units) = 45 kg total, average casualty area = 1.8 m^2, casualty probability = 4.11e-5, max downrange = 21,782.9 km

Battery Cells (6 units) = 7.4 kg total, average casualty area = 0.89 m^2, casualty probability = 2.03e-5, max downrange = 21,974.1 km

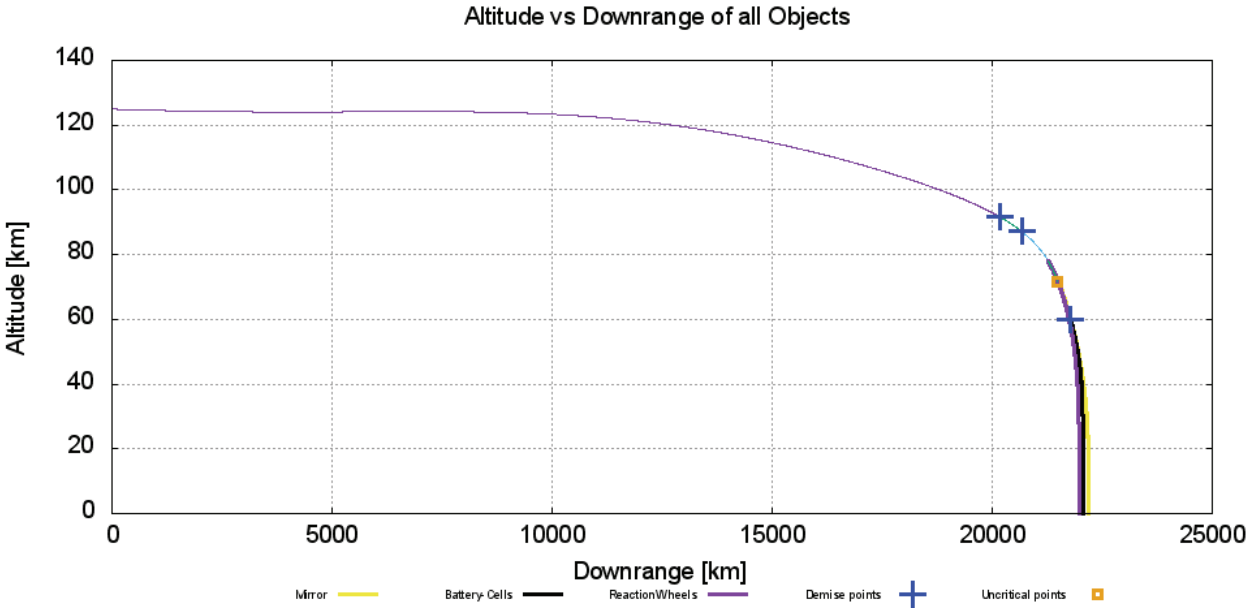

Figure 7.5-4. Altitude vs Downrange Distance for Minimum Drag Case
The shallower entry angle results in a longer flight path through the upper atmosphere.

Higher Fidelity Random Tumbling Results (Appendix B):

Total Impact Mass = 2083.27 kg

Total Casualty Area = 120.4 m^2

Total Casualty Probability (1D projection):

Medium Variant = 2.71e-3

Table 7.5-2 Summary of HST Fragment Impact Parameters

Object Name	Qty	Material	Downrange (km)	Debr. Cas. Area (m^2)	Impact Mass (kg)	Impact Energy (J)
TLx_MagneticTroquer	1	drama-Iron	16614.259	1.2425	38.78	103818.54
TRx_MagneticTroquer	1	drama-Iron	16614.259	1.2425	38.78	103818.54
BLx_MagneticTroquer	1	drama-Iron	16614.259	1.2425	38.78	104212.92
BRx_MagneticTroquer	1	drama-Iron	16614.259	1.2425	38.78	104212.92
Antenna_Ballast_block	4	drama-Tungsten	16810.628	0.4711	3.68	35650.19
Primary_Mirror	1	drama-FusedSilicaProxy	16740.570	5.6175	1005.16	6152355.25
Secondary_Mirror	1	drama-ZerodurProxy	16471.181	1.0783	12.80	15736.81
Axial_Fittings	1	drama-A316	16611.963	0.9756	23.10	64037.47
Base_Disk	1	drama-Molybdenum	16709.401	0.4522	0.76	1996.84
Mast_Base	1	drama-TiAl6v4	16566.835	0.6821	5.90	12700.34
Bracket_Assy	1	drama-TiAl6v4	16462.936	0.8529	6.80	7869.80
Opt._Bench_Struct.	1	drama-Invar	16532.022	0.7262	6.10	10561.09
Main_Ring	1	drama-TiAl6v4	16543.530	7.3183	449.06	842213.94
Battery-Cells	138	drama-Inconel718	16553.207	0.6637	2.34	2154.58
ReactionWheels	4	drama-A316	16619.309	1.0641	20.05	39813.86

The region of potential impact is geographically constrained between latitudes +/- 28.5º which correspond to HST's inclination.

A Monte Carlo simulation was conducted under a controlled re-entry scenario, randomly perturbing the true anomaly at the start of the simulation within a range +/- 1º, generating 50 distinct trajectories.

The resulting spread in the ground tracks revealed a broad range of potential impact locations with longitudes spanning from -172.26º to 175.69º and latitudes constrained to HST's inclination band of +/- 28.5º. Differences in impact regions led to variations in estimated casualty risk. Two methods for computing casualty risk were used and defined in ESA's risk model. The 2D method more accurately captures the influence of regional demographics and is summarized as:

2D Casualty Probability:

Minimum = 0.0

Maximum = 4.59e-2

Mean = 2.55e-3

Standard Deviation 7.83e-3

The accepted upper limit for casualty probability is 1e-4 (1:10,000). The results of this analysis indicated that multiple trajectories, specifically those leading to landfall over densely populated areas, exceed this threshold. The highest risk scenarios involve trajectories over India or Southeast Asia. (**F-9**)

7.5.2 Reentry Predictions using Marshall Aerospace VEhicle Representation In C (MAVERIC)

Two primary functions for this analysis were performed. First, an updated calculation of the uncontrolled reentry casualty risk of HST was conducted to assess compliance with NASA-STD-8719.14C. Second, an HST reentry footprint was created using MAVERIC, the 6DOF simulation tool used to assess controlled reentry of the Space Launch System (SLS). Details of both functions are provided in this section.

7.5.2.1 Updated Risk Analysis

Determining the risk of an uncontrolled HST reentry has been studied previously. Smith et al. assessed HST reentry in 2005 using ORSAT version 5.8. Reference 3 modeled approximately 75% of pre-SM4 HST mass using more than 600 different types of objects, which totaled more than 2000 modeled objects when considering multiples of the same type. The 25% mass that was not modeled included primarily wire harnesses and cabling. Using ORSAT, Smith et al. tracked the more than 2000 modeled HST components throughout reentry, applying models for heating and ablation to determine at what altitude objects would likely liberate from the main HST body, and which components would survive the atmospheric heating to impact the ground. Smith et al. found that 221 objects accounting for 2055 kg of the total HST mass (17%) was predicted to survive to impact and would contribute to the casualty risk. Using their surviving debris list and population estimates, Smith et al. calculated the risk of human casualty from the years 2011 to 2025 in accordance with NASA-STD-8719.14. The process dictated by the standard is:

– Calculate total debris casualty area (DCA, D_A). Smith et al. used Eq. 13, where N is the number of objects that survive reentry with more than 15 J of energy, and A_i is the average cross-sectional area of each individual surviving piece.

$$D_A = \sum_{i=1}^{N} \left(0.6\, m + \sqrt{A_i}\right)^2$$

Equation 13.

– Calculate human casualty expectation using Eq. 14, where D_A is equal to the total debris casualty area and P_D is equal to the total average population density for the particular orbit.

$$E = D_A * P_D$$

Equation 14.

E must be less than 0.0001 (1:10,000) for compliance with the uncontrolled reentry standard, NASA-STD-8719.14 Req. 4.7-1.

To determine the population density term P_D in Eq. 14, Smith et al. used the global population function described in Opiela and Matney 2003. Opiela and Matney's population model predicts global population density as a function of latitude by combining the population distribution and annual predicted growth of each country in the world. The data for Opiela and Matney's country-level population distributions came from the Gridded Population of the World, Version 2 (GPWv2) database, released in 1995, and the annual growth predictions came from the U.S. Census Bureau's International Programs Center International Data Base (IDB), released in 1998.

Using the debris list they had previously generated, Smith et al. computed a D_A of 146 m^2 using 75% of the modeled HST mass, which in conjunction with the Opiela and Matney population model led to an estimated risk of human casualty of 1:340 for a reentry in 2021. After adjusting for the 25% unmodeled mass, the DCA was 199 m^2, and the estimated risk of human casualty was 1:250. Both of these E values significantly violate the 1:10,000 requirement. Figure 7.6-5 shows the risk computed by Smith et al. for reentries between 2011 and 2025.

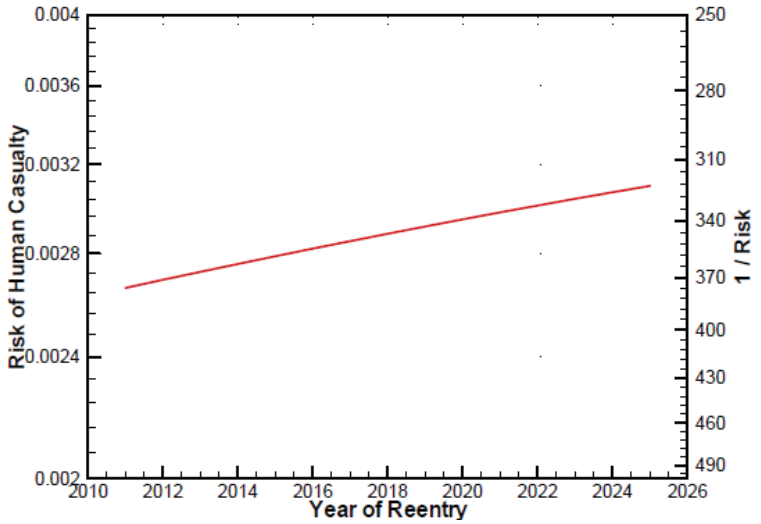

Figure 7.5-5. Risk vs. Year of Reentry Predicted by Smith et al.

Smith et al. performed a robust and detailed analysis in 2004, and much of the original data and analysis still applies today. There are, however, a few configuration changes to HST made as part of servicing missions that occurred after the time of the original analysis. Smith et al. included debris from the Wide Field Planetary Camera 2 (WFPC-II), which was superseded by the Wide Field Camera 3 (WFC3) as part of the 2009 SM4 and added 124 kg of mass to HST. The Corrective Optics Space Telescope Axial Replacement (COSTAR) optical instrument was also included in the 2004 study, which was replaced by the 94 kg heavier Cosmic Origins Spectrograph (COS) as part of the same servicing mission. Additionally, SM4 added a 110 kg Soft Capture Mechanism to HST to enable potential future missions that would require mating HST to another spacecraft, such as a controlled reentry mission. These and other small changes to HST since the 2004 analysis result in approximately 400 kg additional mass that is not included in the original Smith et al. analysis and change some of the debris expected to impact in the case of uncontrolled reentry.

To model these mass and component changes at the level of detail used in Smith et al., additional time and software capabilities would be required. For the purposes of this quick turnaround study, the high-fidelity data used by Smith et al. were adjusted to approximate the properties of the updated HST hardware. The DCA of WFC3 was computed from WFPC-II data by linearly scaling the existing WFPC-II values proportionally to the increased WFC3 mass; the same mass-scaling was applied to COS using COSTAR data. The Soft Capture Mechanism was modeled based on the HST Main Ring and was also mass-scaled to the appropriate value.

This updated analysis also included methodological updates for the DCA calculation compared to the Smith et al. 2004 analysis and leverages the latest available data and models for global population. In 2019, NASA ODPO released a new, more accurate DCA model (Ostrom 2019), which was shown to improve DCA estimates compared to the Opiela-Matney formulation proposed in 2003 while also simplifying the calculation. As in Eq. 13, N is the number of objects that survive reentry with more than 15 J of energy and A_i is the average cross-sectional area of each debris piece:

$$D_A = \sum_{i=1}^{N} \left(0.278\, m^2 + A_i + 1.39\, m * \sqrt{A_i}\right)$$

Equation 15.

The updated model predicts lower DCA values for debris fragments with a small area, compared to the 2003 model, and slightly higher DCA for larger debris pieces. Because much of the HST debris predicted to impact is small, the updated formulation results in a lower overall predicted DCA. Figure 7.5-6 provides a demonstration of this effect by directly comparing the DCA predicted by each method for several selected HST debris pieces.

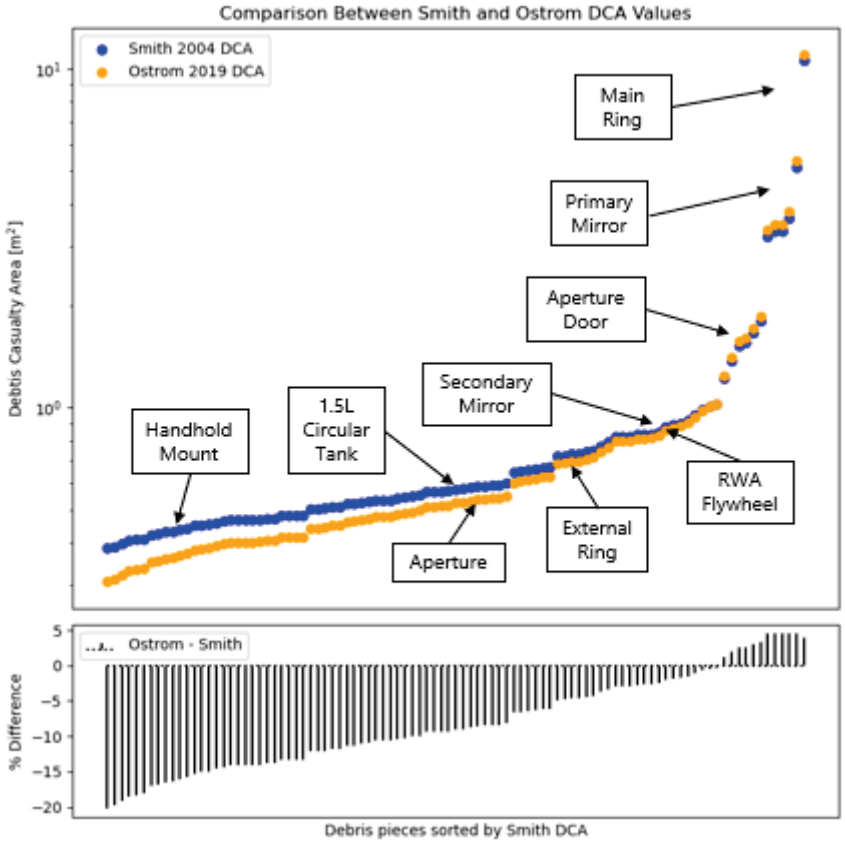

Figure 7.5-6. DCA Comparison for Selected Debris Between Opiela-Matney 2003 (blue) and Ostrom 2019 (orange)

Updated population data and population growth estimates are also available now compared to what was available to Smith et al. in 2004, and the faster-than-predicted population growth that has occurred over the past two decades has increased the probability of a casualty during reentry. Gridded Population of the World (GPW) data, which was on version 2 at the time of Smith et al., is now on version 4 revision 11 as of July 2021. GPWv4 includes updated population census data compared to the previous versions. The IDB growth projections have also been updated since the time of Smith et al., and the latest growth data is included in the updated analysis. Updating the population and growth estimates to the latest data leads to a significant difference from Smith et al.; for instance, the actual 2020 population data was approximately 10% higher than the projections made in 2005.

Figure 7.6-7 shows the updated 2020-2040 population density as a function of orbital inclination using the latest GPWv4 and IDB data. Total population projection was used to scale the density profile through 2040, which results in approximately a 17% population increase from 2020 to 2040. Figure 7.6-7 also provides the 2020 and 2040 population density specific values for the HST orbit (approximately 28.5 degree inclination).

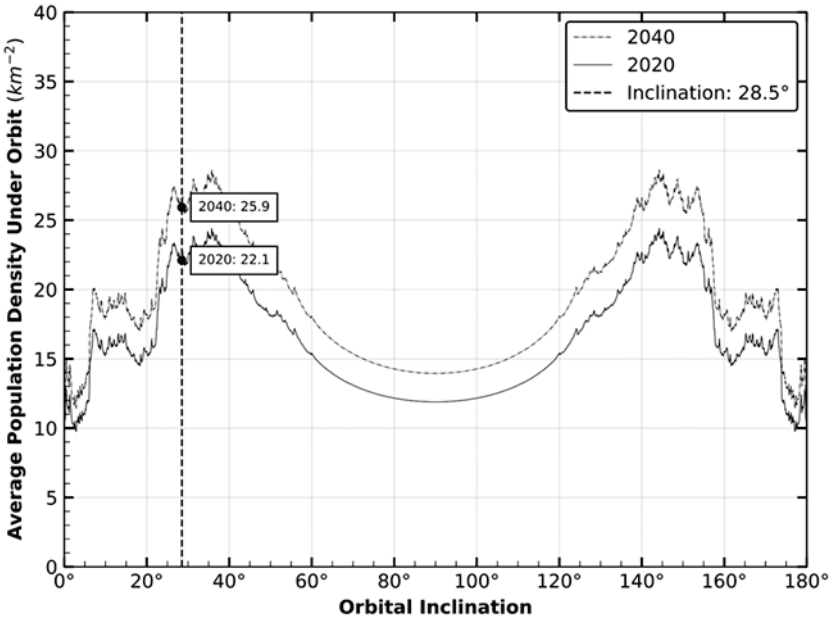

Figure 7.5-7. 2020-2040 Population Density Using Updated Population Model

For the updated risk assessment, the NASA-STD-8719.14C risk equation was recalculated using the updated Ostrom DCA model and latest population models and growth predictions. The previous Smith et al. equations were also recomputed using the updated DCA model as a point of comparison. Computing the DCA using the original HST mass properties in Smith et al. 2004 and the updated Ostrom DCA equation, the Smith et al. unscaled total DCA reduces from 146 m^2 to 137 m^2 and slightly reduces the overall risk from 1:250 to 1:267 in 2021. Accounting for the HST hardware changes made during SM4, the updated DCA estimate is 143.6 m^2. Using the same mass-scaling approach as Smith et al. 2004 to adjust for the 25% unmodeled HST mass (wire harnesses, cables, etc.), the final updated DCA value is 191.0 m^2 using all the latest methods and data; the original, mass-scaled Smith et al. estimate was 199 m^2.

Figure 7.5-8 compares the original Smith 2004 results for their two bounding DCA values (orange) with our updated projections, using the updated DCA values and updated population densities (blue). Updated risk projections are approximately 5% higher than Smith et al. despite predicting a lower overall DCA; the increased risk is driven by faster-than-anticipated population growth. For a 2035 reentry, the updated risk assessment falls between 1: 209 and 1: 278. This updated risk value violates the 1:10,000 risk level dictated by NASA-STD-8719.14C for uncontrolled reentries.

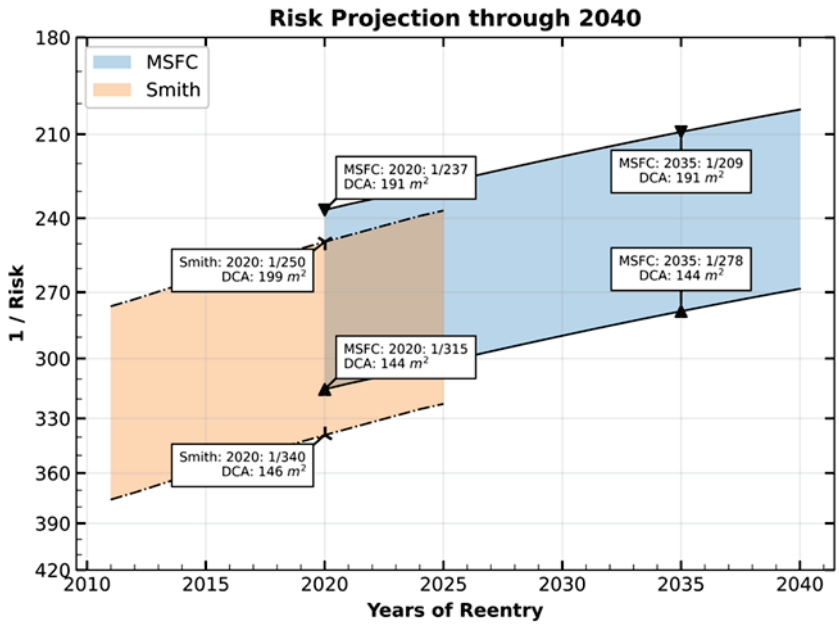

Figure 7.5-8. Smith (2005) Results Compared with MSFC Updated Projections

To provide a frame of reference for the magnitude of the HST reentry risk violation relative to the standard, an additional analysis was done to determine how much debris could survive a generic satellite reentry to comply with NASA-STD-8719.14C. This calculation inverted the risk equation to back out a DCA based on a 1:10,000 risk level and the latest population data. It was found that, for a satellite reentering at 28.5 degrees orbital inclination (the approximate orbit of HST), the maximum acceptable DCA is 4.5 m^2. (**F-6**) Therefore, the debris predicted to result from an uncontrolled HST reentry is more than 30 times larger than the acceptable DCA limit. Figure 7.5-9 provides a visual representation of the magnitude of the DCA violation for an HST uncontrolled reentry.

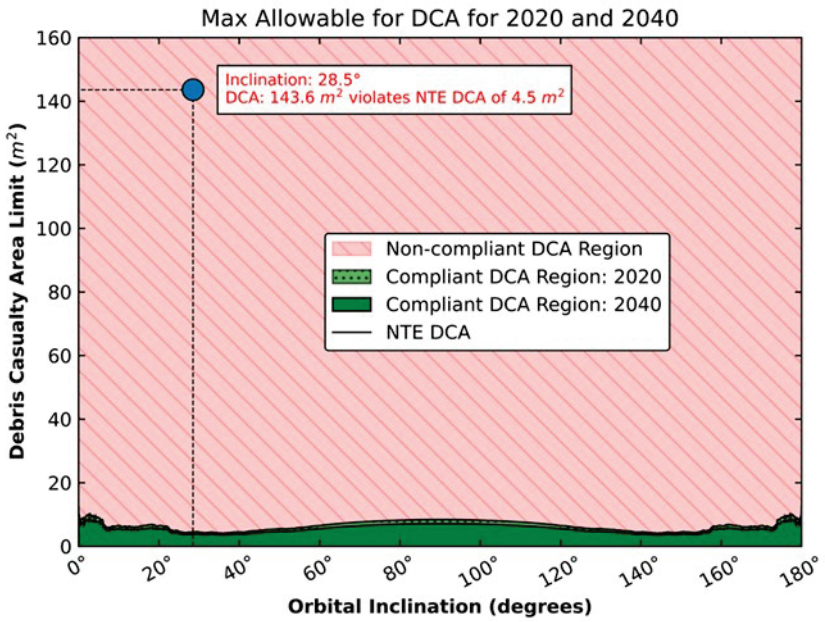

Figure 7.5-9. Acceptable DCA to Meet 1:10,000 Requirement in 2020

7.5.2 MAVERIC and Footprint Analysis

A high-fidelity HST debris footprint was created to quantify the expected range and spread of impacting debris. MAVERIC is a high fidelity 6DOF simulation tool in use at MSFC for Guidance, Navigation, and Control (GN&C)/6DOF design and analysis for Artemis SLS ascent, in-space, and reentry events and Mars Ascent Vehicle. MAVERIC enables Monte Carlo analysis by dispersing subsystem and environmental inputs, such as randomizing mass properties, timing latencies, hardware misalignments, temperature, and atmosphere/winds.

For SLS, MAVERIC is used to show SLS Core Stage (CS) reentry requirement compliance to the NASA-STD-8719.14C requirement for controlled reentry: "No surviving debris impact with a kinetic energy > 15 J within 70 km from foreign landmasses, or 50 km from U.S and Antarctica" (ref. 5). MAVERIC SLS CS reentry Monte Carlo analysis leverages a breakup debris catalog, which provides breakup altitudes, ballistic coefficients, lift-to-drag ratios, and ΔVs from residual propellant explosions for each debris piece and combines the debris properties with dispersed environmental conditions to generate a footprint of the SLS CS debris upon reentry. Selected debris pieces from the Shuttle Columbia Public Entry Risk Assessment (PERA) are also included in the SLS CS analysis to bound the likely "heel" and "toe" of the footprint. Figure 7.5-10 provides an example of the SLS CS debris footprint generated using MAVERIC's Monte Carlo capabilities; the edges of the footprint are compared to the "keep out zones" around land masses as dictated by NASA-STD-8719.14C (ref. 5).

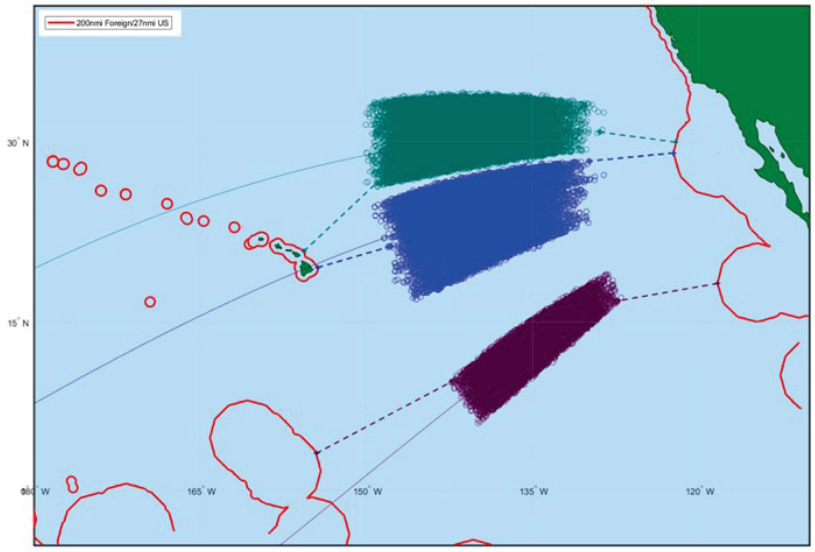

Figure 7.5-10. Example SLS CS Reentry Footprint Created with MAVERIC

NESC Independent Verification & Validation (IV&V) of the MAVERIC SLS Core Stage reentry analysis has shown good agreement, and MAVERIC simulations also showed good agreement with available Artemis I post-flight data for CS reentry. Figure 7.5-11 shows the nominal Artemis I trajectory predicted by MAVERIC and the location of the likely CS tank rupture, detected by the Geostationary Operational Environmental Satellites (GOES) Geostationary Lightning Mapper (GLM). The detected likely location of Artemis I CS rupture location lies very close to the predicted trajectory. This provides confidence in using MAVERIC to adapt and model a HST reentry and footprint.

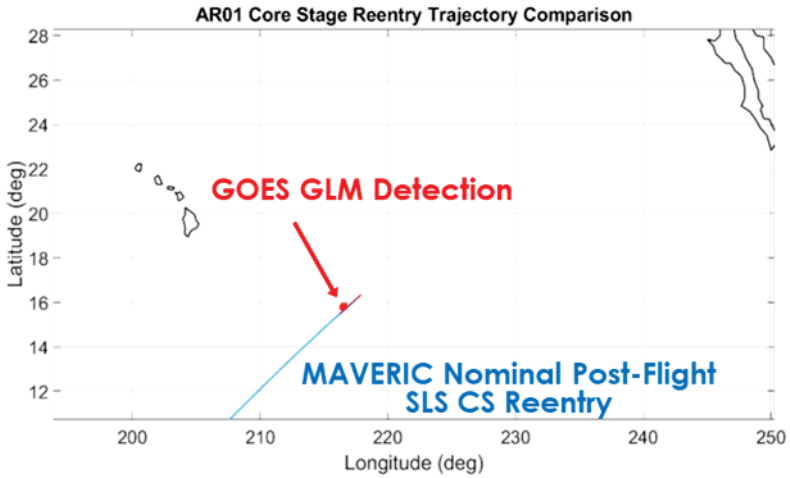

Figure 7.5-11. AR01 Core Stage Reentry Trajectory Comparison

A similar approach to the previously-described SLS CS reentry was taken for the HST uncontrolled reentry footprint analysis. Smith et al. 2004 generated a debris catalog for HST which included debris masses, ballistic coefficients, and debris liberation altitudes as determined by their aerothermal and ablation codes. These inputs in combination with reentry initial conditions were used to generate a HST dispersed footprint using MAVERIC. A detailed description of the footprint modeling process follows.

For the MAVERIC HST debris footprint simulation, the initial conditions were supplied from the FreeFlyer results generated as part of the broader HST analysis (see Section 7.2). For the specific set of initial conditions used for this analysis, HST is located at approximately 122 km in altitude above the north-east coast of Papua New Guinea. HST is assumed to enter a tumble as it enters the atmosphere, and an intact, tumbling BC of 82 kg/m^2 is applied to HST per Baker 2019 until HST breakup. As each demise altitude is reached as dictated by the Smith et al. catalog for surviving debris pieces, fragments are released from the main HST body and propagated to the ground with their own ballistic coefficients, lift-to-drag ratios, and dispersed bank angle. By tracking each released debris piece from the breakup altitude of the parent component to the ground, a debris footprint can be created. The lift-to-drag ratios for debris fragments were estimated using the simple geometry classification for each piece from the Smith et al. catalog and comparing with similar SLS CS debris data, assuming each piece is tumbling. The ballistic coefficients were also taken from the Smith et al. debris catalog. A simplifying assumption for the MAVERIC analysis was using a single static ballistic coefficient per debris piece throughout the entire descent; MAVERIC specifically used the ballistic coefficient for each piece at the time of impact. Figure 7.5-12 provides a summary of the MAVERIC reentry analysis compared to ORSAT v 5.8, which was used by Smith et al.

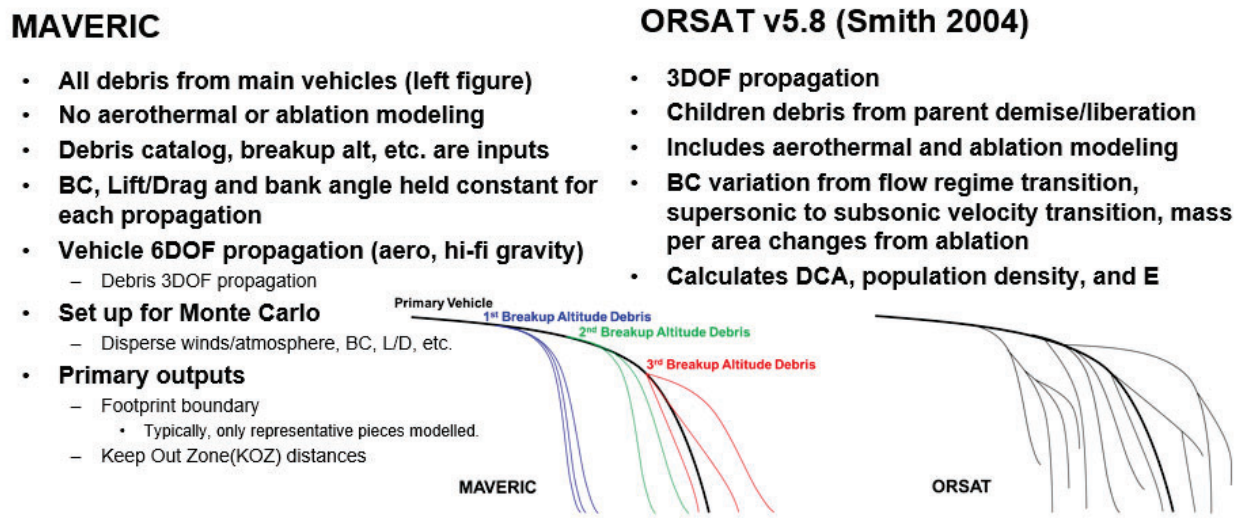

Figure 7.5-12. MAVERIC vs. ORSAT

MAVERIC and ORSAT have different purposes and as such simulate the reentry event in different ways. For instance, MAVERIC maintains one primary HST body throughout the reentry, and debris fragments are always released from that main body; in ORSAT, debris is able to release other debris, leading to more "branching" during the separation. MAVERIC does not implement any aerothermal or ablation models, and therefore relies on the previous ORSAT work to supply the debris list. Also, ORSAT dynamically changes the ballistic coefficient for each debris piece depending on the current conditions, while MAVERIC maintains a static value. MAVERIC can provide a reasonable bounding estimate of the expected debris footprint by leveraging MAVERIC's Monte Carlo capabilities and by including bounding debris pieces in the analysis. (**O-8**) By dispersing the atmospheric (including wind) properties and aerodynamic force direction for each Monte Carlo case, MAVERIC's footprint grows in cross-track as well as length, while the Smith et al. footprint is strictly one-dimensional. A dispersed Global Reference

Atmospheric Model (GRAM) atmospheric and wind model was used, which adds further variation to the debris trajectories. Engineering judgment was used to disperse the breakup altitudes, ballistic coefficients, and lift-to-drag ratios of each debris piece, accounting for further uncertainty in simulated parameters. Bounding high and low ballistic coefficient debris pieces from the Space Shuttle PERA database were also released at the highest and lowest breakup altitude to provide maximal bounds on the length of the dispersed footprint.

Although the MAVERIC HST Monte Carlo analysis results from a single set of initial reentry conditions, the inclusion of a large number of dispersed parameters during the simulation generates a footprint that demonstrates the large possible variation in debris impact location even when the reentry location, attitude, and rates are held constant. Including all dispersed runs and bounding Columbia PERA debris, the possible HST footprint spans 4,261 km with a width of 70 km. (**O-7**) Each Monte Carlo case shows a spread of up to 800 km, but the uncertainty in exactly where along the orbital track the debris will fall stretches the possible impact locations more than 5 times beyond the footprint size for an individual run. Figure 7.5-13 shows the dispersed HST reentry footprint on the globe, demonstrating the scale of the potential debris impact area. Figure 7.5-14 provides a histogram for the footprint lengths of each individual Monte Carlo run; in this figure, the bounding PERA pieces are not included, and the mode of the footprint length including only HST debris pieces is 800 km.

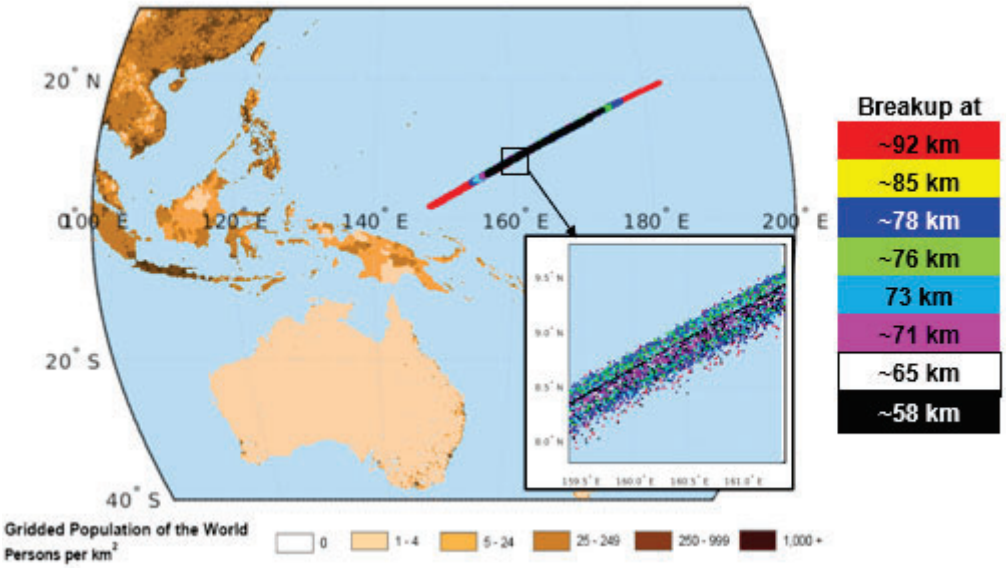

Figure 7.5-13. MAVERIC Dispersed HST Debris Footprint

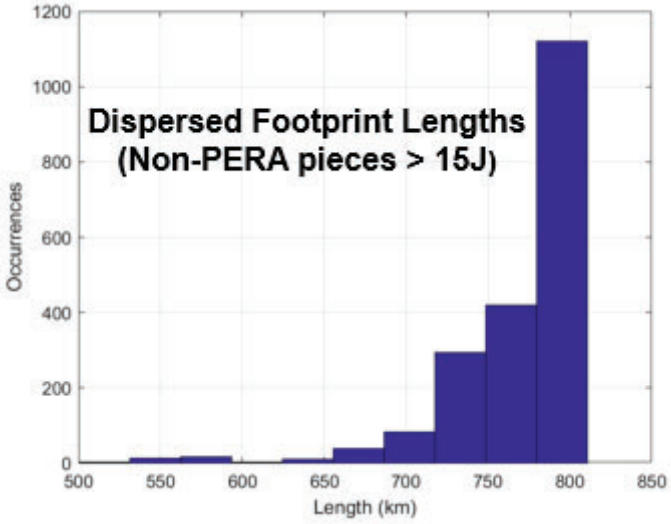

Figure 7.5-14. Per Run Footprint Lengths Not Including Bounding PERA Debris

7.5.3 Risk to the Public

Public risk from objects that survive atmospheric reentry can be quantified by the expectation of casualty (E_c) as described in NASA-STD-8719.14C. The following quantities are defined in NASA-STD-8719.25.

- ***Probability of Impact*** (P_i) is the probability that one or more pieces of debris will impact a specified location *i*. In other words, P_i is the chance of a person or property being struck by debris, regardless of the potential for the debris to cause damage.
- ***Casualty*** is an injury requiring overnight hospitalization or worse, including death.
- ***Expectation of casualty*** (E_c) is the average number of casualties expected per an event if a large number of events could be carried out under identical circumstances.
- ***Collective risk*** is the total combined risk to all individuals exposed to one or more hazards during a specified event. The collective risk is the mean number of casualties expected (E_c) during an established event due to the combination of all hazards associated with the operation.

The risk to the public or expectation of casualty (E_c) is calculated as a function of the debris casualty area (DCA), probability of impact in a specified region, and population density (ρ) in that region.

$$E_c = DCA * P * \rho$$

Equation 16.

Eq. (3) can be modified to compute the average number of casualties across *n* locations.

$$E_c = \sum_{i=1}^{n} DCA * P_i * \rho_i$$

Equation 17.

The DCA for HST reentry is 143.558149 m^2 as calculated in the MAVERIC Monte Carlo analysis (see Section 7.5.2.1).

As discussed in Section 7.5.2.1, HST debris could impact the ground anywhere between 28.5° N and 28.5° S (see Figure 7.5-15). Given the radius of Earth is 6,371 km (3,959 mi), the total area between 28.5° N and 28.5° S is

$$\begin{aligned} \textit{Total area between 28.5° N and 28.5° S} &= 2\pi R^2 * (sin(latitude\ 1) - sin(latitude\ 2)) \\ &= 2\pi * (6371^2) * (sin\ 28.5 - sin(\text{-}28.5)) \\ &= 243{,}381{,}731\ \text{km}^2 \end{aligned}$$

Then the probability of impact in a given region is calculated as

$$P_i = \frac{Area\ of\ region\ i}{Total\ area\ between\ 28.5°\ N\ and\ 28.5°\ S} = \frac{Area\ of\ region\ i}{243{,}381{,}731\ km^2}$$

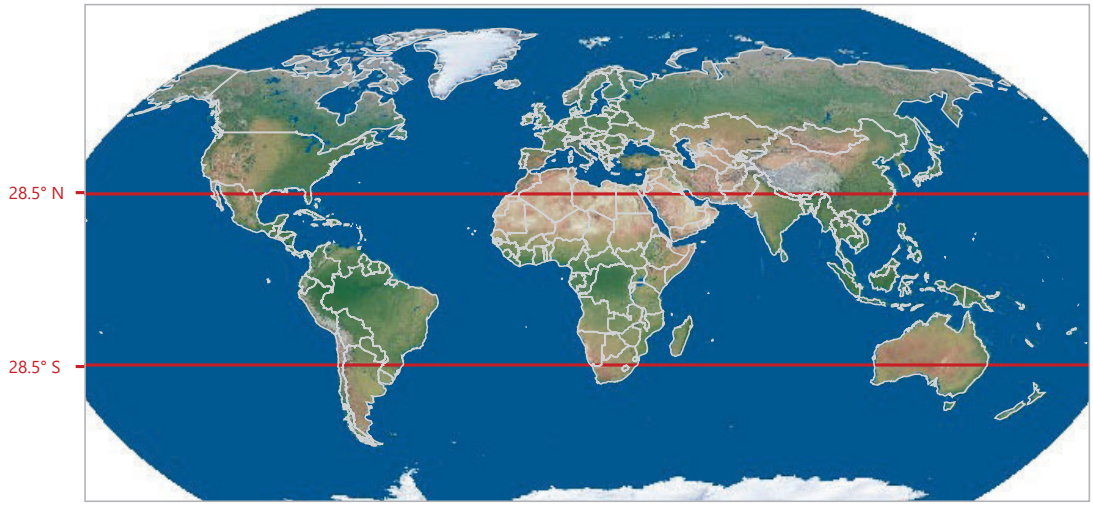

Figure 7.5-15. Map of possible HST impact area between 28.5° N and 28.5° S

Previous NASA studies estimating expected casualties from reentering space debris used the Gridded Population of the World (GPW) database, which models the global distribution of human population. The GPW is a product of NASA's Socioeconomic Data and Applications Center (SEDAC) which integrates Earth science and socioeconomic data for use in research and policy-making. Unfortunately, SEDAC data, including the GPW, were not available at the time of this study, so an alternative data source had to be identified. (**F-4**)

This study used the United Nations World Population Prospects (WPP) 2024 database to model global population distribution. The WPP consists of population estimates from 1950 to the present for 237 countries or areas. It also contains population projections to the year 2100 that reflect a range of plausible outcomes at the global, regional, and national levels. To calculate population density projections, the WPP was merged with land area data from the FAOSTAT database maintained by the Food and Agriculture Organization of the United Nations. The population density projection for 2033 is visualized in Figure 7.5-17.

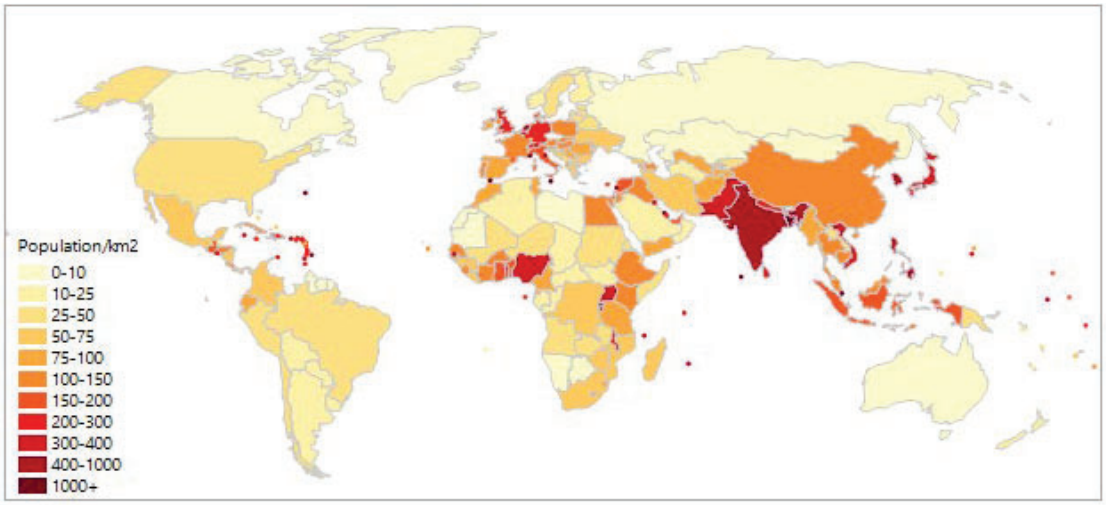

Figure 7.5-17. Map of Population Density (people per km^2) projection for 2033

The following assumptions are made for the E_c calculations.

- The HST debris will impact the ground between 28° N and 28° S latitude
- The probability of impact distribution is uniform within area *i*.
- The population density distribution is uniform within area *i*.

The average number of casualties, E_c, for HST reentry calculated using Eq. (4) are shown in Table 7.5-3 and Figure 7.5-18. The risk was calculated for reentry in years 2025 through 2040 based on the projected population median and 95% lower and upper bounds. Note that this is an overall average risk for the entire area between 28° N and 28° S, including land and ocean. For an orbital decay reentry in the year 2033 with a 28.5° inclination, the casualty risk is 1:330. This is significantly higher than the NASA-STD-8719.14C requirement that E_c for the public be less than or equal to 1:10,000. (**F-8**)

The worst-case scenario would occur if the HST debris impacted in Macao, where between two and four casualties would be expected due to its high population density. At least one casualty would also be expected if it impacted in Hong Kong or Singapore.

Table 7.5-3. HST Casualty Risk for Median Projected Population with 95% Upper and Lower Bounds by Reentry Year

Year	95% Lower Bound	Median	95% Upper Bound
2025	1:366	1:362	1:359
2026	1:363	1:358	1:352
2027	1:361	1:353	1:346
2028	1:359	1:349	1:340
2029	1:357	1:345	1:334
2030	1:356	1:341	1:328
2031	1:354	1:338	1:323
2032	1:352	1:334	1:317
2033	1:351	1:330	1:312
2034	1:350	1:327	1:306
2035	1:348	1:324	1:301
2036	1:347	1:320	1:296
2037	1:346	1:317	1:291
2038	1:345	1:314	1:287
2039	1:344	1:311	1:282
2040	1:343	1:308	1:278

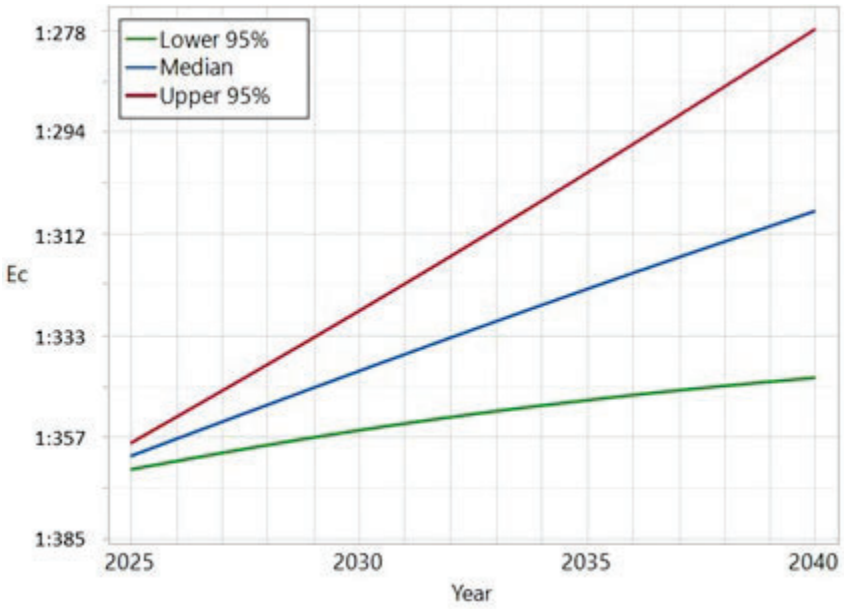

Figure 7.5-18. HST Casualty Risk for Median Projected Population with 95% Upper and Lower Bounds by Reentry Year

7.6 Brief Survey of Related HST Deorbit Studies

Several papers and reports are summarized here that have relevant information on the influence of solar activity to orbital decay and in particular to the HST decay study presented here. Paper references are provided at the end of this report.

Summary of "Orbit Decay Prediction Sensitivity to Solar Flux Variations", Naasz, Berry, Schatten, AAS-07-264.

1. **Solar Activity Impact**: The paper examines how variations in solar activity (particularly solar flux) affect the accuracy of satellite orbit decay predictions, highlighting the 11-year solar cycle and 27-day solar rotation effects on atmospheric density.
2. **Statistical Analysis**: The research presents a statistical approach to quantifying orbit decay prediction uncertainties, showing that atmospheric density variations due to solar flux fluctuations create non-Gaussian distributions in reentry time predictions.
3. **Lifetime Uncertainty**: For the cases analyzed, satellite lifetime prediction uncertainties were approximately 5% due to solar flux variations, though the distribution of possible reentry times showed significant asymmetry with "fat tails."
4. **Early Reentry Risk**: The analysis identified scenarios where some satellites might reenter nearly 2 years before the mean predicted time, which has important implications for risk assessment of uncontrolled reentries.
5. **Solar Activity Modeling**: The paper describes both observed and simulated solar flux patterns, including the 27-day solar rotation periodicity that significantly impacts short-term atmospheric density variations.
6. **Geomagnetic Activity Correlation**: The research also examines the relationship between solar flux (F10.7) and geomagnetic activity (Ap index), noting that both follow roughly log-normal distributions with visible 11-year cycle effects.
7. **Practical Applications**: The findings suggest that for certain applications, short-term flux variations might be reasonably ignored, or a standardized error margin could be applied to all predictions.

The purpose of the paper is to provide a Monte Carlo approach to sampling solar activity indices for satellite orbit forecasting, taking into account the daily variations and tying it to solar behavior not just the smoothed predictions. This research provides valuable insights for satellite operators and mission planners who need to accurately predict spacecraft orbital lifetimes and reentry times, particularly for risk assessment and mission extension planning.

Summary of "Reentry Survivability Analysis of the Hubble Space Telescope (HST)", Space and Life Sciences Directorate, Orbital Debris Program Office, JSC-62599, May 2004.

1. **Analysis Purpose**: The document reports a detailed reentry survivability analysis of the HST using the Object Reentry Survival Analysis Tool (ORSAT).
2. **Component Breakdown**: The paper includes a detailed inventory of HST components with specific information about:
    1. Material composition (primarily aluminum alloys, with some magnesium and steel components)

2. Dimensions and geometric characteristics
3. Mass properties
4. Component locations within the spacecraft structure

3. **Spacecraft Structure**: The analysis identifies key structural elements including:
    1. Optical Telescope Assembly (OTA) components
    2. Support Systems Module (SSM) components organized by bay locations
    3. Electronics boxes (DIU, CCC, OSC, PCU-R, etc.)
    4. Reaction Wheel Assemblies (RWA)
4. **Analytical Framework**: The document references ORSAT Version 5.0 and subsequent upgrades to Version 5.5, indicating the analysis used sophisticated modeling to determine which components might survive atmospheric reentry.
5. **Similar Analyses**: The document references comparable reentry survivability analyses conducted for other spacecraft including:
    1. Compton Gamma Ray Observatory (CGRO)
    2. Upper Atmosphere Research Satellite (UARS)
    3. Earth Observing System (EOS) satellites
    4. Delta IV Launch Vehicle upper stages
6. **Mass Properties**: Many HST components are precisely characterized with masses ranging from approximately 1.36 kg for smaller components to over 45 kg for larger assemblies.
7. **Results:** The analysis shows that 98 different components are expected to survive reentry from natural orbital decay. These components produce a debris casualty area of 156 m^2, a surviving mass of 2055 kg, and a main footprint length of 1220 km. Some of these surviving components impact with a kinetic energy below a lethality limit of 15J and might be ignored for purposes of determining human casualty risk. The resulting debris casualty area would then be 146 m^2. For a 28.5 inclination and orbital decay in the year 2020, a casualty risk of approximately 1:340 was obtained for a standard breakup altitude of 78 km. Only 75% of the spacecraft mass was characterized and analyzed, therefore, a possible increase in risk is posed by the unmodeled mass. Risk of remaining mass is scaled based on the results of the modeled mass then the adjusted risk for the year 2020 is 1:250.

Summary of "Public Entry Risk Assessment for the Space Shuttle Program", JSC-63062, Mission Operations Directorate, Flight Design and Dynamics Division, June 2006.

1. **Purpose**: The document appears to be a comprehensive risk assessment framework for evaluating public safety hazards associated with Space Shuttle reentries.
2. **Assessment Structure**: The document is organized into sections that methodically address different aspects of entry risk assessment, including:
    - Technical evaluations and verification processes

- Surviving debris models and casualty area definitions
- Probabilistic vs. catalog-based approaches to debris analysis

3. **Methodology Development**: The paper describes:
    - Implementation of models in MATLAB code
    - Testing and validation procedures
    - Independent verification by external entities (including ISI, who delivered a final report on July 2, 2004)
4. **Technical Approach**: The document distinguishes between:
    - Macroscopic/continuous (probabilistic) approaches
    - Microscopic/discrete (debris catalog) methodologies for risk assessment
5. **Documentation**: The paper mentions a forthcoming supplementary report that would describe:
    - Algorithms resulting from various models
    - Their implementation in MATLAB code
    - Test cases that validated the code
6. **Analysis Components**: The risk assessment includes considerations of:
    - Harmful debris models
    - Casualty area definitions
    - Sensitivity analysis
    - Uncertainty quantification
    - Assumption limitations

This document represents a systematic approach to quantifying and managing the risks associated with Space Shuttle reentries, specifically focusing on the potential hazards to the public from surviving debris.

Summary of "An Early Study of Disposal Options For the Hubble Space Telescope", Griffin et al. 6th European Conference on Space Debris, April 2013.

1. **Purpose**: The paper examines disposal options for the HST to comply with orbital debris mitigation guidelines.
2. **Timeline**: As of the study, HST was expected to remain operational for at least another decade, with its orbit remaining above 500 km until at least 2024, providing about 5 years before a disposal approach needed to be finalized.
3. **HST Context**: The paper notes HST is an international partnership between NASA and ESA, considered one of NASA's most successful international collaborations.
4. **Propulsion Options Evaluated**:
    - Chemical propulsion (both monopropellant and bipropellant)

- Drag enhancement (ballutes, solar sails, tethers)
- Electric propulsion methods (electrodynamic tethers, solar electric)

5. **Key Findings**:
    - Bipropellant chemical propulsion was determined to be better than monopropellant in terms of thrust per unit mass
    - However, even bipropellant designs would require impractical amounts of propellant to reach the 2000 km defined storage orbit
    - Drag enhancement techniques provide insufficient control for targeted reentry
    - Electrodynamic tethers and solar electric propulsion could work for slow orbit changes but insufficient for targeted reentry
6. **Recommendations**: The study concluded it would be advantageous to delay the final decision on disposal approach to gain better knowledge of key decision factors.
7. **Scope**: While focused on minimizing impacts to the orbital environment, the paper acknowledges reentry risk to the public as an important aspect of the study.

The paper represents a comprehensive analysis of HST disposal options with contributions from multiple NASA centers (GSFC, MSFC), industry partners, and technical advisors.

Summary of "Increased Ephemeris Accuracy Using Attitude-Dependent Aerodynamic Force Coefficients for Inertially Stabilized Spacecraft", Folta, D. and Baker, David F., date unknown of publication.

1. **Purpose:** Current techniques for generating spacecraft ephemerides typically use a constant value of the ballistic coefficient during orbit propagation. This is due to the complexities of calculating attitude-dependent aerodynamic forces and in part to the inaccuracy in the prediction of the atmospheric density, which results in substantial orbital position errors even if the ballistic coefficient were to be determined exactly at all times.
2. **Context:** Assuming constant ballistic coefficients introduces equally large errors as those caused by density uncertainty.
3. **Results:** Error can be reduced by calculating orbit-averaged ballistic coefficients for each viewing attitude, or by calculating aerodynamic force coefficients for the appropriate geometry at each integration step.
4. **Scope:** This report describes the FREEMAC program used to generate aerodynamic coefficients and results show improvement in the predicted semi-major axis and along-track positions that would seem to be worth the added computational effort.
5. **Recommendations:** The techniques described in the paper were applied to HST and report that the use of attitude-dependent drag coefficients resulted in improved ephemeris accuracy, particularly when these coefficients were determined at each orbit integration step.

8.0 Findings, Observations, and NESC Recommendations

8.1 Findings

F-1. As spacecraft dip lower in the atmosphere, density increases, and model uncertainties have a stronger effect on decay predictions. This may require adjusting C_d due to inaccuracies in density models.

F-2. Historical solar activity records show peaks of extreme activity on 11/4/2003, 9/9/2005, 12/6/2006, 03/07/2011, where the F10.7 magnitudes are factors higher than the measurements before and after these days, causing the MSIS atmosphere model to fail to produce an atmospheric density value.

F-3. CelesTrak (T.S. Kelso) assumes MSAFE predicted F10.7 values are adjusted to account for Earth eccentricity and incorrectly loads these values in the 'adjusted' column of his space weather file. These values are then adjusted by a $1/\text{radius}^2$ scaling factor and loads those values into the 'observed' column. MSFC MSAFE model developers confirm using observed F10.7 data to generate predictions.

F-4. Population density data are necessary for calculating the casualty probabilities under the ground track of reentering spacecraft. This analysis had to rely on alternate data due to population density data being removed from NASA's SocioEconomic Data and Applications Center (SEDAC) and EarthData websites in March 2025.

F-5. Given Swift Observatory's current altitude, small changes in solar predictions make a big difference in predicting reentry times; there are new solar activity models based on the physics of the Sun and approaches that consider the stochastic nature of daily solar flux values that may improve predictions in this case.

F-6. To meet the 1:10,000 requirement for uncontrolled reentry, a satellite in a 28.5º inclination orbit reentering in 2025 would need a maximum debris casualty area of only ~4 m^2; this maximum allowable DCA value will decrease in time, due to population increases; the smallest HST DCA estimates (140 m^2) are ~30x larger than this maximum allowable value and the HST Primary Mirror (expected to survive to impact) DCA is greater than the maximum allowable DCA by itself.

F-7. For average projected area, average expected solar activity and derived drag coefficient of 1.74, HST is projected to reenter Earth's atmosphere in the fall of 2033.

F-8. For HST reentries over "densely populated" regions of the globe and constrained by HST's inclination, the risk exceeds the requirement of 1:10,000 for all analyses and variants performed.

F-9. For average projected area, average expected solar activity and derived drag coefficient of 1.55, Swift is projected to reenter Earth's atmosphere in mid-summer of 2026.

8.2 Observations

O-1. Satellite orbital decay predictions are dependent on solar activity data. NOAA Space Weather Prediction Center is a source of predicted space weather phenomenon and relied upon by industry and other government agencies. There are international organizations that provide space weather observations as well.

O-2. Satellite drag coefficients are critical for determining the neutral mass densities that contribute to spacecraft operating in the thermosphere. This study utilized a range of C_d values and derived specific values to match the recent HST and Swift Observatory decay profiles. The determinations of satellite drag coefficients are ultimately tied to spacecraft shape *and* thermospheric factors like temperature and density.

O-3. A single TLE can influence the decay time, by up to a month or more in some cases. Each TLE is a single observation with an unknown orientation; Monte Carlo simulations from multiple TLEs and considering the uncertainty a single propagated TLE contributes can improve the results.

O-4. The NESC team continues to be made aware of additional tools and models, such as a density model developed by the Department of Defense/Orbitron High Accuracy Satellite Drag Model (HASDM), which includes phases and amplitudes of the diurnal and semidiurnal variations of thermospheric density, based on observations from a set of Low Earth Orbit (LEO) calibration satellites.

O-5. Some of the runs do not make it to the 100 km altitude cutoff before terminating due to entering the reference ellipsoid caused by variable time step; once the propagation hits about 200 km it starts to decay rapidly using a variable step size or even a 10min step size, within 1/2 steps it can essentially crash into Earth.

O-6. FF Simulation was unable to propagate epochs across periods of extremely high solar F10.7 values, a bug report was issued, and AI solutions discovered the underlying MSIS model was in error. AI solutions is investigating a patch for FF. Previous solar cycles with similarly high values processed normally as cycles with a steady increase in solar activity did not result in simulation interruptions.

O-7. The Public Entry Risk Assessment (PERA) for Space Shuttle reports a 0.5 Ballistic Coefficient for a Shuttle tile piece that bounds the heel of the footprint and was used as a bounding value for the HST 6DOF Monte Carlo reentry predictions. This assumption is 3x smaller than the assumption used in the last ORSAT reentry run (2005) for equivalent BC pieces greater than the 15 J minimum threshold.

O-8. Higher fidelity debris reentry software tools exist , NASA's Orbital Debris Program Office uses ORSAT, and ESA uses SCARAB; GSFC SMD missions rely on high fidelity Monte Carlo simulations from the FDF. This study relied on lower fidelity tools to meet the schedule.

8.3 NESC Recommendations

To the Swift Observatory Project Office:

R-1. Given Swift Observatory has a predicted reentry within two years, conduct an ORSAT evaluation through the ODPO with the most current information. (**F-1**, **F-5**, **O-2**, **O-8**)

To the GSFC FDF (and other organizations conducting reentry predictions):

R-2. Consider using physics-based solar prediction models for near term reentry predictions, such as Swift Observatory. (**F-1**, **F-5**, **O-1**)

R-3. Use more stochastic models over 'smoothed' solar cycle predictions for near term reentry predictions. Models inclusive of the naturally occurring peaks in activity produce more

accurate decay reentry predictions. Further studies should be conducted that include variations in geomagnetic conditions on top of smoothed predictions. (**F-1**, **O-1**, **O-4**)

To the HST Project Office:

R-4. Using the attitude profile flown during the observation schedule may reveal 'trends' favoring certain orientations that allow for better estimates of area as a function of time, in addition to estimates of C_d based on free molecular flow models which would improve estimates for decay predictions. (**F-1**, **F-2**, **F-7**, **O-2**, **O-3**, **O-4**)

R-5. Conduct an updated HST uncontrolled reentry survivability and population risk analysis using the latest version of ORSAT against the final (post SM-4) HST configuration inclusive of the latest population densities and growth projections. Predictions should include detailed aerothermal analysis to determine demise fragment properties under varying conditions for improved footprint analyses. (**F-4**, **F-6**, **O-8**)

To the Office of Safety and Mission Assurance:

R-6. Update NASA-STD-8719.14C Process for Limiting Orbital Debris to include the new Debris Casualty Area equation from the Orbital Debris Program Office. (**F-6**)

To CelesTrak Developer T.S. Kelso:

R-7. The CelesTrak space weather file should use the unadjusted MSAFE observed F10.7 values in the 'observed' column of the publicly distributed space weather file. (**F-3**, **O-1**)

To FreeFlyer and NRL MSIS Developers:

R-8. The FreeFlyer simulation tool utilizes the Naval Research Lab MSIS atmosphere model to produce atmospheric densities for orbital decay calculations and should implement a workaround for cases where extreme F10.7 values disrupt the density calculations; NRL MSIS developers should address the errors resulting from extreme values of F10.7 that are out-of-family from surrounding measurements. (**F-2**, **O-6**)

9.0 Alternate Technical Opinion(s)

No alternate technical opinions were identified during the course of this assessment by the NESC assessment team or the NESC Review Board (NRB).

10.0 Other Deliverables

No unique hardware, software, or data packages, other than those contained in this report, were disseminated to other parties outside this assessment.

11.0 Recommendations for the NASA Lessons Learned Database

No recommendations for NASA lessons learned were identified as a result of this assessment.

12.0 Recommendations for NASA Standards, Specifications, Handbooks, and Procedures

Consider updating NASA-STD-8719.14C Process for Limiting Orbital Debris section 4.7.4.1 to include the new Debris Casualty Area equation from the Orbital Debris Program Office

published in 2019 by Ostrom with methodological updates. Consider specifying that the most current population density prediction be used or specifying a source of population density prediction data.

From eqtn 4.7-1:

$$D_A = \sum_{i=1}^{N} \left(0.6\, m + \sqrt{A_i}\right)^2$$

To eqtn 4.7-1:

$$D_A = \sum_{i=1}^{N} \left(0.278\, m^2 + A_i + 1.39\, m * \sqrt{A_i}\right)$$

Equation 18.

13.0 Definition of Terms

Corrective Action	Changes to design processes, work instructions, workmanship practices, training, inspections, tests, procedures, specifications, drawings, tools, equipment, facilities, resources, or material that result in preventing, minimizing, or limiting the potential for recurrence of a problem.
Finding	A relevant factual conclusion and/or issue that is within the assessment scope and that the team has rigorously based on data from their independent analyses, tests, inspections, and/or reviews of technical documentation.
Lesson Learned	Knowledge, understanding, or conclusive insight gained by experience that may benefit other current or future NASA programs and projects. The experience may be positive, such as a successful test or mission, or negative, as in a mishap or failure.
Observation	A noteworthy fact, issue, and/or risk, which is not directly within the assessment scope, but could generate a separate issue or concern if not addressed. Alternatively, an observation can be a positive acknowledgement of a Center/Program/Project/Organization's operational structure, tools, and/or support.
Problem	The subject of the independent technical assessment.
Proximate Cause	The event(s), including any condition(s) that existed immediately before the undesired outcome, that directly resulted in its occurrence.
Recommendation	A proposed measurable stakeholder action directly supported by specific Finding(s) and/or Observation(s) that will correct or mitigate an identified issue or risk.
Root Cause	One or multiple causes (including adverse or unplanned events, conditions, or organizational factors) that contributed to or created the

	proximate cause(s) and subsequent undesired outcome and, if eliminated or modified, should have prevented the undesired outcome.
Supporting Narrative	A paragraph, or section, in an NESC final report that provides a detailed explanation of a succinctly worded finding or observation. For example, the logical deduction that led to a finding or observation; descriptions of assumptions, exceptions, clarifications, and boundary conditions.

14.0 Acronyms and Nomenclature List

1D	One-Dimensional
2D	Two-Dimensional
6-DOF	Six Degrees of Freedom
AOCS	Attitude and Orbit Control Subsystem
BC	Ballistic Coefficient
BSTAR	B*
CGRO	Compton Gamma Ray Observatory
COS	Cosmic Origins Spectrograph
COSTAR	Corrective Optics Space Telescope Axial Replacement
CS	Core Stage
DAS	Debris Assessment Software
DCA	Debris Casualty Area
DRAMA	Debris Risk Assessment and Mitigation Analysis
DRAO	Dominion Radio Astrophysical Observatory
DTM	Drag Temperature Model
EGM	Earth Gravity Model
EOS	Earth Observing System
ESA	European Space Agency
EUV	Extreme Ultraviolet
FDF	Flight Dynamics Facility
FF	FreeFlyer
GLM	Geostationary Lightning Mapper
GN&C	Guidance, Navigation, & Control
GOES	Geostationary Operational Environmental Satellites
GPW	Gridded Population of the World
GRAM	Global Reference Atmospheric Model

HST	Hubble Space Telescope
IDB	International Data Base
ISS	International Space Station
IV&V	Independent Verification & Validation
JB	Jacchia-Bowman
JR	Jacchia-Roberts
JWST	James Webb Space Telescope
MAVERIC	Marshall Aerospace VEhicle Representation In C
MSAFE	Marshall Solar Activity Future Estimation
MSIS	Spectrometer Incoherent Scatter
NESC	NASA Engineering and Safety Center
NOAA	National Oceanic and Atmospheric Administration
NORAD	NORth American Aerospace Defense
NRL	Naval Research Laboratory
NRLMSIS	Naval Research Laboratory's Mass Spectrometer Incoherent Scatter
ODAR	Orbital Debris Assessment Report
ODPO	Orbital Debris Program Office
ORDEM	Orbital Degree Engineering Model
ORSAT	Object Reentry Survival Analysis Tool
PERA	Public Entry Risk Assessment
RWA	Reaction Wheel Assemblies
SEDAC	SocioEconomic Data and Applications Center
SERAM	Spacecraft Entry Risk Analysis Module
SESAM	Spacecraft Entry Survival Analysis Module
SLS	Space Launch System
SM-4	Servicing Mission 4
SOAP	Satellite Orbital Analysis Program
SRP	Solar Radiation Pressure Model
SSM	Support Systems Module
STK	System Tool Kit
TLE	Two-Line Element
UARS	Upper Atmosphere Research Satellite
UT	Universal Time

UV	Ultraviolet
VOP	Variation of Parameters
WFPC-II	Wide field Planetary Camera 2
WPP	World Population Prospects

15.0 References

1. “Annual Lifetime Predictions Flight Dynamics Facility (FDF),” Flight Dynamics Support Services-III Task Order 109, Document Control Number: FDSS-III-109-0002, Version 8.1, February 13, 2025.

2. Griffin, T. et al., “An Early Study of Disposal Options for the Hubble Space Telescope,” 6th European Conference on Space Debris, Volume 6, Issue 1, 2013.

3. Smith, R. et al., “Reentry Survivability analysis of the Hubble Space Telescope (HST)” Proceedings of the 4th European Conference on Space Debris (ESA SP-587), April 2005.

4. Baker, K. et al., “An Updated Re-entry Analysis of the Hubble Space Telescope,” First International Orbital Debris Conference, 2019.

5. NASA Technical Standard NASA-STD-8719.14C, “Process for Limiting Orbital Space Debris,” November 5, 2021.

6. Woodburn, J., Lynch, S., “A Numerical Study of Orbit Lifetime,” AAS 05-297, 2005.

7. Naasz, B., Berry, K., Schatten, K., “Orbit Decay Prediction Sensitivity to Solar Flux Variations,” AAS 07-264, 2007.

8. Jacchia, 1971, 1977 (Jacchia, L.G., "Revised Static Models of the Thermosphere and Exosphere with Empirical Temperature Profiles", Smithson. Astrophys. Special Report 332, 1971.

9. Roberts, C.E. An analytic model for upper atmosphere densities based upon Jacchia's 1970 models. *Celestial Mechanics* 4, p. 368-377 (1971). https://doi.org/10.1007/BF01231398.

10. Hedin, A. E. (1991), Extension of the MSIS Thermosphere Model into the middle and lower atmosphere, *J. Geophys. Res.*, 96(A2), 1159–1172, doi:10.1029/90JA02125.

11. Picone, J. M., A. E. Hedin, D. P. Drob, and A. C. Aikin, NRLMSISE-00 empirical model of the atmosphere: Statistical comparisons and scientific issues, *J. Geophys. Res.*, 107(A12), 1468, doi:10.1029/2002JA009430, 2002.

12. Bowman, B.R., et al., "The Thermospheric Semiannual Density Response to Solar EUV Heating," Journal of Atmospheric and Solar-Terrestrial Physics, doi:10.1016/j.jastp.2008.04.020, 2008

13. Bruinsma, S., “The DTM-2013 thermosphere model,” J. Space Weather Space Clim.

Volume 5, doi: 10.1051, 2015.

14. Emmert, et al., “NRLMSIS 2.0: A Whole-Atmosphere Empirical Model of Temperature and Neutral Species Densities,” *Earth and Space Science*, doi: 10.1029/2020EA001321, 2020.

15. Bruinsma, S., et al., “Thermosphere modeling capabilities assessment: geomagnetic storms,” J. Space Weather Space Climate, Volume 11, doi: 10.1051/swsc/2021001, 2021.

16. Bruinsma, et al., “Description and comparison of 21st century thermosphere data,” *Advances in Space* Research, Volume 72, Issue 12, p. 5476-5489, 2023.

17. Tapping, K., “The 10.7 cm solar radio flux ($F_{10.7}$),” *Space Weather*, volume 11, Issue 7, p. 394-406, 2013.

18. Schatten, K “Solar Activity Forecasting For Use in Orbit Propagation,” 2001

19. Folta, D., Baker, D., “Increased Ephemeris Accuracy Using Attitude-Dependent Aerodynamic Force Coefficients for Inertially Stabilized Spacecraft,” *Flight Mechanics Estimation Theory Symposium*, 1991.

20. Ostrom, C., et al., “Operational and Technical Updates to the Object Reentry Survival Analysis Tool”, International Orbital Debris Conference (IOC), 2019

21. Opiela, J., and Matney, M., Improvements to NASA’s Estimation of Ground Casualties from Reentering Space Objects, 54th International Astronautical Congress, IAC-03-IAA.5.4.03, Sept 29 – Oct 3, 2003, Bremen, Germany.

22. Baker, K., et. al, “An updated re-entry analysis of the Hubble Space Telescope”, First Int'l. Orbital Debris Conference, 2019.

23. NASA-STD-8719.25 Range Flight Safety Requirements

24. NASA Handbook 8719.14 - Handbook for Limiting Orbital Debris

25. United Nations, Department of Economic and Social Affairs, Population Division (2024). World Population Prospects 2024, Online Edition.

26. https://www.fao.org/faostat/en/#home United Nations, Food and Agriculture Organization, Statistics Division.

Appendix A Compliance Verification Summary using the DRAMA Tool Suite: Hubble re-entry Simulations

Western Science
Department of Physics and Astronomy
Western University

Compliance verification summary using the Debris Risk Assessment and Mitigation Analysis (DRAMA) tool suite

Hubble re-entry simulations

April 16, 2025

Author:
Maximilian Vovk

DRAMA Version: 3.1.0
SARA-REENTRY 2.1.3
ESA-DRAMA

Contents

List of Figures

List of Tables

1 Entry Assumptions

In this study, we simulate the atmospheric re-entry of the Hubble Space Telescope using ESA's DRAMA software suite. Specifically, we employ the SARA module to compute the re-entry trajectory and survivability of spacecraft components.

The orbital parameters for Hubble are extracted from publicly available two-line element sets (TLEs) provided by Heavens Above website[1].

The following TLE corresponds to the Hubble orbit on 2025/04/14 at 04:07:15.920 UTC:

```
1 20580U 90037B   25104.17171204  .00009507  00000-0  36811-3 0  9992
2 20580  28.4666 118.5846 0002299 110.7701 249.3139 15.24425514723164
```

The orbital elements derived from this TLE and used in the simulation are listed below:

Tab. 1–1: Orbital Elements of the Hubble Space Telescope (J2000)

Orbital Element	Value	Units
Semi-major axis (a)	6877.064	km
Eccentricity (e)	0.001326055	–
Inclination (i)	28.60851	degrees
Right Ascension of Ascending Node (Ω)	118.141975	degrees
Argument of Perigee (ω)	33.72206	degrees
True Anomaly (ν)	326.41296	degrees

Since the TLE-derived state lies well above the atmospheric interface, the re-entry trajectory must be propagated down to the re-entry boundary using the OSCAR module in DRAMA [1]. OSCAR accounts for long-term orbital decay under atmospheric drag, solar activity, and geomagnetic conditions by using the latest space weather forecasts and empirical density models provided by ESA.

Once the spacecraft descends below an altitude of 150 km, the simulation transitions from the OSCAR module to the SARA module. This handoff marks the beginning of the aerothermal re-entry phase, during which detailed modeling of fragmentation, thermal loads, and ground impact risk is performed.

Atmospheric density profiles during this phase are derived using the NRLMSISE-00 model, an empirical global reference atmosphere extending from the surface to space [1]. For middle- and upper-atmosphere wind fields, the HWM14 model is employed, providing latitude-, altitude-, and time-dependent horizontal wind components [1]. These models ensure physically consistent representation of the aerodynamic environment for breakup and survivability analysis.

[1] https://www.heavens-above.com/

2 Satellite structure

In this study, we use the material options available within the DRAMA framework, prioritizing those included in ESA's ESTIMATE database. The European Space maTerIal deMisability dATabasE (ESTIMATE)[1], developed by ESA's Space Debris Office, provides a curated list of commonly used spacecraft materials along with their thermophysical and structural properties relevant for re-entry survivability modeling.

We modeled the Hubble Space Telescope as a composite structure comprising a cylindrical main body with attached solar panels and four magnetictorquers. The main body houses both the payload and the satellite bus subsystems. The geometry and rough dimensions of each subsystem were defined based on publicly available NASA sources:

- Main body and mirror: https://science.nasa.gov/mission/hubble/overview/about-hubble/
- Electrical subsystem (battery cells and casing): https://science.nasa.gov/mission/hubble/observatory/design/electrical-power/
- Attitude control (magnetorquers and reaction wheels): https://science.nasa.gov/mission/hubble/observatory/design/pointing-control/

All four magnetic torquers and the solar panels are considered mechanically connected to the *Main Body*. A 3D representation of the modeled spacecraft assembly within DRAMA is shown in Figure 2–1.

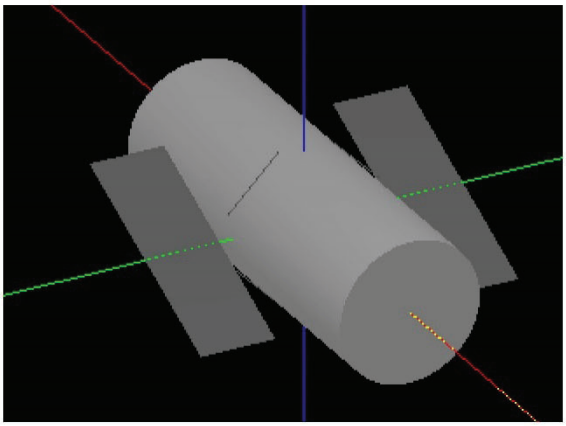

Fig. 2–1: DRAMA assembly view of the Hubble Space Telescope showing the cylindrical main body, four magnetorquers, and solar panels. The axes indicate 3D orientation. Red/yellow arrows indicate the direction of motion.

[1] https://estimate.sdo.esoc.esa.int/

We assume that the *Main Body* demises at approximately 78 km altitude, triggering the release of all internal subcomponents (referred to as children) at that point. This breakup altitude reflects dynamic pressure and thermal stress thresholds typically observed in re-entry events, consistent with empirical studies from Aerospace Corporation [2] and modeling assumptions in Smith et al. [3].

Table 2–1 summarizes the modeled subsystems, including their geometry, dimensions, masses, and associated materials from `ESTIMATE` or `DRAMA`'s internal library.

Tab. 2–1: Each object Mass, Geometry, and Material. Children of the *Main Body* are grouped below it (excluding Magnetic Torquers and Solar Panels).

Name	Quantity	Geometry	Dimensions	Mass [kg]	Material
– MagneticTorquers –					
TLx MagneticTroquer	1	Cylinder	Radius: 0.02 m, Height: 2.4 m	10	drama-Copper
TRx MagneticTroquer	1	Cylinder	Radius: 0.02 m, Height: 2.4 m	10	drama-Copper
BLx MagneticTroquer	1	Cylinder	Radius: 0.02 m, Height: 2.4 m	10	drama-Copper
BRx MagneticTroquer	1	Cylinder	Radius: 0.02 m, Height: 2.4 m	10	drama-Copper
– Solar Panels –					
Rx Solar panels	1	Box	Width: 2.44 m, Height: 0.01 m, Length: 7.54 m	27.60	drama-SolarPanel-Mat
Lx Solar panels	1	Box	Width: 2.44 m, Height: 0.01 m, Length: 7.54 m	27.60	drama-SolarPanel-Mat
Main Body	1	Cylinder	Radius: 2.3 m, Height: 13.0 m	1243.15	drama-AA7075
Battery Casing	2	Box	Width: 1.0 m, Height: 0.2 m, Length: 0.2 m	2.0	drama-Inconel718
Battery-Cells	3	Box	Width: 0.45 m, Height: 0.191 m, Length: 0.232 m	18.0	drama-Bat-NiCd
Mirror	1	Cylinder	Radius: 1.2 m, Height: 0.1 m	828.0	drama-FusedSilicaProxy
ReactionWheels	2	Cylinder	Radius: 0.5 m, Height: 0.2 m	45.0	drama-A316
Low Gain Antenna	2	Cylinder	Radius: 0.02 m, Height: 1.0 m	2.0	drama-AA7075

Each geometry will start to lose mass when the average temperature of the body reaches the melting temperature [4], as governed by the thermal energy balance:

$$Q = Q_c + Q_r + Q_d - \sigma \varepsilon T^4 A_r \tag{2–1}$$

$$\frac{\mathrm{d}m}{\mathrm{d}t} = 0 \qquad \frac{\mathrm{d}T}{\mathrm{d}t} = \frac{Q}{c_p m} \qquad for \quad T < T_{melt} \tag{2–2}$$

$$\frac{\mathrm{d}m}{\mathrm{d}t} = -\frac{Q}{H} \qquad \frac{\mathrm{d}T}{\mathrm{d}t} = 0 \qquad for \quad T \geq T_{melt} \tag{2–3}$$

Where $\frac{dm}{\mathrm{d}t}$ is the fraction of mass loss in time, T is the average temperature, c_p the specific heat capacity, H the specific heat of melting of the material and Q is the total heat flux where Q_c is convective incoming heat flux, Q_r is radiative incoming heat flux and Q_d conductive heat flux while ε is the material emissivity, σ is the Stefan-Boltzmann constant and A_r is the effective radiation surface.

The *Main Body* shields internal components until it demises or reaches the predefined breakup altitude of 78 km, at which point all children are released at a nominal temperature of 300 K.

The children at the relies are :

- the two **battery casing** (which houses 3 **battery cells**),

- the two **Low Gain Antenna** (LGA), and
- the four **Reaction Wheels**

Each comes from a different modeled subsystem :

- The **internal power subsystem** is modeled via the battery casing and battery cells.
- The **Attitude and Orbit Control Subsystem (AOCS)** is represented by the four magnetorquers and reaction wheels.
- The **Communication subsystem** is represented by the two low gains antennas (LGAs) mounted on the bus.

This modular separation between payload and platform is consistent with the breakdown used in Smith et al. [3], and enables independent survivability assessments of each subsystem during re-entry.

3 Re-entry Simulation Results

The re-entry simulation was conducted using ESA's DRAMA SARA module under the assumption of an uncontrolled, circular orbital decay trajectory.

During the simulations, the demise altitude triggers the release of child objects. Fragments are classified as uncritical once their impact kinetic energy falls below the 15 J casualty threshold, consistent with DRAMA's lethality criteria.

The re-entry simulation or the casualty probability was conducted under the assumption of an uncontrolled circular orbital decay trajectory with a global casualty threshold of 15 J [4] and using 3 different population growth scenarios : LOW VARIANT, MEDIUM VARIANT and HIGH VARIANT.

3.1 Effect of Spacecraft Orientation on Re-entry Conditions

Prior to breakup, the satellite is expected to generally align with the direction of motion; however, the exact orientation depends on the spacecraft's mass distribution and aerodynamic stability. To reflect these uncertainties, three orientation configurations of the Hubble were tested, one that maximize the drag, one that minimize the drag and a random tumbling state. In all cases, released subcomponents (children) were assumed to enter a random tumbling state upon separation, consistent with DRAMA's default behavior and the expected dynamics of spacecraft fragmentation.

It is important to note that the exact geodetic and dynamic conditions at the atmospheric entry interface—where the simulation transitions from OSCAR to SARA—differ depending on the spacecraft orientation and drag profile. To account for this, we provide a set of entry state tables that summarize the geodetic coordinates and trajectory angles at the first time step of SARA for each tested configuration.

In these tables, the heading angle is measured clockwise from true north, such that a value of 90° corresponds to an eastward trajectory.

3.1.1 Maximizing the Drag Coefficient

In this run, the Hubble Space Telescope was modeled with its main cylindrical body aligned to its widest cross-section in the direction of motion, thereby maximizing its drag coefficient and accelerating orbital decay.

Tab. 3–1: Initial Re-entry State at SARA Entry Interface (Highest Drag Configuration)

Parameter	Value	Unit
Altitude	125.031	km
Latitude	20.022	degrees
Longitude	-0.898	degrees
Velocity	7.422	km/s
Flight Path Angle	-0.03820	degrees
Heading Angle	113.15244	degrees

Key results:

- **Total number of fragments:** 11 (3 unique)
- **Total impact mass:** 1068.1 kg
- **Total casualty area:** 17.22 m^2
- **Total casualty probability (1D) for different population variant:** LOW 3.82×10^{-4} MEDIUM 3.80×10^{-4} HIGH 3.84×10^{-4}

Surviving Fragments and Associated Risk:

- **Primary Mirror:** 828 kg; average casualty area: 4.69 m^2; casualty probability: 1.04×10^{-4}; Max Downrange 13480.644 km
- **Reaction Wheels (4 units):** 45 kg total; average casualty area: 1.80 m^2; casualty probability: 3.97×10^{-5}; Max Downrange 13122.044 km
- **Battery Cells (6 units):** 10.02 kg total; average casualty area: 0.89 m^2; casualty probability: 1.96×10^{-5}; Max Downrange 13297.987 km

Max downrange difference between fragments : 358.6 km

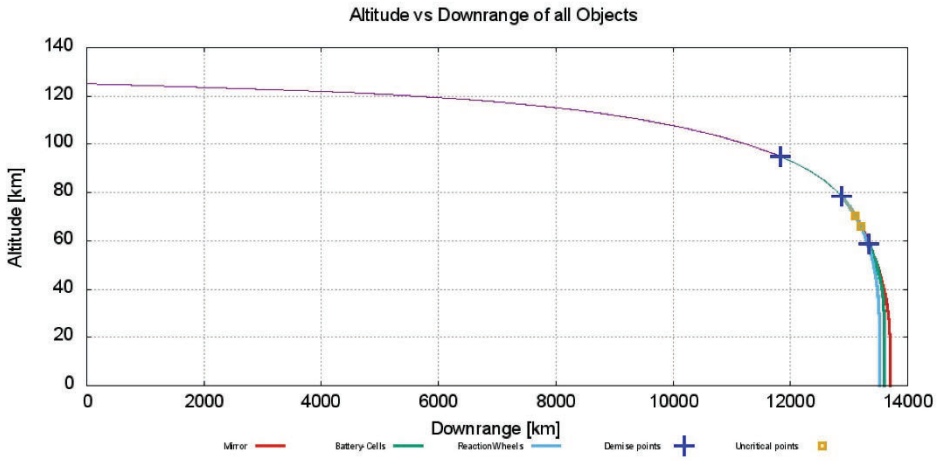

Fig. 3–1: Altitude vs. Downrange distance for the main body during re-entry. The steep descent profile reflects the high drag configuration of the satellite.

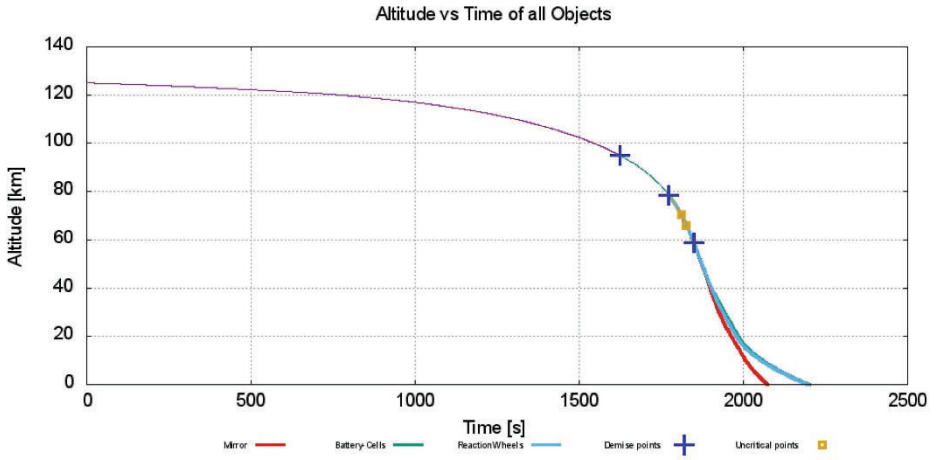

Fig. 3–2: Altitude vs. Time for the main body from re-entry interface to fragmentation. Breakup occurs near 78 km, followed by rapid descent of surviving fragments.

3.1.2 Minimizing the Drag Coefficient

To assess the range of possible outcomes for Hubble's re-entry, an additional run was conducted assuming the spacecraft's main body was aligned to minimize drag — i.e., oriented such that the narrowest cross-sectional area faced the direction of motion.

Tab. 3–2: Initial Re-entry State at SARA Entry Interface (Lowest Drag Configuration)

Parameter	Value	Unit
Altitude	124.962	km
Latitude	17.301	degrees
Longitude	14.550	degrees
Velocity	7.422	km/s
Flight Path Angle	-0.02363	degrees
Heading Angle	115.05219	degrees

Key results:

- **Total number of fragments:** 11 (3 unique)
- **Total impact mass:** 1052.4 kg
- **Total casualty area:** 17.22 m^2
- **Total casualty probability (1D) for different population variant:** LOW 3.98×10^{-4} MEDIUM 3.94×10^{-4} HIGH 4.02×10^{-4}

Surviving Fragments and Associated Risk:

- **Primary Mirror:** 828 kg; average casualty area: 4.69 m^2; casualty probability: 1.07×10^{-4}; Max Downrange 22188.211 km
- **Reaction Wheels (4 units):** 45 kg total; average casualty area: 1.80 m^2; casualty probability: 4.11×10^{-5}; Max Downrange 21782.931 km
- **Battery Cells (6 units):** 7.40 kg total; average casualty area: 0.89 m^2; casualty probability: 2.03×10^{-5}; Max Downrange 21974.146 km

Max downrange difference between fragments : 405.28 km

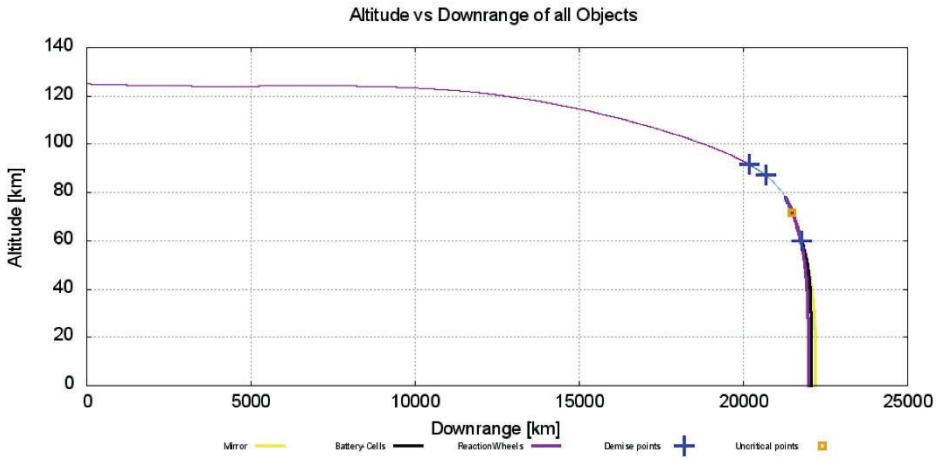

Fig. 3–3: Altitude vs. Downrange distance for the minimum drag case. The shallower entry angle results in a longer flight path through the upper atmosphere.

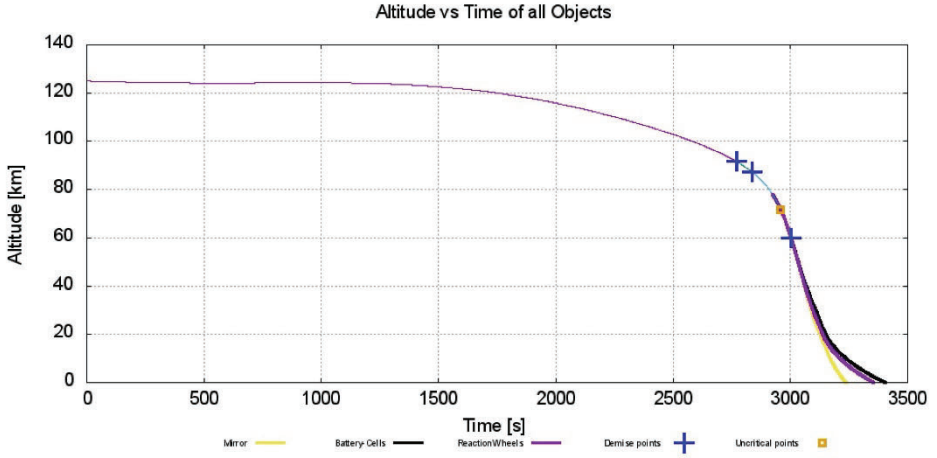

Fig. 3–4: Altitude vs. Time for the minimum drag configuration. The descent duration is extended, leading to a longer heating phase.

3.1.3 Random Tumbling Configuration

A third simulation scenario was conducted assuming the Hubble Space Telescope entered a random tumbling state prior to breakup. This represents a realistic and frequently observed condition for uncontrolled re-entry objects, where attitude control is lost during decay and aerodynamic torques induce chaotic rotation.

Tab. 3–3: Initial Re-entry State at SARA Entry Interface (Random Tumbling Configuration)

Parameter	Value	Unit
Altitude	124.957	km
Latitude	-16.523	degrees
Longitude	-94.997	degrees
Velocity	7.420	km/s
Flight Path Angle	-0.03150	degrees
Heading Angle	65.09831	degrees

Key results:

- **Total number of fragments:** 11 (3 unique)
- **Total impact mass:** 1047.4 kg
- **Total casualty area:** 17.22 m^2
- **Total casualty probability (1D) for different population variant:** LOW 3.82×10^{-4} MEDIUM 3.80×10^{-4} HIGH 3.84×10^{-4}

Surviving Fragments and Associated Risk:

- **Primary Mirror:** 828 kg; average casualty area: 4.69 m^2; casualty probability: 1.04×10^{-4}; Max Downrange 15093.366 km
- **Reaction Wheels (4 units):** 45 kg total; average casualty area: 1.80 m^2; casualty probability: 3.97×10^{-5}; Max Downrange 14883.104 km
- **Battery Cells (6 units):** 6.56 kg total; average casualty area: 0.89 m^2; casualty probability: 1.96×10^{-5}; Max Downrange 14960.080 km

Max downrange difference between fragments : 210.262 km

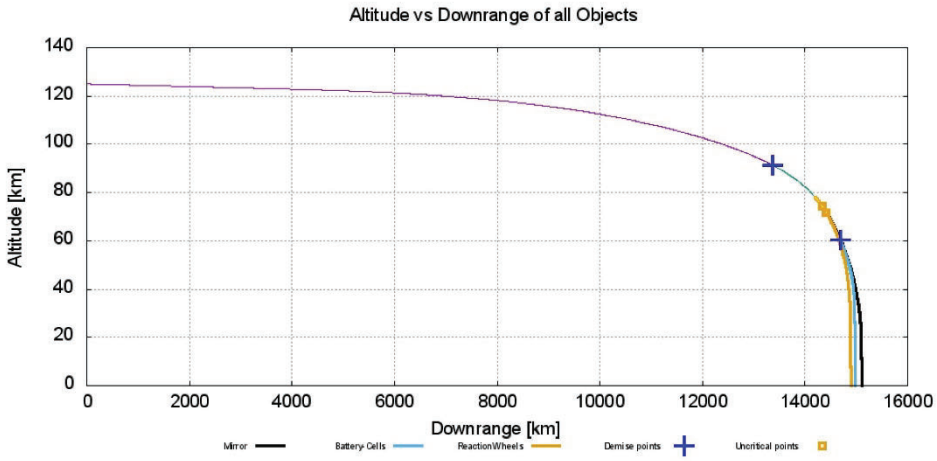

Fig. 3–5: Altitude vs. Downrange distance for the tumbling configuration. The flight path is intermediate between high and low drag scenarios.

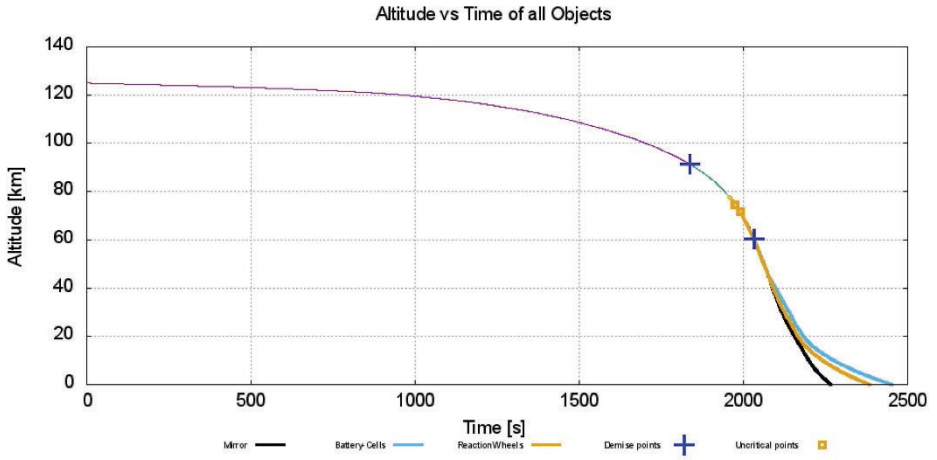

Fig. 3–6: Altitude vs. Time profile of the tumbling Hubble main body during re-entry. Dynamic variation in drag leads to complex descent behavior.

3.2 Impact and Casualty Probability Distributions

The re-entry simulations were performed using ESA's DRAMA SARA module under the assumption of an uncontrolled, circular orbital decay trajectory. Several global population growth scenarios— Low-Variant, Medium-Variant, and High-Variant —were evaluated using DRAMA's built-in configuration options. However, as the Hubble Space Telescope orbits at an inclination of $28.5°$, the region of potential impact is geographically constrained to latitudes between $-28.5°$ and $+28.5°$. As a result, overall casualty risk distributions remained broadly similar across the different population models.

After fragmentation, SARA propagates the surviving fragments and computes both impact and casualty probabilities using a one-dimensional (1D) population density projection along latitude. A fragment contributes to the casualty probability only if its kinetic energy upon impact exceeds the predefined threshold—set in this study to the default value of 15 J. This threshold approximates the minimum energy at which a fragment is likely to cause injury to a person on the ground [4].

The resulting latitude-dependent 1D impact and casualty probability distributions for the uncontrolled re-entry are shown in Figures 3–7 and 3–8, respectively.

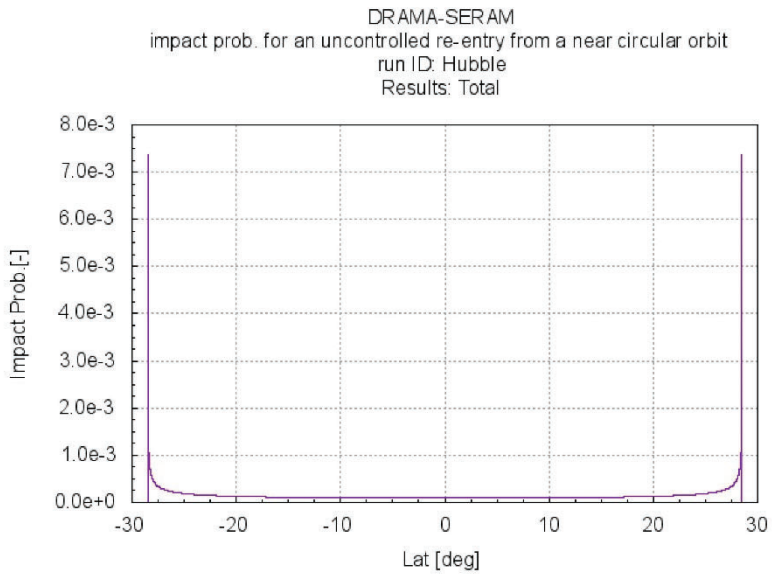

Fig. 3–7: 1D impact probability distribution by latitude for an uncontrolled circular re-entry at $28.5°$ inclination.

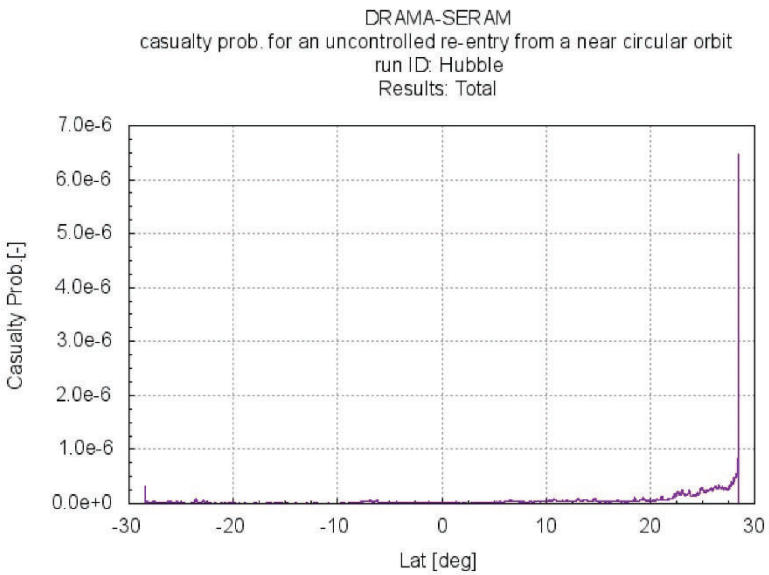

Fig. 3–8: Casualty probability distribution by latitude for fragments with impact energy exceeding 15 J.

3.2.1 Re-entry Risk Sensitivity to Impact Location

To illustrate how impact location influences casualty risk—particularly between sparsely and densely populated regions—a Monte Carlo analysis was performed under a controlled re-entry scenario. The initial true anomaly was randomly perturbed within a range of $\pm 1^\circ$ across 50 trajectories, introducing realistic targeting uncertainties.

This allowed us to assess the sensitivity of risk outcomes to small changes in entry timing and trajectory, which in turn affect the final impact location. The analysis was repeated across three global population growth scenarios—`Low-Variant`, `Medium-Variant`, and `High-Variant`—to account for demographic variability.

Tab. 3–4: Casualty Probability Summary by Population Growth Scenario (Monte Carlo Analysis)

Scenario	Min Prob.	Max Prob.	Mean Prob.	Standard Dev.
Low-Variant	4.03×10^{-5}	1.28×10^{-3}	3.70×10^{-4}	3.75×10^{-4}
Medium-Variant	3.21×10^{-5}	1.36×10^{-3}	3.96×10^{-4}	4.06×10^{-4}
High-Variant	3.67×10^{-5}	1.25×10^{-3}	3.14×10^{-4}	3.06×10^{-4}

These simulations show a wide spread in potential impact points, with longitudes ranging from -172.26° to 175.69°, and latitudes confined to the ±28.5° band. While overall trends were consistent across the three scenarios, localized differences in ground

tracks and regional population density led to variation in the calculated casualty probabilities.

According to ISO 24113:2019(E), the accepted upper limit for casualty probability in a re-entry scenarios is 1×10^{-4} [5]. In the Monte Carlo simulations, several trajectories exceed this threshold, particularly those resulting in landfall over highly populated regions. The lowest-risk scenario corresponds to an impact in the remote South Pacific Ocean near Point Nemo, yielding a casualty probability of approximately 3.2×10^{-5}. Conversely, the highest-risk case—approaching 1.3×10^{-3}—results from an impact over India, one of the most densely populated areas on the planet.

These findings underscore the critical importance of precision targeting and controlled de-orbit planning for large spacecraft like the Hubble Space Telescope.

Bibliography

[1] ESA/ESOC Space Debris Office, *DRAMA Software User Manual*, 2023, version 3.0. [Online]. Available: https://sdup.esoc.esa.int/drama/downloads/documentation/DRAMA-Software-User-Manual.pdf

[2] O. Refling, R. Stern, and C. Potz, "Review of orbital reentry risk predictions," The Aerospace Corporation, Tech. Rep. ATR-92(2835)-1, Jul 1992.

[3] R. Smith, K. Bledsoe, J. Dobarco-Otero, W. Rochelle, N. Johnson, A. Pergosky, and M. Weiss, "Reentry survivability analysis of the hubble space telescope (hst)," vol. 587, p. 527, 2005.

[4] ESA/ESOC Space Debris Office, "Drama 3.0 final report," European Space Agency (ESA), Tech. Rep., 2023, dRAMA-3.0.0-Final-Report. [Online]. Available: https://sdup.esoc.esa.int/drama/downloads/documentation/DRAMA-3.0.0-Final-Report.pdf

[5] International Organization for Standardization, "ISO 24113:2019 - space systems – space debris mitigation requirements," https://www.iso.org/standard/72383.html, 2019, third edition, ISO 24113:2019(E).

4 Appendix

4.1 Comparison with Previous Hubble Re-entry Results

Our simulation results show strong agreement with previous Hubble re-entry analyses performed using NASA's `ORSAT` tool [3], particularly regarding the survivability of major components such as the primary mirror and the reaction wheel assemblies. The most notable divergence lies in the fate of the battery subsystem. In our study, the battery cells—modeled with Inconel casings—survive atmospheric re-entry, whereas Smith et al. [3] did not report battery survival. This discrepancy likely arises from differences in modeling assumptions, such as the treatment of thermal shielding, material properties, or the orbital decay trajectory used at the point of breakup.

Importantly, the battery subsystem is among the most borderline components in terms of ablation survivability. It is more prone to ablation than other surviving elements such as the mirror or reaction wheels, and slight changes in re-entry conditions can render the batteries non-critical by the time they reach lower altitudes. As such, the outcome for the battery system is sensitive and could vary between studies depending on implementation specifics.

Another key distinction lies in the fragmentation approach. Smith et al. [3] modeled a significantly higher number of fragments, which led to a cumulative casualty area of 146.2 m^2 for an orbital decay re-entry at 28.5° inclination. This resulted in an overall casualty risk of approximately 2.94×10^{-3}—an order of magnitude above the accepted safety threshold of 1×10^{-4} as defined in ISO 24113:2019(E) [5].

Although our study employs a more conservative fragmentation scheme with fewer unique fragments, all configurations still yielded casualty probabilities above the NASA threshold. Specifically, the calculated 1D casualty probabilities for uncontrolled re-entry scenarios ranged between 3.80×10^{-4} and 4.02×10^{-4}.

These findings reaffirm the Hubble Space Telescope's high-risk profile in the event of an uncontrolled re-entry and underscore the importance of pursuing a controlled de-orbit strategy to ensure compliance with international safety guidelines.

Appendix B Compliance Verification Summary using the DRAMA Tool Suite: Hubble Re-entry Simulations with ORSAT Paper Data

Western Science
Department of Physics and Astronomy
Western University

Compliance verification summary using the Debris Risk Assessment and Mitigation Analysis (DRAMA) tool suite

Hubble re-entry simulations with ORSAT paper data

April 21, 2025

Author:
Maximilian Vovk

DRAMA Version: 3.1.0
SARA-REENTRY 2.1.3
ESA-DRAMA

Contents

List of Figures

List of Tables

1 Entry Assumptions

In this study, we simulate the atmospheric re-entry of the Hubble Space Telescope using ESA's DRAMA software suite. Specifically, we employ the SARA module to compute the re-entry trajectory and survivability of spacecraft components.

The orbital parameters for Hubble are extracted from publicly available two-line element sets (TLEs) provided by Heavens Above website[1].

The following TLE corresponds to the Hubble orbit on 2025/04/14 at 04:07:15.920 UTC:

```
1 20580U 90037B   25104.17171204  .00009507  00000-0  36811-3 0  9992
2 20580  28.4666 118.5846 0002299 110.7701 249.3139 15.24425514723164
```

The orbital elements derived from this TLE and used in the simulation are listed below:

Tab. 1–1: Orbital Elements of the Hubble Space Telescope (J2000)

Orbital Element	Value	Units
Semi-major axis (a)	6877.064	km
Eccentricity (e)	0.001326055	–
Inclination (i)	28.60851	degrees
Right Ascension of Ascending Node (Ω)	118.141975	degrees
Argument of Perigee (ω)	33.72206	degrees
True Anomaly (ν)	326.41296	degrees

Since the TLE-derived state lies well above the atmospheric interface, the re-entry trajectory must be propagated down to the re-entry boundary using the OSCAR module in DRAMA [1]. OSCAR accounts for long-term orbital decay under atmospheric drag, solar activity, and geomagnetic conditions by using the latest space weather forecasts and empirical density models provided by ESA.

Once the spacecraft descends below an altitude of 150 km, the simulation transitions from the OSCAR module to the SARA module. This handoff marks the beginning of the aerothermal re-entry phase, during which detailed modeling of fragmentation, thermal loads, and ground impact risk is performed.

Atmospheric density profiles during this phase are derived using the NRLMSISE-00 model, an empirical global reference atmosphere extending from the surface to space [1]. For middle- and upper-atmosphere wind fields, the HWM14 model is employed, providing latitude-, altitude-, and time-dependent horizontal wind components [1]. These models ensure physically consistent representation of the aerodynamic environment for breakup and survivability analysis.

[1] https://www.heavens-above.com/

2 Satellite structure

In this study, we use the material options available within the DRAMA framework, prioritizing those included in ESA's ESTIMATE database. The European Space maTerIal deMisability dATabasE (ESTIMATE)[1], developed by ESA's Space Debris Office, provides a curated list of commonly used spacecraft materials along with their thermophysical and structural properties relevant for re-entry survivability modeling. The rest of the dimensions has been taken from the excel sheet given.

We modeled the Hubble Space Telescope as a composite structure comprising a cylindrical main body with attached solar panels, four magnetictorquers and Aperture Door. All four magnetictorquers, the solar panels and Aperture Door are considered mechanically connected to the *Main Body*. The *Main Body* houses both the payload and the satellite bus subsystems. A 3D representation of the modeled spacecraft assembly within DRAMA is shown in Figure 2–1.

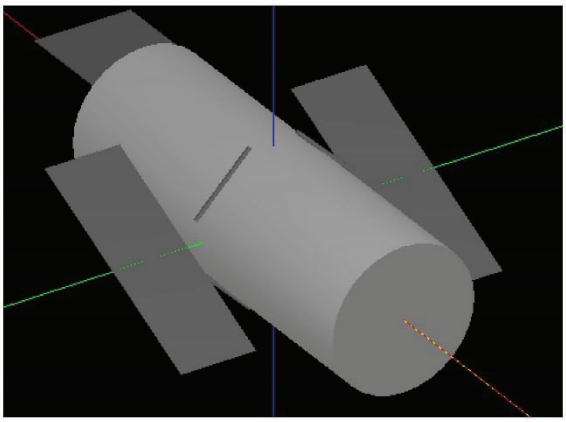

Fig. 2–1: DRAMA assembly view of the Hubble Space Telescope showing the cylindrical main body, four magnetorquers, solar panels and Aperture Door. The axes indicate 3D orientation. Red/yellow arrows indicate the direction of motion.

We assume that the *Main Body* demises at approximately 78 km altitude, triggering the release of all internal subcomponents (referred to as children) at that point. This breakup altitude reflects dynamic pressure and thermal stress thresholds typically observed in re-entry events, consistent with empirical studies from Aerospace Corporation [2] and modeling assumptions in Smith et al. [3].

Table 2–1 summarizes the modeled subsystems, including their geometry, dimensions, masses, and associated materials from ESTIMATE or DRAMA's internal library.

[1] https://estimate.sdo.esoc.esa.int/

Tab. 2–1: Each object Mass, Geometry, and Material. Children of the *Main Body* are grouped below it (excluding Magnetic Torquers and Solar Panels).

Name	Quantity	Geometry	Dimensions	Mass [kg]	Material
– Magnetic Torquers –					
TLx MagneticTroquer	1	Cylinder	Radius: 0.066 m, Height: 2.489 m	43.00	drama-Iron
TRx MagneticTroquer	1	Cylinder	Radius: 0.066 m, Height: 2.489 m	43.00	drama-Iron
BLx MagneticTroquer	1	Cylinder	Radius: 0.066 m, Height: 2.489 m	43.00	drama-Iron
BRx MagneticTroquer	1	Cylinder	Radius: 0.066 m, Height: 2.489 m	43.00	drama-Iron
– Solar Panels –					
Rx Solar Panels	1	Box	Width: 2.44 m, Height: 0.01 m, Length: 7.54 m	27.60	drama-SolarPanel-Mat
Lx Solar Panels	1	Box	Width: 2.44 m, Height: 0.01 m, Length: 7.54 m	27.60	drama-SolarPanel-Mat
Aperture Door	1	Box	Width: 3.099 m, Height: 0.038 m, Length: 3.099 m	41.78	drama-AA7075
Main Body	1	Cylinder	Radius: 2.3 m, Height: 13.0 m	1243.15	drama-AA7075
Battery Enclosure	2	Box	Width: 0.914 m, Height: 0.808 m, Length: 0.363 m	49.24	drama-AA7075
Battery-Cells	69	Cylinder	Radius: 0.09 m, Height: 0.236 m	2.34	drama-Inconel718
Primary Mirror	1	Box	Width: 2.195 m, Height: 2.195 m, Length: 0.33 m	1005.16	drama-FusedSilicaProxy
Secondary Mirror	1	Cylinder	Radius: 0.322 m, Height: 0.058 m	12.80	drama-ZerodurProxy
RWA Housing	2	Cylinder	Radius: 0.301 m, Height: 0.527 m	46.72	drama-AA7075
ReactionWheels	2	Cylinder	Radius: 0.24 m, Height: 0.254 m	20.05	drama-A316
Low Gain Antenna Fwd	1	Box	Width: 0.113 m, Height: 0.059 m, Length: 5.224 m	9.89	drama-AA7075
Low Gain Antenna Shield	1	Box	Width: 0.113 m, Height: 0.059 m, Length: 7.812 m	14.79	drama-AA7075
Main Ring	1	Cylinder	Radius: 1.5 m, Height: 0.381 m	449.06	drama-TiAl6v4
Antenna Ballast Block	4	Box	Width: 0.203 m, Height: 0.027 m, Length: 0.041 m	3.68	drama-Tungsten
Axial Fittings	1	Box	Width: 0.146 m, Height: 0.228 m, Length: 0.715 m	23.10	drama-A316
Base Disk	1	Box	Width: 0.07 m, Height: 0.04 m, Length: 0.07 m	1.92	drama-Molybdenum
Bracket Assy	1	Box	Width: 0.357 m, Height: 0.036 m, Length: 0.5 m	6.80	drama-TiAl6v4
Mast Base	1	Cylinder	Radius: 0.089 m, Height: 0.276 m	5.90	drama-TiAl6v4
Opt. Bench Struct.	1	Box	Width: 0.305 m, Height: 0.016 m, Length: 0.381 m	6.10	drama-Invar

Each geometry will start to lose mass when the average temperature of the body reaches the melting temperature [4], as governed by the thermal energy balance:

$$Q - Q_c + Q_r + Q_d - \sigma \varepsilon T^4 A_r \tag{2–1}$$

$$\frac{\mathrm{d}m}{\mathrm{d}t} = 0 \qquad \frac{\mathrm{d}T}{\mathrm{d}t} = \frac{Q}{c_p m} \qquad for \quad T < T_{melt} \tag{2–2}$$

$$\frac{\mathrm{d}m}{\mathrm{d}t} = -\frac{Q}{H} \qquad \frac{\mathrm{d}T}{\mathrm{d}t} = 0 \qquad for \quad T \geq T_{melt} \tag{2–3}$$

Where $\frac{\mathrm{d}m}{\mathrm{d}t}$ is the fraction of mass loss in time, T is the average temperature, c_p the specific heat capacity, H the specific heat of melting of the material and Q is the total heat flux where Q_c is convective incoming heat flux, Q_r is radiative incoming heat flux and Q_d conductive heat flux while ε is the material emissivity, σ is the Stefan-Boltzmann constant and A_r is the effective radiation surface.

The *Main Body* shields internal components until it demises or reaches the predefined breakup altitude of 78 km, at which point all children are released at a nominal temperature of 300 K.

This modular separation between payload and platform is consistent with the breakdown used in Smith et al. [3], and enables independent survivability assessments of each subsystem during re-entry.

3 Re-entry Simulation Results

The re-entry simulation was conducted using ESA's DRAMA SARA module under the assumption of an uncontrolled, circular orbital decay trajectory.

During the simulations, the demise altitude triggers the release of child objects. Fragments are classified as uncritical once their impact kinetic energy falls below the 15 J casualty threshold, consistent with DRAMA's lethality criteria.

The re-entry simulation or the casualty probability was conducted under the assumption of an uncontrolled circular orbital decay trajectory with a global casualty threshold of 15 J [4] and using `Medium-Variant` population growth scenario.

To compute the casualty risk, a 1D latitude-based population model was used. This simplification is standard practice when the re-entry orbit is not precisely defined or the satellite's final breakup location is uncertain. By assuming a uniform distribution of population along latitude bands, the model captures the dominant effect of the satellite's orbital inclination on the potential impact zones. This approach is particularly suitable for early-stage analyses or general risk estimates, where detailed targeting information is not available. When precise orbit and satellite data are available precise 2D risk can be assessed.

3.1 Effect of Spacecraft Orientation on Re-entry Conditions

It is important to note that the exact geodetic and dynamic conditions at the atmospheric entry interface—where the simulation transitions from OSCAR to SARA—differ depending on the spacecraft orientation and drag profile. To account for this, we provide a table that summarize the geodetic coordinates and trajectory angles at the first time step of SARA where the downrange is considered 0.

In these tables, the heading angle is measured clockwise from true north, such that a value of 90° corresponds to an eastward trajectory.

3.1.1 Random Tumbling Configuration

The simulation scenario was conducted assuming the Hubble Space Telescope entered a random tumbling state prior to breakup. This represents a realistic and frequently observed condition for uncontrolled re-entry objects, where attitude control is lost during decay and aerodynamic torques induce chaotic rotation.

Tab. 3–1: Initial Re-entry State at SARA Entry Interface (Random Tumbling Configuration) where Downrange = 0

Parameter	Value	Unit
Altitude	90.984	km
Latitude	-13.455	degrees
Longitude	124.474	degrees
Velocity	7.315	km/s
Flight Path Angle	-0.55386	degrees
Heading Angle	116.77993	degrees

- **Total casualty area:** 120.40 m^2
- **Total impact mass:** 2083.27 kg
- **Total casualty probability (1D projection):** 2.71×10^{-3}

Maximum Downrange: 16,810.63 km at Latitude: $-20.70°$, Longitude: $141.31°$ (Antenna_Ballast_block)
Minimum Downrange: 16,462.94 km at Latitude: $-19.54°$, Longitude: $138.22°$ (Bracket_Assy)
Max downrange difference between fragments: 347.69 km

Tab. 3–2: Summary of Fragment Impact Parameters

Object Name	Qty	Material	Downrange (km)	Debr. Cas. Area (m^2)	Impact Mass (kg)	Impact Energy (J)
TLx_MagneticTroquer	1	drama-Iron	16614.259	1.2425	38.78	103818.54
TRx_MagneticTroquer	1	drama-Iron	16614.259	1.2425	38.78	103818.54
BLx_MagneticTroquer	1	drama-Iron	16614.259	1.2425	38.78	104212.92
BRx_MagneticTroquer	1	drama-Iron	16614.259	1.2425	38.78	104212.92
Antenna_Ballast_block	4	drama-Tungsten	16810.628	0.4711	3.68	35650.19
Primary_Mirror	1	drama-FusedSilicaProxy	16740.570	5.6175	1005.16	6152355.25
Secondary_Mirror	1	drama-ZerodurProxy	16471.181	1.0783	12.80	15736.81
Axial_Fittings	1	drama-A316	16611.963	0.9756	23.10	64037.47
Base_Disk	1	drama-Molybdenum	16709.401	0.4522	0.76	1996.84
Mast_Base	1	drama-TiAl6v4	16566.835	0.6821	5.90	12700.34
Bracket_Assy	1	drama-TiAl6v4	16462.936	0.8529	6.80	7869.80
Opt._Bench_Struct.	1	drama-Invar	16532.022	0.7262	6.10	10561.09
Main_Ring	1	drama-TiAl6v4	16543.530	7.3183	449.06	842213.94
Battery-Cells	138	drama-Inconel718	16553.207	0.6637	2.34	2154.58
ReactionWheels	4	drama-A316	16619.309	1.0641	20.05	39813.86

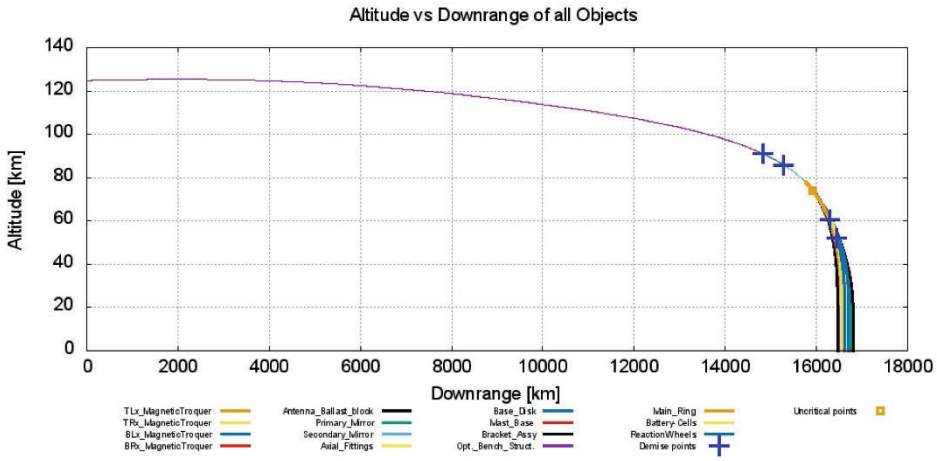

Fig. 3–1: Altitude vs. Downrange distance for the tumbling configuration. The flight path is intermediate between high and low drag scenarios.

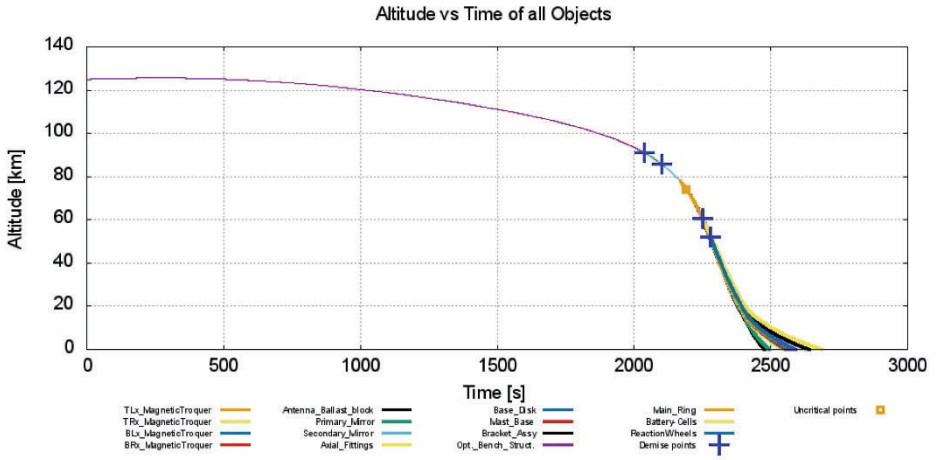

Fig. 3–2: Altitude vs. Time profile of the tumbling Hubble main body during re-entry. Dynamic variation in drag leads to complex descent behavior.

3.2 Impact and Casualty Probability Distributions

The re-entry simulations were performed using ESA's DRAMA SARA module under the assumption of an uncontrolled, circular orbital decay trajectory. As the Hubble Space Telescope orbits at an inclination of 28.5°, the region of potential impact is geographically constrained to latitudes between -28.5° and $+28.5^\circ$. As a result, overall casualty risk distributions remained broadly similar across the different population models.

After fragmentation, SARA propagates the surviving fragments and computes both impact and casualty probabilities using a one-dimensional (1D) population density projection along latitude. A fragment contributes to the casualty probability only if its kinetic energy upon impact exceeds the predefined threshold—set in this study to the default value of 15 J. This threshold approximates the minimum energy at which a fragment is likely to cause injury to a person on the ground [4].

The resulting latitude-dependent 1D impact and casualty probability distributions for the uncontrolled re-entry are shown in Figures 3–3 and 3–4, respectively.

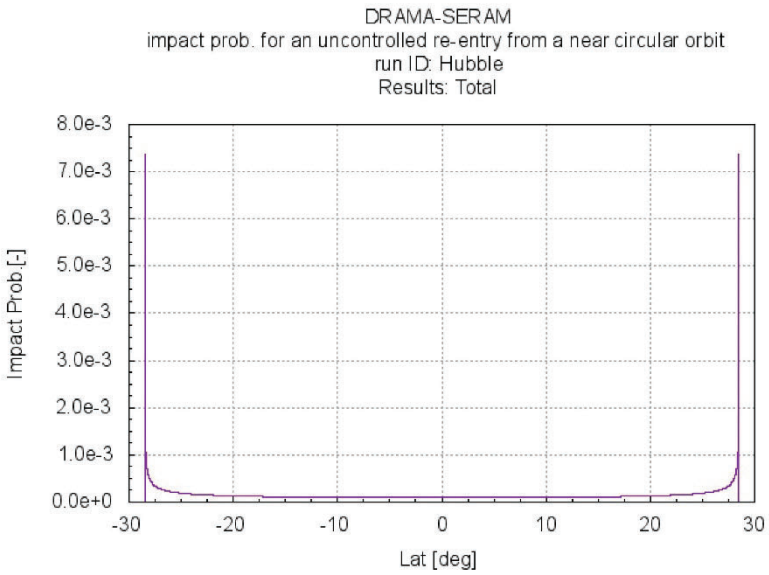

Fig. 3–3: 1D impact probability distribution by latitude for an uncontrolled circular re-entry at 28.5° inclination.

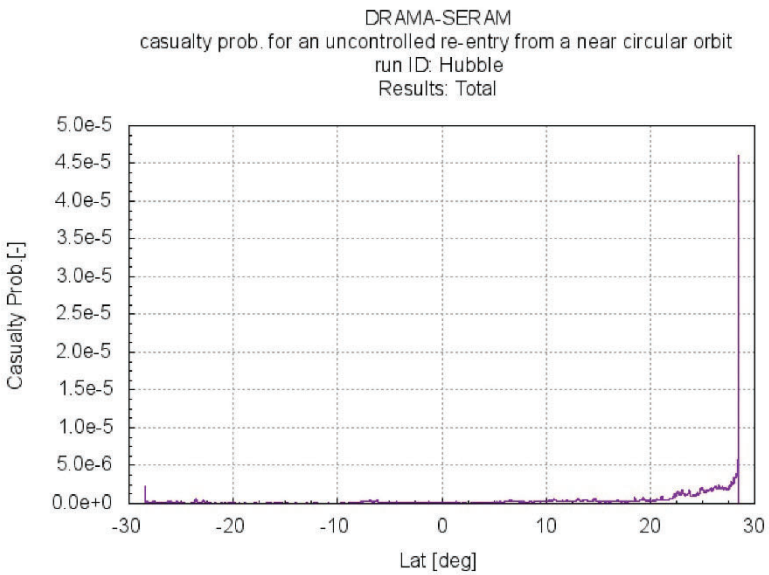

Fig. 3–4: Casualty probability distribution by latitude for fragments with impact energy exceeding 15 J.

3.2.1 Re-entry Risk Sensitivity to Impact Location

To investigate how the impact location affects casualty risk—particularly with respect to regional population density—a Monte Carlo simulation was conducted under a controlled re-entry scenario. The true anomaly at the start of the simulation was randomly perturbed within a range of $\pm 1^\circ$, generating 50 distinct trajectories.

The resulting spread in ground tracks revealed a broad range of potential impact locations, with longitudes spanning from -172.26° to 175.69°, and latitudes confined within the spacecraft's inclination band of $\pm 28.5^\circ$. While the general footprint of re-entry remained consistent, differences in impact regions led to notable variations in estimated casualty risk.

Casualty probability was evaluated using both the 1D and 2D methods defined in ESA's risk model. The 1D method integrates the impact probability across latitude bands, assuming a uniform longitudinal distribution used for uncontrolled reentry. In contrast, the 2D method accounts for both latitude and longitude, incorporating realistic population density maps to provide geographically weighted estimates used or controlled reenry. Consequently, the 2D method more accurately captures the influence of regional demographics.

- **1D Casualty Probability (TotalCasualty1D):**
  - Minimum: 2.60×10^{-4}

  - Maximum: 8.96×10^{-3}
  - Mean: 2.37×10^{-3}
  - Standard Deviation: 2.45×10^{-3}
- **2D Casualty Probability (TotalCasualty2D):**
  - Minimum: 0.00
  - Maximum: 4.59×10^{-2}
  - Mean: 2.55×10^{-3}
  - Standard Deviation: 7.83×10^{-3}

According to ISO 24113:2019(E), the accepted upper limit for casualty probability in spacecraft re-entry scenarios is 1×10^{-4} [5]. The results of this analysis indicate that multiple trajectories—particularly those leading to landfall over densely populated areas—exceed this threshold. The lowest-risk case, yielding a near-zero 2D casualty probability, corresponds to an impact near Point Nemo in the remote South Pacific Ocean. Conversely, the highest-risk scenarios involve trajectories intersecting densely populated regions such as India or Southeast Asia.

These results highlight the critical importance of controlled de-orbit strategies for large spacecraft such as the Hubble Space Telescope.

Bibliography

[1] ESA/ESOC Space Debris Office, *DRAMA Software User Manual*, 2023, version 3.0. [Online]. Available: https://sdup.esoc.esa.int/drama/downloads/documentation/DRAMA-Software-User-Manual.pdf

[2] O. Refling, R. Stern, and C. Potz, "Review of orbital reentry risk predictions," The Aerospace Corporation, Tech. Rep. ATR-92(2835)-1, Jul 1992.

[3] R. Smith, K. Bledsoe, J. Dobarco-Otero, W. Rochelle, N. Johnson, A. Pergosky, and M. Weiss, "Reentry survivability analysis of the hubble space telescope (hst)," vol. 587, p. 527, 2005.

[4] ESA/ESOC Space Debris Office, "Drama 3.0 final report," European Space Agency (ESA), Tech. Rep., 2023, dRAMA-3.0.0-Final-Report. [Online]. Available: https://sdup.esoc.esa.int/drama/downloads/documentation/DRAMA-3.0.0-Final-Report.pdf

[5] International Organization for Standardization, "ISO 24113:2019 - space systems – space debris mitigation requirements," https://www.iso.org/standard/72383.html, 2019, third edition, ISO 24113:2019(E).

Appendix C: Swift Observatory Decay Results

The Swift Observatory was at an altitude of 451 km as of April 2025 with 20.5-degree inclination and a nearly circular eccentricity. The Swift Observatory is already at a lower altitude than HST, has a much higher area-to-mass ratio; as a result, it is twice as sensitive to atmospheric drag than HST. The mass is approximately 1456 kg[11].

Similarly to HST, a run matrix was generated varying the key parameters in the decay equation such as area, drag coefficient, atmosphere model, TLEs and various interpretations of the solar activity model to produce a range of possible Swift reentry dates. Given the shortened time to produce results, a complete statistical analysis was not possible. Using extreme and average values can provide insight into the possible reentry timeframes acknowledging uncertainty exists in every part of this process.

As described above in section 7.2, the same process was followed to derive the drag coefficient that is bounded by the actual measured decay trend, Table C-1 shows the simulation results against the derived value.

Table C-1. Swift Simulation is Validated, Bounds Actual Swift Decay

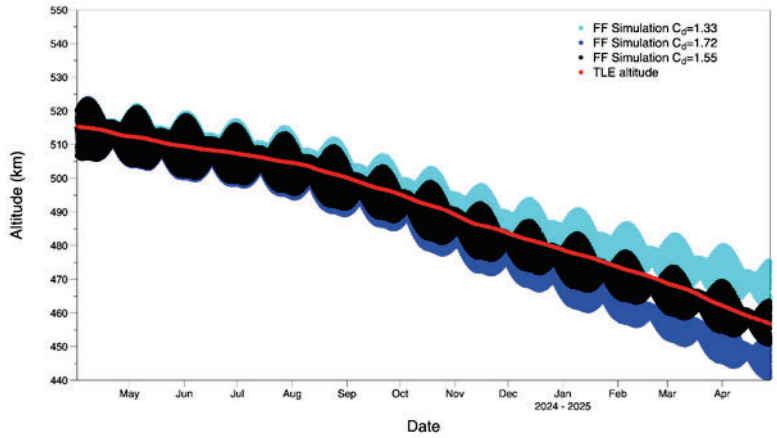

Results for an average cross-sectional area of 17.1 m^2, derived C_d of 1.55, MSIS atmosphere model, and 50th percentile solar activity prediction, MSAFE file produces a possible Swift reentry in June 2026. (F-10)

Assuming a higher projected area increases drag and shows earlier reentry times as early as December 2025. Using the minimal projected area pushes out that reentry. Varying drag coefficients to a higher +1 sigma value has a stronger effect on drag and reentry leading to a 2025 possibility, while a -1 sigma value pushes out the reentry into 2027. Likewise, an extreme solar prediction environment of 95th percentile produces a February of 2026 reentry, and a 5th percentile environment produces a later December 2026 date.

With this shortened decay timeline, there were little observed differences in dates between the JR and MSIS atmosphere models, and correcting the MSAFE space weather file to remove the Earth eccentricity variation amounted to a few days difference.

[11] *https://web.archive.org/web/20180624050438/http://swift.sonoma.edu/about_swift/general_faq.html*

Simulation setup included the following assumptions, models, environments and settings:

Initial Orbit Characteristics: TLE 04/25/2025 02:53:15.02

Height: 451.82 km

Eccentricity = 0.000567300

Inclination = 20.5547 degrees

Mass = 1456 kg

Effective Drag Area (Projected Surface Area) = 17.10 m^2

Drag Coefficient C_d = 2.18

Updated FF Simulations to use:

- Bodies – Sun, Earth, Moon
- Spherical SRP Model
- Gravitational Model 8x8 with solid tides
- SpaceTrak TLE from April 25, 2025, 02:53:15, initializes state
- Bulirsch-Stoer VOP, Integrator with Variable Step size
- Decay Altitude cutoff – 100km
- Updated space weather CelesTrak file- up to date observations through April 25, 2025

The results are shown in Figure 7.5-1. (O-2)

Table C-2. Swift Run Matrix Results for Various Parameters

Run No.	Solar Cycle	Atmosphere	Area (m^2)	Cd	Reentry Date	
1a	Celestrak MSAFE 50%	MSIS	17.08	2.2	January 31,2026	
2a	Celestrak MSAFE 50%	MSIS	17.08	2.5	December 25, 2025	
3a	Celestrak MSAFE 50%	MSIS	17.08	1.8	April 04,2026	
4a	Celestrak MSAFE 50%	MSIS	30.24	2.2	October 13, 2025	
4b	Celestrak MSAFE 50%	MSIS	30.24	2.18	October 14,2025	
4c	Celestrak MSAFE 50%	MSIS	30.24	1.55	December 07,2025	
5a	Celestrak MSAFE 50%	MSIS	22.92	2.2	November 23, 2025	
5b	Celestrak MSAFE 50%	MSIS	22.92	2.18	November 24, 2025	
5c	Celestrak MSAFE 50%	MSIS	22.92	1.55	February 17, 2026	
6a	Celestrak MSAFE 50%	JR	17.08	2.2	January 22, 2026	
7a	Celestrak MSAFE 50%	JR	17.08	2.5	December 21, 2025	
8a	Celestrak MSAFE 50%	MSIS	17.08	2.32	January 16, 2026	
10a	Celestrak MSAFE 50%	MSIS	17.08	2.37	January 10, 2026	
11a	Celestrak MSAFE 50%	MSIS	17.08	0.97	May 22, 2027	
12a	Celestrak MSAFE 50%	MSIS	17.08	3.77	October 17, 2025	
13a	MSAFE 5th (*)	MSIS	17.08	2.18	April 27, 2026	
14a	MSAFE 50th (*)	MSIS	17.08	2.18	January 29, 2026	
15a	MSAFE 50th (*)	MSIS	17.08	3.48	October 22, 2025	+1.3 1 sigma
16a	MSAFE 50th (*)	MSIS	17.08	0.88	October 9, 2027	-1.3 1 sigma
17a	MSAFE 95th (*)	MSIS	17.08	2.18	December 03, 2025	
18a	Celestrak MSAFE 50%	MSIS	17.08	1.55	June 08, 2026	
19a	MSAFE 50th (*)	MSIS	17.08	1.55	May 31, 2026	
20a	MSAFE 5th (*)	MSIS	17.08	1.55	December 02, 2026	
21a	MSAFE 95th (*)	MSIS	17.08	1.55	February 26, 2026	

* MSAFE 50th, removed oscillation of F10.7 due to variations in Earth's eccentricity

Considered Nominal Avg Cross-Sectional Area and Avg Cd

As with HST, the major takeaways from this run matrix confirm that extreme area presentations, extreme drag coefficients or extreme environments can dramatically alter the predicted reentry

times.(F-5) Notably, Swift is twice as sensitive to atmospheric drag because the (A/m) ratio is 2x bigger than HST even though the Swift Observatory is much smaller.

Comparing the NESC simulation results above for the nominal expected environment, area and drag, are within the family of the GSFC FDF probability distribution prediction results for Swift Observatory. See Figure C-2 below.

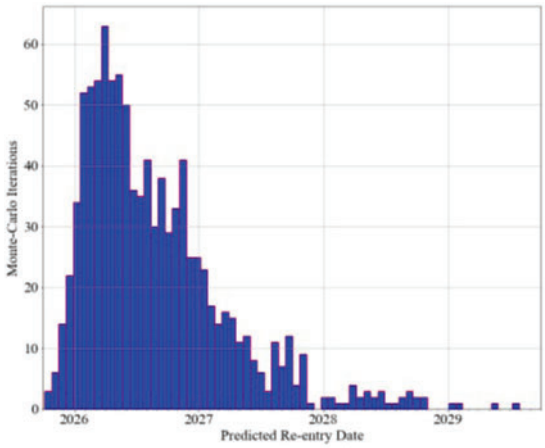

Figure C-1. GSFC FDF Probability Distribution of Swift Observatory Reentry Predictions

Reentry footprint and casualty risk were not analyzed for Swift due to the late request. It is recommended that given the earlier prediction timeline for Swift a formal analysis with higher fidelity modeling and tools be performed and reported to the appropriate Agency authority.

Appendix D: Stakeholder Briefing

Hubble Orbit Decay Study
TI-25-02088
May 21, 2025

NESC Lead, Heather Koehler
Technical Fellow Flight Mechanics

Hubble Space Telescope (HST) orbital decay is highly sensitive to the solar and geomagnetic activity, attitude and associated drag, and ballistic coefficient.

This study evaluated extreme predicted environments, historical sweep of actual environments, minimum and maximum projected HST areas and upper, lower, and nominal drag coefficients to bound possible reentry timelines.

The compressed timeline and available resources limited a more extensive study, but several findings, observations, and NASA Engineering and Safety Center (NESC) recommendations are included for consideration.

Results of the NESC study indicate that for *nominal* predicted solar activity, *average* projected area, and *expected* Coefficient of Drag (Cd), HST reentry is most likely to occur within a couple years of **2033**.

NESC also conducted a brief evaluation of the Swift decay and found in *nominal* cases, **reentry could be in mid 2026.**

HST Reentry/Footprint calculations show **casualty risk as high as 1:341** from 6 Degrees of Freedom (6DOF) Monte Carlo, exceeding the $1x10^{-4}$ limit over highest population landmass under the ground track; underscores critical importance of precision targeting and controlled de-orbit planning.

Analysis

- Driving Factors for Analysis
  - Hubble (HST) Overview
  - Solar Environment, Predictions
  - Spacecraft Drag Coefficient, Estimations
- Orbit Decay Simulation Results
  - FreeFlyer (FF) modeling inputs and results
- Reentry Simulation Results
  - Marshall Aerospace VEhicle Representation In C (MAVERIC) – 6DOF Monte Carlo simulation
  - ESA's Debris Risk Assessment Mitigation Analysis (DRAMA) tool suite
- Quick assessment of Swift Orbital Decay
- Findings, Observations, and NESC Recommendations
- Backup
  - Survey of HST Decay Predictions and Relevant Works (not included here today)

Hubble Overview

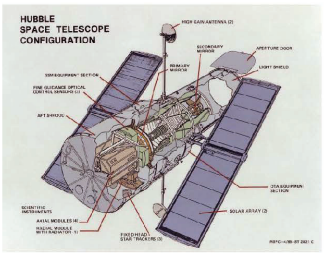

- Hubble currently at 489 km above Earth's surface, 28.46° inclination, near circular orbit
- (03/2025) GSFC Flight Dynamics Facility (FDF) reports actual orbital decay, dropping ~ 45 km since January 2022 and 5-6 km since January 2025
- Last servicing mission (2009) added ~400 kg, resulting in a 12,264 kg telescope

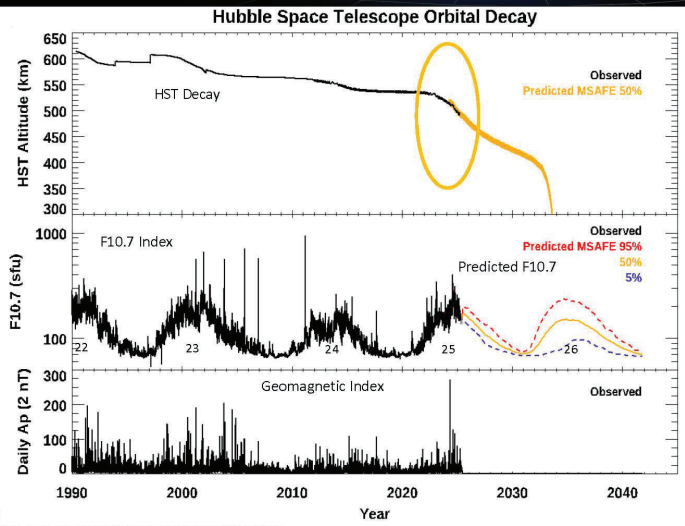

NESC Document #:

Restricted distribution to NE
This is for status only and does not represent complete engineering analysis.

Solar Cycle Predictions, F10.7 cm Index

- Solar emission intensity measured at 10.7-centimeter (cm) wavelength by Dominion Radio Astrophysical Observatory (Canada) , reported as the F10.7 index
  - F10.7 Correlates well with Ultra-Violet (UV)/Extreme Ultra-Violet (EUV) emissions responsible for heating Earth's upper atmosphere but measured from surface of Earth
  - Geomagnetic Indices Ap, Kp are measures of magnetic field disturbances and are proxies for magnetospheric energy input to Earth's upper atmosphere
  - Models of Earth's upper atmosphere use F10.7 solar activity index and the Ap or Kp geomagnetic index to produce neutral density values for computing drag force

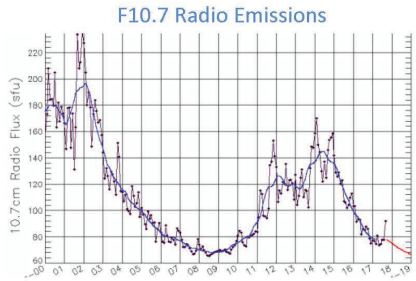

Marshall Solar Activity Future Estimation(MSAFE) Technique

- McNish-Lincoln linear regression method used for predicting remainder of current solar cycle
- Analysis of the past 24 complete solar cycles used to generate statistical estimates of F10.7 for the next complete solar cycle
- Most methods that predict solar and geomagnetic activity produce 'smoothed' F10.7 and Ap time series, but don't include observed daily F10.7 and Ap variability due to solar and geomagnetic activity, respectively

1 sfu = 10-22 W*m-2*Hz-1

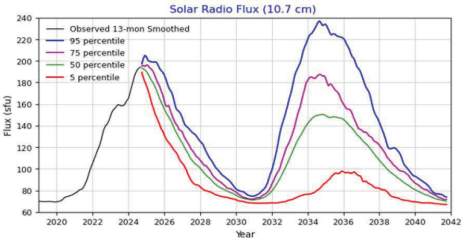

Spacecraft Drag Coefficient Estimations

"Virtually every term in the atmospheric drag force equation has a significant uncertainty." (Naasz, Berry, Schatten, AAS 07-264)

- NESC determined the average Coefficient of Drag, Cd, using the measured altitude decay profile in the equation for the loss in orbital energy

$$C_d = -\frac{2\pi m}{A\rho v^2 P}\frac{dR}{dt}$$

- Uncertainties in the atmospheric density and area to mass ratio cause wide scatter in the Cd's computed at the epoch of each state vector

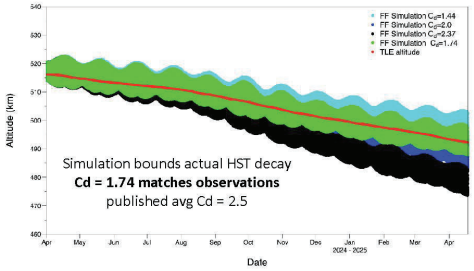

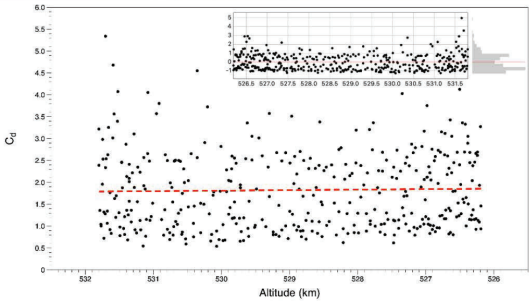

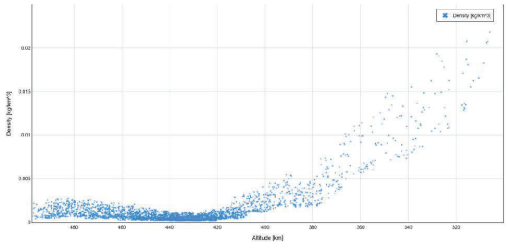

HST Decay Prediction Results

"The computation of orbit lifetime is extremely challenging. The abundance of uncertainty makes the results of any one prediction suspect." (Woodburn, Lynch, 2005)

- Varied area's: max, min, avg cross-sectional area's
- Average cross-sectional area = 71 m^2
- Expected Cd = 1.74-1.8
- Two atmosphere models, Jacchia-Roberts (JR) and NRL-MSIS
  - Differences of ~9-16 months with JR trending earlier
- MSAFE Space Weather File underpins both JR and MSIS models
- MSAFE Nominal 50%, extreme bounds of 5% and 95% select cases
- Running a different TLE (Epoch) ~ 1 mos difference
- CelesTrak space weather file has incorrect implementation of MSAFE
- Corrected MSAFE 50th solar activity file makes ~days difference in reentry over this time period

- Higher projected area could mean as early as fall 2030
- Lower projected area could mean as late as 2050's
- +1 sigma Cd as early as 2026 or -1sigma as late as 2043
- 95th environment could mean as early as 2027
- 5th environment means as late as 2034

- Nominal predicted HST reentry avg area, Cd=1.74, 50th environment = **Fall 2033**

Extreme area presentations, extreme drag coefficients or extreme environments dramatically alters the predicted reentry times

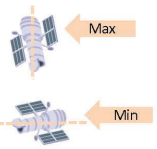

Run No.	Solar Weather Pred	Atmosphere	Area (m^2)	Cd	Reentry Date	
1a	Celestrak MSAFE 50%	MSIS	71	2.5	July 07, 2029	
2a	Celestrak MSAFE 50%	MSIS	92	2.5	October 08, 2027	
2ab	Celestrak MSAFE 50%	MSIS	92	1.74	November 06, 2030	
3a	Celestrak MSAFE 50%	MSIS	55	2.5	December 26, 2032	
3ab	Celestrak MSAFE 50%	MSIS	55	1.74	April 14, 2035	
4a	Celestrak MSAFE 50%	MSIS	13.8	2.5	>2050's	
4ab	Celestrak MSAFE 50%	MSIS	13.8	1.74	>2050's	
5a	Celestrak MSAFE 50%	MSIS	74	2.5	February 29, 2029	
6a	Celestrak MSAFE 50%	MSIS	71	1.31	June 15, 2035	25% lwr bd
7a	Celestrak MSAFE 50%	MSIS	71	3.26	September 28, 2027	75% upr bd
8a	Celestrak MSAFE 50%	JR	71	2.5	October 16, 2028	
9a	Celestrak MSAFE 50%	JR	92	2.5	June 11, 2027	
10a	Celestrak MSAFE 50%	JR	55	2.5	August 11, 2031	
11a	Celestrak MSAFE 50%	JR	13.8	2.5	>2050's	
12a	MSAFE 50th (*)	MSIS	71	2.5	July 09, 2029	
13a	MSAFE 50th (*)	MSIS	71	4.19	November 27, 2026	+1 sigma
14a	MSAFE 50th (*)	MSIS	71	0.79	May 01, 2043	-1 sigma
15a	MSAFE 5th (*)	MSIS	71	2.5	January 31, 2034	
16a	MSAFE 95th (*)	MSIS	71	2.5	June 13, 2027	
17a	Celestrak MSAFE 50%	MSIS	71	2.0	April 09, 2031	April 1,2024 TLE
18a	MSAFE 50th (*)	MSIS	71	2.0	May 26, 2030	April 1,2024 TLE
19a	Celestrak MSAFE 50%	MSIS	71	1.74	November 02, 2033	April 9,2025 TLE
19a2	MSAFE 50th (*)	MSIS	71	1.74	October 29, 2033	
20a	Celestrak MSAFE 50%	MSIS	71	1.74	October 02, 2033	April 1,2024 TLE

* MSAFE 50th, removed oscillation of F10.7 due to variations in Earth's eccentricity
Considered Nominal Avg Cross-Sectional Area and Avg Cd

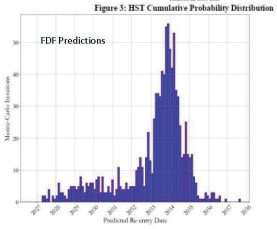

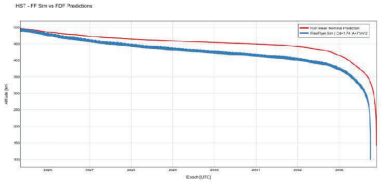

Historical Survey

To check the best/worst case deorbit times under 'actual' solar activity

- Solar cycle has a clear effect on deorbit time
- Currently in Solar Cycle 25 trending from solar maxima -> minima
- **Based on historical data, current deorbit time could extend out as the cycle moves towards the minima**

A trough in deorbit time corresponds to peak in solar activity

F10.7 spikes (magenta) caused simulation issues, since out of family from surrounding days

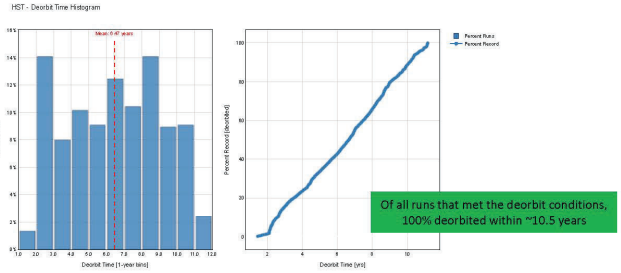

Of all runs that met the deorbit conditions, 100% deorbited within ~10.5 years

***Current cycle 25, is more like cycle 23, than 24 with regard to magnitude of the peak.**

Solar Cycle	Start	End	Maxima Start	Maxima End	Avg. Deorbit Time [years]
19	2/1/1954	10/31/1964	1/1/1957	12/31/1960	6.496
20	11/1/1964	6/30/1976	1/1/1967	12/31/1971	6.302
21	7/1/1976	9/30/1986	1/1/1978	12/31/1982	4.329
22	10/1/1986	5/31/1996	1/1/1988	12/31/1992	5.031
23	6/1/1996	12/31/2008	1/1/1999	12/31/2003	7.426
24	1/1/2009	12/31/2019	1/1/2012	12/31/2016	8.936
25	1/1/2020	---	1/1/2023	---	---

Solar Maxima/Minima	Avg. Deorbit Time [years]
Maxima	6.059
Minima	6.815

MAVERIC Reentry and Footprint Analysis

- HST initial conditions at ~122 km using FF results
  - Non-dispersed
- Reused material from (Smith, 2004) where available
  - Modeled all predicted surviving debris pieces
  - Used BCs at impact
  - Parent/child debris liberations for staggered breakup altitudes from the primary vehicle
- HST intact tumbling Ballistic Coefficient(BC) from (Baker 2019)
- Estimated Lift/Drag aero coefficients for surviving debris pieces using simple shape models (cylinders, boxes, flat plates)
- Perturbed atmosphere and winds
- Leveraged MAVERIC's Monte Carlo capabilities to disperse parameters
  - Engineering judgement used for dispersions on breakup altitude, individual and intact Ballistic Coefficient, Lift/Drag, intact mass properties
- Included bounding Columbia debris to provide a bounding footprint range

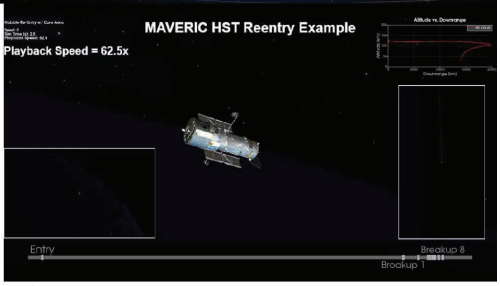

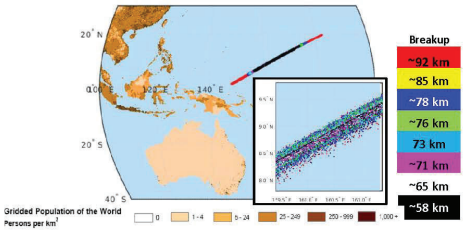

Dispersed Footprint length = 4,261 km, width = 70 km
Includes all dispersed runs, and bounding Columbia PERA debris
Single run spread w/o PERA pieces ~800 km

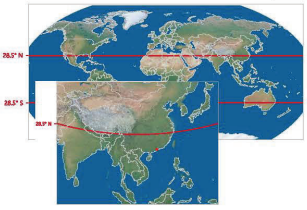

Impact zone +/- 28.5° Lat
Median # casualties = 3, 2035

Year	95% Lower Bound	Median	95% Upper Bound
2030	1:356	1:341	1:328
2035	1:348	1:324	1:301
2040	1:343	1:308	1:278

Overall Risk to Public, >1:10,000

ESA DRAMA Reentry and Footprint Analysis

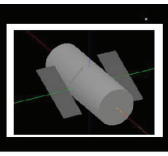

- Main Body shields internal components until demise or reaches altitude of 78 km, releases children at nominal temperature of 300 K
- Three reentry configurations were analyzed
  - Maximum drag orientation
  - Minimal drag orientation
  - **Higher Fidelity Results - Random tumbling state (below)**

Total casualty area: 120.40 m2
Total impact mass: 2083.27 kg
Total casualty probability (1D projection): 2.71×10^{-3} (1:369)

Maximum Downrange: 16,810.63 km at Latitude: −20.70°, Longitude: 141.31° (Antenna Ballast block)
Minimum Downrange: 16,462.94 km at Latitude: −19.54°, Longitude: 138.22° (Bracket Assy)
Max downrange difference between fragments: 347.69 km

Scenario	Min Prob.	Max Prob.	Mean Prob.	Standard Dev.
Low-Variant	4.03×10^{-5}	1.28×10^{-3}	3.70×10^{-4}	3.75×10^{-4}
Medium-Variant	3.21×10^{-5}	1.36×10^{-3}	3.96×10^{-4}	4.06×10^{-4}
High-Variant	3.67×10^{-5}	1.25×10^{-3}	3.14×10^{-4}	3.06×10^{-4}

Casualty Probability by Population Growth Model, Monte Carlo approach to reentry

Several trajectories exceeded $1x10^{-4}$ limit; (1:10,000)
Lowest risk scenario reentry over South Pacific Ocean, Point Nemo, $3.2x10^{-5}$ (1:31,250)
Highest risk case results from impact over India, $1.3x10^{-3}$ (1:769)

Tab. 3–2: Summary of Fragment Impact Parameters

Object Name	Qty	Material	Downrange (km)	Debr. Cas. Area (m²)	Impact Mass (kg)	Impact Energy (J)
TLx_MagneticTroquer	1	drama-Iron	16614.259	1.2425	38.78	103818.54
TRx_MagneticTroquer	1	drama-Iron	16614.259	1.2425	38.78	103818.54
BLx_MagneticTroquer	1	drama-Iron	16614.259	1.2425	38.78	104212.92
BRx_MagneticTroquer	1	drama-Iron	16614.259	1.2425	38.78	104212.92
Antenna_Ballast_block	4	drama-Tungsten	16810.628	0.4711	3.68	35650.19
Primary_Mirror	1	drama-FusedSilicaProxy	16740.570	5.6175	1005.16	6152355.25
Secondary_Mirror	1	drama-ZerodurProxy	16471.181	1.0783	12.80	15736.81
Axial_Fittings	1	drama-A316	16611.963	0.9756	23.10	64037.47
Base_Disk	1	drama-Molybdenum	16709.401	0.4522	0.76	1996.84
Mast_Base	1	drama-TiAl6v4	16566.835	0.6821	5.90	12700.34
Bracket_Assy	1	drama-TiAl6v4	16462.936	0.8529	6.80	7869.80
Opt._Bench_Struct.	1	drama-Invar	16532.022	0.7262	6.10	10561.09
Main_Ring	1	drama-TiAl6v4	16543.530	7.3183	449.06	842213.94
Battery-Cells	138	drama-Inconel718	16553.207	0.6637	2.34	2154.58
ReactionWheels	4	drama-A316	16619.309	1.0641	20.05	39813.86

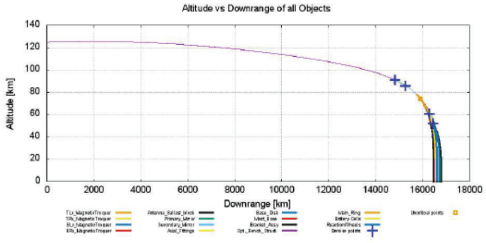

Fig. 3–1: Altitude vs. Downrange distance for the tumbling configuration. The flight path is intermediate between high and low drag scenarios.

Swift Decay Prediction Results

Swift is twice as sensitive to atmospheric drag because the (A/m) ratio is 2x greater than HST even though Swift is much smaller

- Swift currently at 451km altitude, nearly circular orbit, 20.5° inclination
- Swift Mass is 1456 kg
- Average Cross-Sectional Area = 17.10m^2 with max 30.24m^2 and min 22.92m^2
- Derived average Cd = 1.55
- Little difference between JR and MSIS atmosphere models
- Corrected MSAFE (Space weather) files makes ~days difference in predictions

- Swift Decay is sensitive to variations in Cd and Area
  - Smaller area longer decay time
  - Smaller Cd longer decay time
  - Larger area shorter decay time
  - Larger Cd shorter decay time

- Higher projected area could mean as early as Dec 2025
- Lower projected area could mean as late as June 2026
- +1 sigma Cd as early as Oct 2025 or -1sigma as late as Oct 2027
- 95th environment could mean as early as Dec 2025
- 5th environment means as late as Dec 2026

- Nominal Predicted Swift Reentry, avg area, Cd = 1.55, 50th environment = **Summer 2026**

Run No.	Solar Cycle	Atmosphere	Area (m^2)	Cd	Reentry Date	
1a	Celestrak MSAFE 50%	MSIS	17.08	2.2	January 31,2026	
2a	Celestrak MSAFE 50%	MSIS	17.08	2.5	December 25, 2025	
3a	Celestrak MSAFE 50%	MSIS	17.08	1.8	April 04,2026	
4a	Celestrak MSAFE 50%	MSIS	30.24	2.2	October 13, 2025	
4b	Celestrak MSAFE 50%	MSIS	30.24	2.18	October 14,2025	
4c	Celestrak MSAFE 50%	MSIS	30.24	1.55	December 07,2025	
5a	Celestrak MSAFE 50%	MSIS	22.92	2.2	November 23, 2025	
5b	Celestrak MSAFE 50%	MSIS	22.92	2.18	November 24, 2025	
5c	Celestrak MSAFE 50%	MSIS	22.92	1.55	February 17, 2026	
6a	Celestrak MSAFE 50%	JR	17.08	2.2	January 22, 2026	
7a	Celestrak MSAFE 50%	JR	17.08	2.5	December 21, 2025	
8a	Celestrak MSAFE 50%	MSIS	17.08	2.32	January 16, 2026	
10a	Celestrak MSAFE 50%	MSIS	17.08	2.37	January 10, 2026	
11a	Celestrak MSAFE 50%	MSIS	17.08	0.97	May 22, 2027	
12a	Celestrak MSAFE 50%	MSIS	17.08	3.77	October 17, 2025	
13a	MSAFE 5th (*)	MSIS	17.08	2.18	April 27, 2026	
14a	MSAFE 50th (*)	MSIS	17.08	2.18	January 29, 2026	
15a	MSAFE 50th (*)	MSIS	17.08	3.48	October 22, 2025	+1.3 1 sigma
16a	MSAFE 50th (*)	MSIS	17.08	0.88	October 9, 2027	-1.3 1 sigma
17a	MSAFE 95th (*)	MSIS	17.08	2.18	December 03, 2025	
18a	Celestrak MSAFE 50%	MSIS	17.08	1.55	June 08, 2026	
19a	MSAFE 50th (*)	MSIS	17.08	1.55	May 31, 2026	
20a	MSAFE 5th (*)	MSIS	17.08	1.55	December 02, 2026	
21a	MSAFE 95th (*)	MSIS	17.08	1.55	February 26, 2026	

* MSAFE 50th, removed oscillation of F10.7 due to variations in Earth's eccentricity
Considered Nominal Avg Cross-Sectional Area and Avg Cd

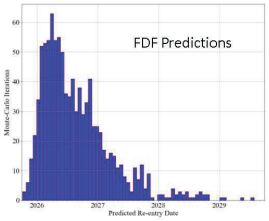

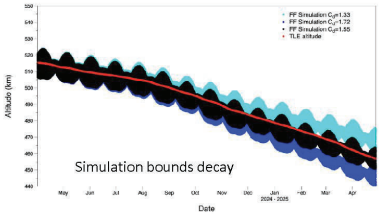

Findings

Space Environment & Input Models

F-1 As spacecraft dip lower in the atmosphere, density increases and model uncertainties have a stronger effect on decay predictions, this may require adjusting Cd due to inaccuracies in density models.

F-2 Historical solar activity records show peaks of extreme activity on 11/4/2003, 9/9/2005, 12/6/2006, 03/07/2011, where the F10.7 magnitudes are factors higher than the measurements before and after these days, causing the MSIS atmosphere model to fail to produce an atmospheric density value.

F-3 CelesTrak (T.S. Kelso) assumes MSAFE predicted F10.7 values are adjusted to account for Earth eccentricity and incorrectly loads these values in the 'adjusted' column of his space weather file. These values are then adjusted by a 1/radius^2 scaling factor and loads those values into the 'observed' column. MSFC MSAFE model developers confirm using observed F10.7 data to generate predictions.

F-4 Population density data are necessary for calculating the casualty probabilities under the ground track of reentering spacecraft. This analysis had to rely on unofficial data due to the population density data being removed from NASA's SocioEconomic Data and Applications Center (SEDAC) and EarthData websites in March 2025.

F-5 Given Swift's current altitude, small changes in solar predictions make a big difference in predicting reentry times; there are new solar activity models based on the physics of the Sun, and approaches that consider the stochastic nature of daily solar flux values that may improve predictions in this case.

Findings Continued

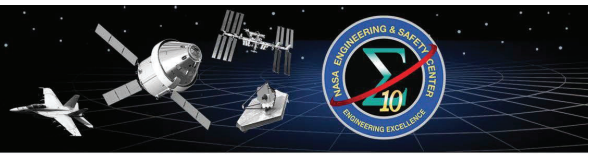

Requirements/Standards

F-6 To meet the 1:10,000 requirement for uncontrolled reentry, a satellite in a 28.5 deg inclination orbit reentering in 2025 would need a max Debris Casualty Area of only ~4m^2; this max allowable DCA value will decrease in time, due to population increases; the smallest HST DCA estimates (140m^2) are ~30x larger than this max allowable value and the HST Primary Mirror (expected to survive to impact) DCA is > max allowable DCA.

F-7 Higher fidelity debris reentry software tools exist, NASA's Orbital Debris Program Office uses ORSAT, and ESA uses SCARAB; GSFC SMD missions rely on high fidelity Monte Carlo simulations from the FDF.

Observations

Inputs

O-1 Satellite orbital decay predictions are dependent on solar activity data. NOAA Space Weather Prediction Center is a source of predicted space weather phenomenon and relied upon by industry and other government agencies. There are international organizations that provide space weather observations as well.

O-2 Satellite drag coefficients are critical for determining the neutral mass densities that contribute to spacecraft operating in the thermosphere. This study utilized a range of Cd values and derived specific values to match the recent HST, and Swift decay profiles. The determinations of satellite drag coefficients are ultimately tied to spacecraft shape *and* thermospheric factors like temperature and density.

O-3 A single Two-Line Element (TLE) can influence the decay time, by up to a month or more in some cases. Each TLE is a single observation with an unknown orientation; Monte Carlo simulations from multiple TLEs and considering the uncertainty a single propagated TLE contributes can improve the results.

O-4 We continue to be made aware of additional tools and models, such as a density model developed by the Department of Defense/Orbitron High Accuracy Satellite Drag Model (HASDM) which includes phases and amplitudes of the diurnal and semidiurnal variations of thermospheric density, based on observations from a set of Low Earth Orbit (LEO) calibration satellites.

Simulation

O-4 Some of the runs do not make it to the 100 km altitude cutoff before terminating due to entering the reference ellipsoid caused by variable time step; once the propagation hits about 200 km it really starts decay rapidly using a variable step size or even a 10min step size, within 1/2 steps it can essentially crash into Earth.

O-5 FF Simulation was unable to propagate epochs across periods of extremely high solar F10.7 values, a bug report was issued, and AI solutions discovered the underlying MSIS model was in error. AI solutions is investigating a patch for FF. Previous solar cycles with similarly high values processed normally as cycles with a steady increase in solar activity did not result in simulation interruptions.

O-6 The Public Entry Risk Assessment (PERA) for Space Shuttle reports a 0.5 Ballistic Coefficient for a Shuttle tile piece that bounds the heel of the footprint and was used as a bounding value for the 6DOF Monte Carlo reentry predictions. This assumption is 3x smaller than the assumption used in the last ORSAT reentry run (2005) for equivalent BC pieces greater than the 15 J minimum threshold.

Recommendations

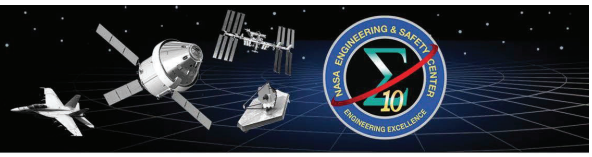

To Swift Project Office:
R-1 Given Swift has a predicted reentry within two years, conduct an ORSAT evaluation through the ODPO with the most current information. (**F-1**, **F-5**, **F-7, O-2**)

To GSFC FDF (and other organizations conducting reentry predictions):
R-2 Consider using physics-based solar prediction models for near term reentry predictions, such as Swift. (**F-1**, **F-5**, **O-1**)

R-3 Use more stochastic models over 'smoothed' solar cycle predictions for near term reentry predictions. Models inclusive of the naturally occurring peaks in activity produce more accurate decay reentry predictions. Further studies should be conducted that include variations in geomagnetic conditions on top of smoothed predictions. (**F-1**, **O-1**, **O-8**)

To HST Project Office:
R-4 Using the attitude profile flown during the observation schedule may reveal 'trends' favoring certain orientations which allow for better estimates of area as a function of time, in addition to estimates of Cd based on free molecular flow models which would improve estimates for decay predictions. (**F-1**, **F-2**, **O-2**, **O-3**, **O-4**)

R-5 Conduct an updated HST uncontrolled reentry survivability and population risk analysis using the latest version of ORSAT against the final (post SM-4) HST configuration inclusive of the latest population densities and growth projections. Predictions should include detailed aerothermal analysis to determine demise fragment properties under varying conditions for improved footprint analyses. (**F-4**, **F-6**, **F-7**)

Recommendations, Continued

To OSMA:

- **R-6** Update NASA-STD-8719.14C Process for Limiting Orbital Debris to include the new Debris Casualty Area equation from the Orbital Debris Program Office. (**F-4**, **F-7**)

To CelesTrak Developer T.S. Kelso:

- **R-7** The CelesTrak space weather file should use the unadjusted MSAFE observed F10.7 values in the 'observed' column of the publicly distributed space weather file. **(F-2, F-3, O-1)**

To Free Flyer and NRL MSIS Developers:

- **R-8** The FreeFlyer simulation tool utilizes the Naval Research Lab MSIS atmosphere model to produce atmospheric densities for orbital decay calculations and should implement a workaround for cases where extreme F10.7 values disrupt the density calculations; NRL MSIS developers should address the errors resulting from extreme values of F10.7 that are out-of-family from surrounding measurements. **(F-2, O-5)**

Value of Activity

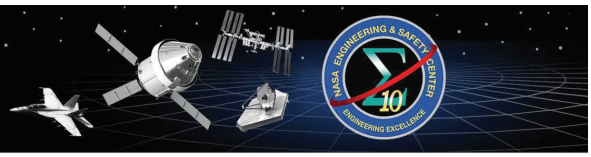

- **Independent assessment of HST/Swift Decay provides:**
  - a cross-validation of results
  - the ability to compare multiple solutions to help quantify prediction uncertainties
  - robustness against model limitations
  - the ability to identify sensitivities
  - increased prediction confidence
- **New collaborations between Space Environments Technical Fellow and GSFC Flight Dynamics Facility to improve solar activity prediction methods benefiting decay predictions**
- **Identified issue in a widely used thermosphere model, with the intention of improving the model relied on by government, industry and academic institutions for a variety of purposes**
- **Identified an incorrect manipulation of data from a NASA solar activity model hosted on a public and widely cited website, correcting this file impacts government, industry and academic institutions using this information**

BACKUP

Problem Background and Assessment Approach

Hubble's decay and demise has been studied extensively and found to be highly sensitive to variations in space weather activity; the reentry and breakup modelling involves complex aerothermal analyses to accurately assess casualty risks for populations living under the ground track. Accurate orbital decay and footprint involve large uncertainties in predicting solar behavior, resulting thermosphere changes and complicated aero-heating analyses on materials coupled with aerodynamic effects on unknown fragmentation.

The orbiting platform has been serviced 5 times since its launch in 1990 to maintain the observatory, replace critical instruments, and extend the lifetime. Recent studies estimate the observatory to decay in the mid 2030's with approximately 20% of the mass of the spacecraft surviving reentry, increasing the probability of casualties on the ground with an uncontrolled reentry. The Flight Dynamics Facility (FDF) study utilized System Tool Kit (STK) for orbital propagation, Monte Carlo sampling of Schatten solar prediction environment, and the Orbital Debris Program Office used their high-fidelity orbital survival analysis tool (ORSAT).

The NESC performed orbital decay simulations using different tools and environment assumptions to provide an independent check on previous reports. The NESC team separated the study into two problems: 1) orbital decay and 2) reentry, footprint, and casualty calculations.

FreeFlyer (FF) was used to model the orbital decay, assessing variations in historical solar cycle for best- and worst-case cycles, predictive solar activity using Mass Spectrometer and Incoherent Scatter (MSIS)-MSFC Solar Activity and Future Estimation (MSAFE) model, varying projected area and drag coefficients as both are sensitive to atmosphere and altitude. Aerospace's reentry analysis tools, like All-Prop were used as a check on FF. Reentry conditions were assessed using two simulations to disperse multiple reentry conditions and the resulting footprint and casualty probabilities: the European Space Agency's (ESA's) open-source Debris Risk Assessment and Mitigation Analysis (DRAMA) tool suite and the Space Launch System (SLS) 6DOF Marshall Aerospace VEhicle Representation In C (MAVERIC) Monte Carlo simulation.

High fidelity reentry analyses and detailed statistical sweeps of all relevant factors and environments were out of scope for this brief study. The intent was to utilize different tools and environments as a check against other higher fidelity analyses and methods.

Derived Cd – 1.74 but may be closer to 1.8
Cd plotted with Daily Sunspot Number

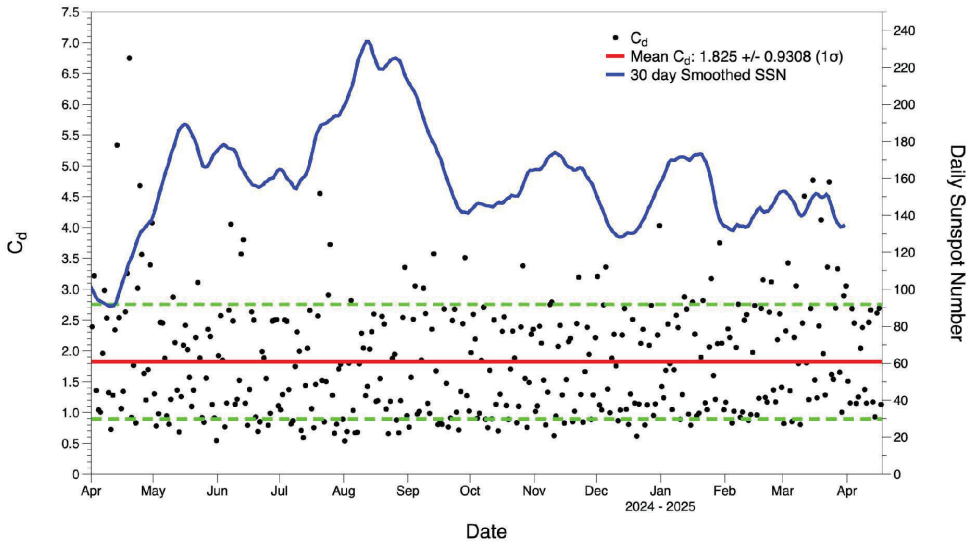

NESC logo inserted *after* NRB approval

Swift Decay Compared to Solar Activity

- Blue/Pink highlighted area indicate matching timespans between the top 2 plots and the bottom plot, notice significant 'spikes' in activity in 2024
- Top plot is the TLE data, with a linear fit to the altitude, Orbit Decays ~520 km to 450 km in a year, ~20 km since January 2025
- Middle plot is observed F10 and Ap, with averages shown as dashed lines
- Bottom plot is the combination of the observed/predicted Solar Spot Number from NOAA
- Bottom plot, blue highlight timespans indicate observed solar data, while the pink indicates predict

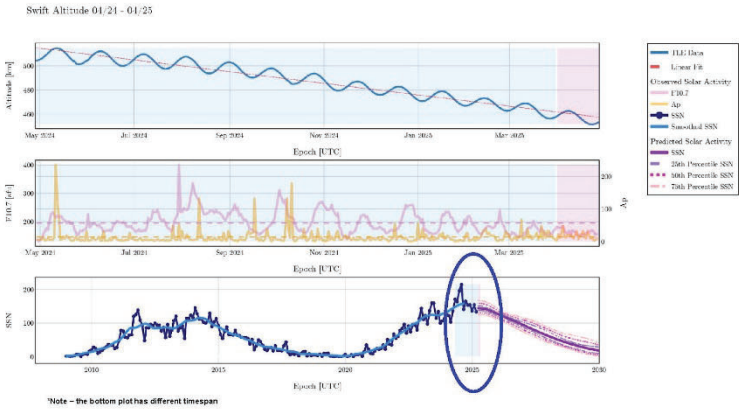

*Note – the bottom plot has different timespan

Presence of second peak last year (2024) and 'spikes' increased solar activity could be impacting MSIS atmospheric density modeling, indicating earlier reentry times than actual decay may lead one to believe

"It is not the amount of variability that is in question, but rather the detail" – Naasz, Berry, Schatten

Primer: NORAD Two Line Element (TLE) Sets

Initialize the HST Orbit for Analysis, Orbital Elements and Epochs

BSTAR Drag Term, 0.00045853 (in Earth radii^{-1} units) – combo of Area, density and drag coefficient

(1) HST
1 20580U 90037B 25099.45794414 .00011761 00000+0 45853-3 0 9990
2 20580 28.4677 150.4913 0002256 65.6904 294.3926 15.24330044722180

"While NORAD maintains specific target tolerances for the overall level of accuracy as a system performance metric, it can be expected that accuracy of a (TLE) will vary depending upon the type of orbit and satellite involved." T.S. Kelso

NORAD Two-Line Element Set Format

Data for each satellite consists of three lines in the following format:

```
AAAAAAAAAAAAAAAAAAAA
1 NNNNU NNNNNAAA NNNNN.NNNNNNNN +.NNNNNNNN +NNNNN-N +NNNNN-N N NNNN
2 NNNNN NNN.NNNN NNN.NNNN NNNNNNN NNN.NNNN NNN.NNNN NN.NNNNNNNNNNNNNN
```

Line 0 is a twenty-four character name (to be consistent with the name length in the NORAD SATCAT).

Lines 1 and 2 are the standard Two-Line Orbital Element Set Format identical to that used by NORAD and NASA. The format description is:

Line 1	
Column	Description
01	Line Number of Element Data
03-07	Satellite Number
08	Classification (U=Unclassified)
10-11	International Designator (Last two digits of launch year)
12-14	International Designator (Launch number of the year)
15-17	International Designator (Piece of the launch)
19-20	Epoch Year (Last two digits of year)
21-32	Epoch (Day of the year and fractional portion of the day)
34-43	First Time Derivative of the Mean Motion
45-52	Second Time Derivative of Mean Motion (Leading decimal point assumed)
54-61	BSTAR drag term (Leading decimal point assumed)
63	Ephemeris type
65-68	Element number
69	Checksum (Modulo 10) (Letters, blanks, periods, plus signs = 0; minus signs = 1)

Line 2	
Column	Description
01	Line Number of Element Data
03-07	Satellite Number
09-16	Inclination [Degrees]
18-25	Right Ascension of the Ascending Node [Degrees]
27-33	Eccentricity (Leading decimal point assumed)
35-42	Argument of Perigee [Degrees]
44-51	Mean Anomaly [Degrees]
53-63	Mean Motion [Revs per day]
64-68	Revolution number at epoch [Revs]
69	Checksum (Modulo 10)

(1) TLE April 09, 2025 10:59:26.37 Ref. Source – CelesTrak 501©(3) non-profit hosted by T.S. Kelso; Identical TLE to Space-Trak.org

NRL MSIS Density Values as Function of Altitude

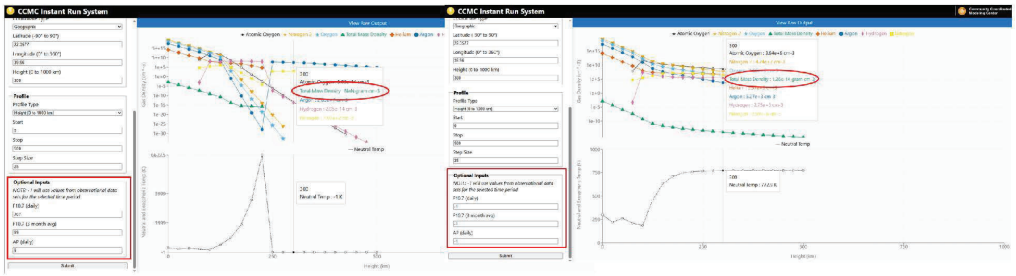

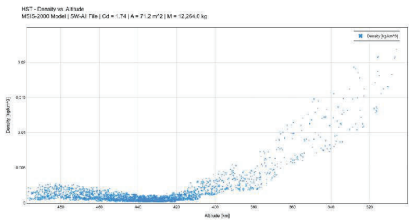

Revision to CelesTrak Space Weather File

Also compared this new space weather file "SW-All.csv" against the *source* data model, MSAFE 50th percentile model (labeled here as SW_predict_MSAFE_50.csv)

The MSAFE_50.csv curve falls along the green revised CelesTrak file, SW-All.csv

The green SW-All.csv has the inserted Earth eccentricity variations but the original MSAFE method does not preserve these variations

The stale F10.7 space weather file (blue) predicted values much lower than current observations leading to later decay prediction times for HST

This demonstrates how sensitive predictions are to Solar Activity

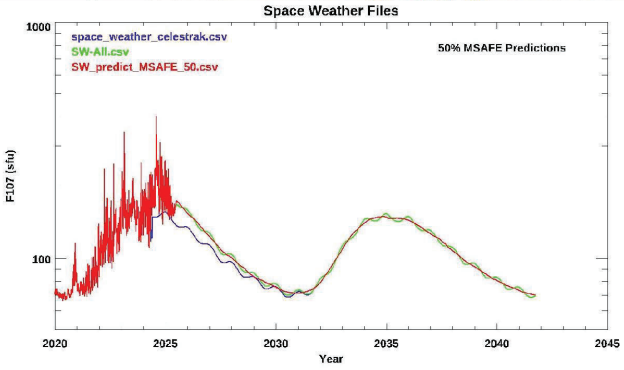

All calculations for orbital decay were re-run against latest Space Weather Data File (SW-All.csv) with some runs including a revised MSAFE without Earth Eccentricity variation

Dominion Radio Astrophysical Observatory (DRAO)
Radio bursts in the 2010 to 2017

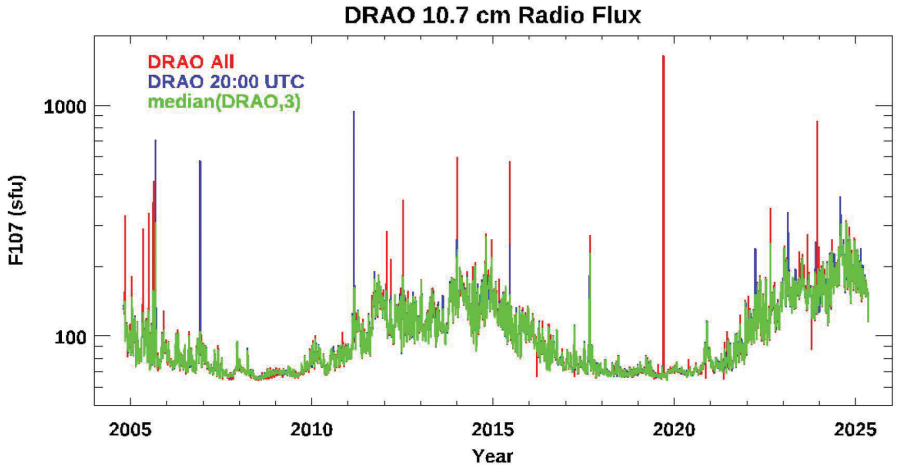

NESC logo inserted *after* NRB approval

Orbital Element Sets Propagation

- **Aerospace Corp has access to several external and internally developed programs to compute Reentry for Air Force Programs**
- **HST Decay computed with several tools using:**
  - General Perturbations (TLE) and Improved version called XP
    - Reentry Predictions
      - TLE: 7 April 2032 (does not include varying F10.7, only relies on a fixed value, linear density variation with altitude)
      - XP: 8 September 2033 (includes more perturbations, slightly higher fidelity density model, same fixed F10.7)

Within family of FDF, NESC

  - Special Perturbations method (more perturbations, better BC)
    - Reentry Predictions
      - Aerospace BC: September 27, 2031
      - Max Area BC: May 22, 2030
  - SOAP Long term(life-time tool specially developed for decay predictions, can read internal solar cycle data or MSAFE)
    - Reentry Predictions
      - 10/12/2028 (constant BC, Constant F10.7 = 180, MSIS-2000)
      - 03/06/2031 (constant BC, Constant F10.7 = 100, MSIS-2000)
  - All Prop (hi-fidelity integration, EGM 21x21,MSIS-2000, MSAFE)
    - Reentry Predictions
      - 05/19/2030
  - TRACE (hi-fidelity integration, EGM 70x70, MSIS-2000, MSAFE)
    - Reentry Predictions
      - 03/01/2029
  - Lifetime (Aerospace) (mean element propagation, constant BC, internal Solar Cycle)
    - Reentry Predictions
      - 05/23/2035

Within family of FDF, NESC

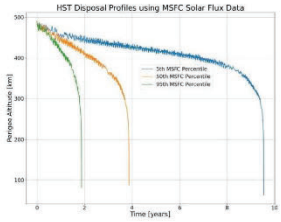

Most Confidence among tools, but not as close to NESC/FDF

NESC Document #:

Restricted distribution to NESC and designated team members until reviewed by the NRB.
This is for status only and does not represent complete engineering analysis.

26

NESC logo inserted *after* NRB approval

Debris Casualty Area Equation Updates

- **NASA ODPO has introduced a more accurate DCA model (Ostrom 2019):**
  - $D_A = \sum_{i=1}^{N}\left(0.278\, m^2 + A_i + 1.39\, m * \sqrt{A_i}\right)$
- **New model results in lower DCA for small debris and slightly higher DCA for large debris**
- **Using the new equation, the Smith 2004 unscaled <u>total</u> DCA reduces from 146 m² to 137 m² and slightly reduces the overall risk:**
  - 1:340 in 2021 → 1:363
  - 1:250 in 2021 (mass scaled) → 1:267

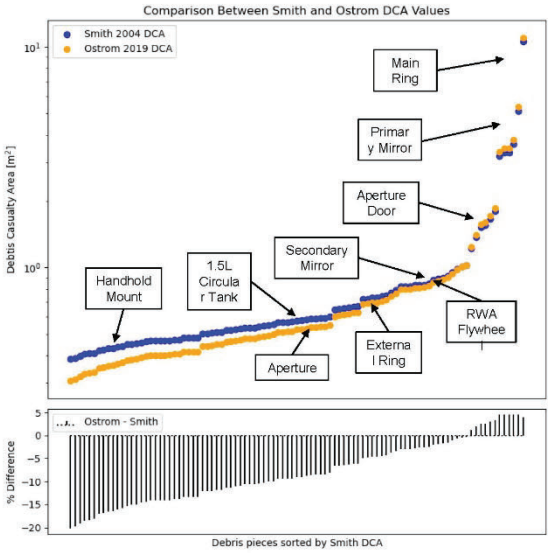

NESC logo inserted *after* NRB approval

MAVERIC Reentry and Example Footprint Analysis

- **MAVERIC is a high-fidelity 6-DOF simulation currently used for:**
  - Artemis SLS ascent, in-space, and reentry GN&C/6-DOF design and analysis
  - MSR Mars Ascent Vehicle GN&C/6-DOF design and analysis
- **MAVERIC is used to show SLS reentry requirement compliance to the NASA-STD-8719.14C requirement for <u>controlled</u> reentry:**
  - No surviving debris impact with a kinetic energy > 15 *J* within 370 km from foreign landmasses, or 50 km from U.S. and Antarctica
- **MAVERIC SLS Core reentry Monte Carlo analysis includes:**
  - Dispersed atmosphere/winds
  - Core Stage(CS) breakup debris catalog with BC, Lift to Drag and explosion ΔVs
  - Bounding debris from Shuttle Columbia PERA
- **NESC IV&V of the MAVERIC SLS Core reentry analysis showed good agreement**
- **The available Artemis I post-flight data for Core reentry showed good agreement with MAVERIC predictions**
- **MAVERIC reentry and footprint analysis can be used to inform risk, determine keep-out-zones, define optimal entry interface**

SLS Dispersed Footprint Examples

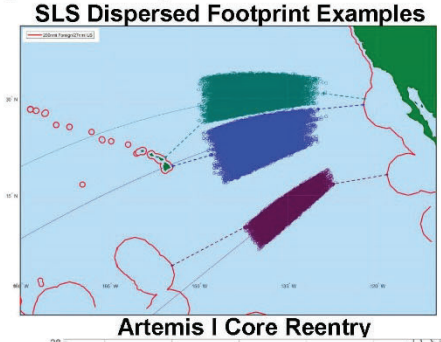

Artemis I Core Reentry

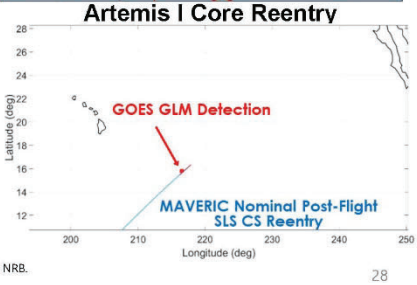

NESC logo inserted *after* NRB approval

Risk Assessment Updates

- **Left figure shows updated 2020-2040 population density as f(inclination) using GPWv4 and IDB**
  - Total population projection used to scale density profile through 2040 (~17% increase from 2020 to 2040)
  - ~10% higher population than Smith projections for 2020
- **Middle figure compares the original Smith 2004 results for their two bounding DCA values (orange) with MSFC's updated projections, using the updated DCA values and updated population densities (blue). Updated projections show slightly higher risk (~5%) than Smith 2004**
  - Updated Risk Assessment: between $1:209$ and $1:278$ risk for a HST reentry in 2035
- **Right figure shows max DCA to meet $1:10,000$: <u>~4.5 m² for HST orbit in 2020; ~3.9 m² in 2040</u>**

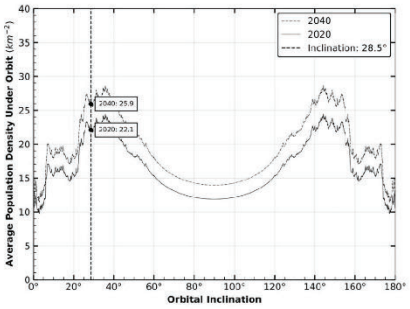

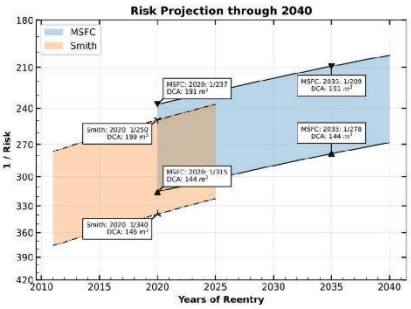

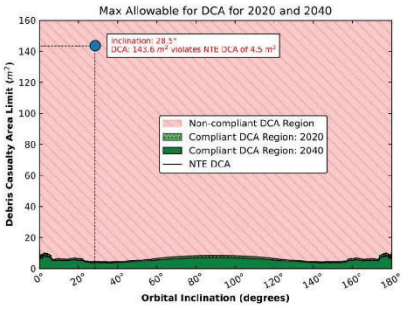

NESC logo inserted *after* NRB approval

Population Model

- **Previous studies used NASA's Socioeconomic Data and Applications Center (SEDAC) Gridded Population of the World (GPW) database**
  - SEDAC data are no longer available as of March 7, 2025
- **This study used United Nations (UN) World Population Prospects (WPP) 2024 database to model global population**
  - 2023 population data from national population censuses for 237 countries or areas
  - Population projections to year 2100 with estimates of uncertainty
- **WPP database was merged with UN data on land area to compute population density projections**

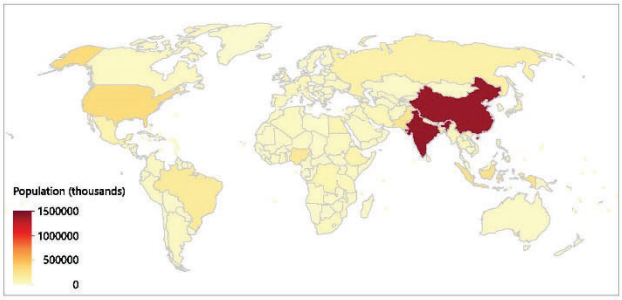

NESC logo inserted *after* NRB approval

Risk to the Public

- **Expected number of casualties can be computed as the product of:**
  - Probability of impact in a region
  - Debris casualty area
  - Population density in the region

$$E_c = P(Impact) * DCA * Pop\ Density$$

NESC logo inserted *after* NRB approval

MAVERIC vs. ORSAT

MAVERIC

- **All debris from main vehicles (left figure)**
- **No aerothermal or ablation modeling**
- **Debris catalog, breakup alt, etc. are inputs**
- **BC, Lift/Drag and bank angle held constant for each propagation**
- **Vehicle 6DOF propagation (aero, hi-fi gravity)**
  - Debris 3DOF propagation
- **Set up for Monte Carlo**
  - Disperse winds/atmosphere, BC, L/D, etc.
- **Primary outputs**
  - Footprint boundary
    - Typically, only representative pieces modelled.
  - Keep Out Zone(KOZ) distances

ORSAT v5.8 (Smith 2004)

- **3DOF propagation**
- **Children debris from parent demise/liberation**
- **Includes aerothermal and ablation modeling**
- **BC variation from flow regime transition, supersonic to subsonic velocity transition, mass per area changes from ablation**
- **Calculates DCA, population density, and E**

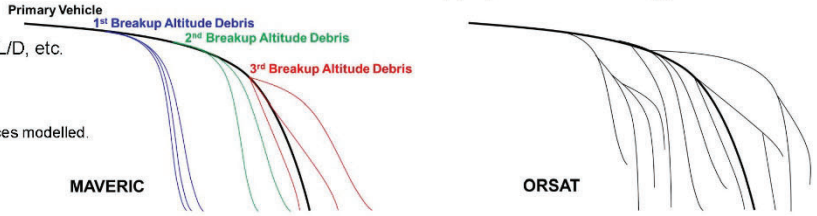

NESC logo inserted *after* NRB

Max Drag Results

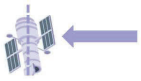

Key results:

- **Total number of fragments:** 11 (3 unique)
- **Total impact mass:** 1068.1 kg
- **Total casualty area:** 17.22 m²
- **Total casualty probability (1D) for different population variant:**
  Low-Variant 3.82×10^{-4} Medium-Variant 3.80×10^{-4} High-Variant 3.84×10^{-4}

Surviving Fragments and Associated Risk:

- **Primary Mirror:** 828 kg; average casualty area: 4.69 m²; casualty probability: 1.04×10^{-4}; Max Downrange 13480.644 km; Lat $-29.163°$ Lon $114.300°$
- **Reaction Wheels (4 units):** 45 kg total; average casualty area: 1.80 m²; casualty probability: 3.97×10^{-5}; Max Downrange 13122.044 km; Lat $-29.043°$ Lon $112.427°$
- **Battery Cells (6 units):** 10.02 kg total; average casualty area: 0.89 m²; casualty probability: 1.96×10^{-5}; Max Downrange 13297.987 km; Lat $-29.103°$ Lon $113.302°$

Max downrange difference between fragments : 358.6 km

Parameter	Value	Unit
Altitude	125.031	km
Latitude	20.022	degrees
Longitude	-0.898	degrees
Velocity	7.422	km/s
Flight Path Angle	-0.03820	degrees
Heading Angle	113.15244	degrees

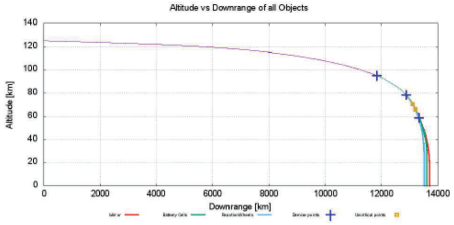

Fig. 3–1: Altitude vs. Downrange distance for the main body during re-entry. The steep descent profile reflects the high drag configuration of the satellite.

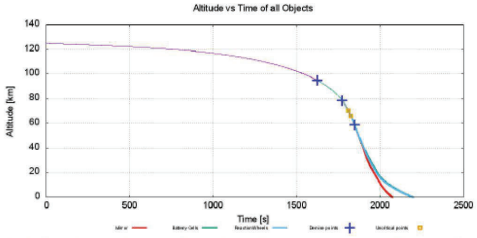

Fig. 3–2: Altitude vs. Time for the main body from re-entry interface to fragmentation. Breakup occurs near 78 km, followed by rapid descent of surviving fragments.

NESC logo inserted *after* NRB

Min Drag Results

Key results:

- **Total number of fragments:** 11 (3 unique)
- **Total impact mass:** 1052.4 kg
- **Total casualty area:** 17.22 m²
- **Total casualty probability (1D) for different population variant:**
  Low-Variant 3.98×10^{-4} Medium-Variant 3.94×10^{-4} High-Variant 4.02×10^{-4}

Surviving Fragments and Associated Risk:

- **Primary Mirror:** 828 kg; average casualty area: 4.69 m²; casualty probability: 1.07×10^{-4}; Max Downrange 22188.211 km; Lat $-3.445°$ Lon $-150.598°$
- **Reaction Wheels (4 units):** 45 kg total; average casualty area: 1.80 m²; casualty probability: 4.11×10^{-5}; Max Downrange 21782.931 km; Lat $-4.427°$ Lon $-152.259°$
- **Battery Cells (6 units):** 7.40 kg total; average casualty area: 0.89 m²; casualty probability: 2.03×10^{-5}; Max Downrange 21974.146 km; Lat $-4.018°$ Lon $-151.562°$

Max downrange difference between fragments : 405.28 km

Parameter	Value	Unit
Altitude	124.962	km
Latitude	17.301	degrees
Longitude	14.550	degrees
Velocity	7.422	km/s
Flight Path Angle	-0.02363	degrees
Heading Angle	115.05219	degrees

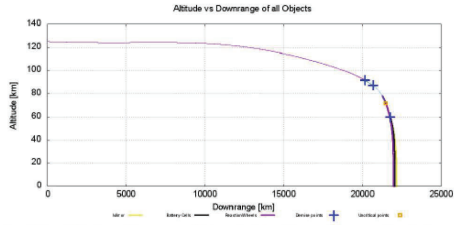

Fig. 3–3: Altitude vs. Downrange distance for the minimum drag case. The shallower entry angle results in a longer flight path through the upper atmosphere.

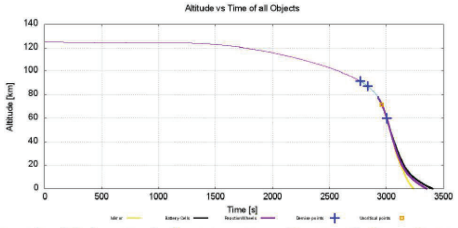

Fig. 3–4: Altitude vs. Time for the minimum drag configuration. The descent duration is extended, leading to a longer heating phase.

NESC logo inserted *after* NRB

Randomly Tumbling Results

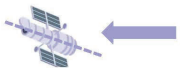

Key results:

- **Total number of fragments:** 11 (3 unique)
- **Total impact mass:** 1047.4 kg
- **Total casualty area:** 17.22 m²
- **Total casualty probability (1D) for different population variant:**
  Low-Variant 3.82×10^{-4} Medium-Variant 3.80×10^{-4} High-Variant 3.84×10^{-4}

Surviving Fragments and Associated Risk:

- **Primary Mirror:** 828 kg; average casualty area: 4.69 m²; casualty probability: 1.04×10^{-4}; Max Downrange 15093.366 km; Lat 27.186° Lon 38.250°
- **Reaction Wheels (4 units):** 45 kg total; average casualty area: 1.80 m²; casualty probability: 3.97×10^{-5}; Max Downrange 14883.104 km; Lat 27.479° Lon 36.163°
- **Battery Cells (6 units):** 6.56 kg total; average casualty area: 0.89 m²; casualty probability: 1.96×10^{-5}; Max Downrange 14960.080 km; Lat 27.374° Lon 36.951°

Max downrange difference between fragments : 210.262 km

Parameter	Value	Unit
Altitude	124.957	km
Latitude	-16.523	degrees
Longitude	-94.997	degrees
Velocity	7.420	km/s
Flight Path Angle	-0.03150	degrees
Heading Angle	65.09831	degrees

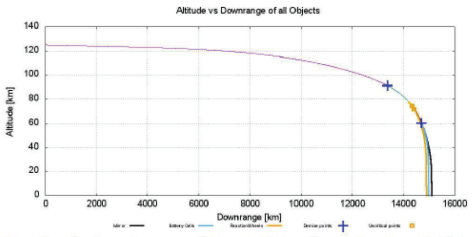

Fig. 3–5: Altitude vs. Downrange distance for the tumbling configuration. The flight path is intermediate between high and low drag scenarios.

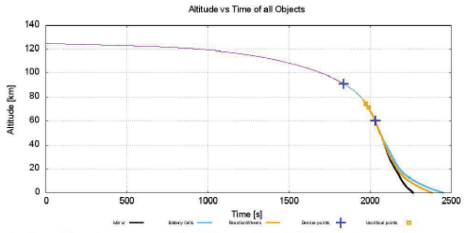

Fig. 3–6: Altitude vs. Time profile of the tumbling Hubble main body during re-entry. Dynamic variation in drag leads to complex descent behavior.